University of Nevada, Reno

Holocene records of climate and pollution from the Northern Rocky Mountains: Integrating perspectives from glacial ice, lake sediments, and tree rings

A dissertation submitted in partial fulfillment of the
requirements for the degree of Doctor of Philosophy in
Hydrology

By

Nathan J. Chellman

Dr. Joseph R. McConnell/Dissertation Advisor

August, 2019

THE GRADUATE SCHOOL

We recommend that the dissertation
prepared under our supervision by

NATHAN J. CHELLMAN

Entitled

Holocene records of climate and pollution from the Northern Rocky Mountains: Integrating perspectives from glacial ice, lake sediments, and tree rings

be accepted in partial fulfillment of the
requirements for the degree of

DOCTOR OF PHILOSOPHY

Joseph R. McConnell, Ph.D., Advisor

Monica M. Arienzo, Ph.D., Committee Member

Gregory T. Pederson, Ph.D., Committee Member

Alan Heyvaert, Ph.D., Committee Member

Adam Csank, Ph.D., Graduate School Representative

David W. Zeh, Ph.D., Dean, Graduate School

August, 2019

Abstract

Reconstructions of past climate and pollution often rely on chemical records preserved in glacial ice, lake sediments, and tree rings. The goal of this dissertation is to combine perspectives on paleoclimate and pollution from paired records developed from these archives to obtain a more complete understanding of past environmental change, as well as to leverage the strengths of each archive to address shortcomings of another. Paired ice-core and tree-ring records were developed from the Upper Fremont Glacier (UFG) and groves of nearby whitebark pines in the Wind River Range, Wyoming. The depth-age scale for the difficult-to-date ice cores was constrained by synchronizing the ice-core water isotopes to the absolutely-dated tree-ring chronology, both proxies for temperature. On the revised depth-age scale, trends in black carbon, thallium, bismuth, and mercury (Hg) in the ice paralleled those observed in Greenland documenting widespread industrial pollution. The record of ice-core Hg subsequently was used to evaluate the viability of tree rings for reconstructing past atmospheric Hg concentrations. Hg trends observed in the trees were temporally offset from the ice core, suggesting radial movement of Hg across ring boundaries.

A well-dated ice core record of water isotopes and ice accumulation was developed from a shallow ice patch on the Beartooth Plateau, Wyoming. Radiocarbon dating indicated the ice patch has persisted for over 10,000 years, and these records represent the first climate records developed from such an archive. In conjunction with a nearby lake sediment record, the ice patch records were shown to document Holocene climate variability, including peak warmth around 4,200 years ago followed by a 1,500 year-long era of colder and wetter winters, generally paralleling human activity in the nearby Bighorn Mountains.

Black carbon (BC) profiles from two Wyoming lakes were used to assess how lake characteristics affect interpretations of lake sediment BC records. Comparisons of BC to charcoal data from Island Lake indicate that BC can be subject to similar depositional mechanisms as

charcoal, leading to locally-biased records. At North Lake, which has a comparatively smaller and less vegetated watershed of the two lakes, comparisons to the UFG BC record and modelling results indicate that the North Lake BC record is primarily atmospherically deposited and therefore represents regional burning. The climate and pollution records presented in this dissertation demonstrate how improved analytical techniques and new paleo archives can lead to a better understanding of environmental changes in the northern Rocky Mountains over past centuries and millennia.

Acknowledgements

I would like to thank my advisor, Joe McConnell, for making this work possible. Joe has been an amazing mentor and has provided me with countless opportunities for research and collaborations. I would also like to thank Monica Arienzo for her advice, assistance, and leadership in the lab, field, and at conferences. I am also grateful for the friendship and camaraderie from Michael Sigl, Olivia Maselli, and Dan Pasteris throughout my time in grad school. I appreciate the expertise of and insights from my committee, including Joe McConnell, Monica Arienzo, Greg Pederson, Adam Csank, and Alan Heyvaert, who were instrumental to this dissertation. Finally, I would like to thank my family for all of their support. Funding for my Ph.D. was provided by the Sulo and Aileen Maki Endowment at the Desert Research Institute. Further acknowledgements specific to each project are provided at the end of each chapter of this dissertation.

Table of Contents

List of Tables

Chapter 3

Chapter 4

List of Figures

Introduction

Understanding past environmental change is crucial for understanding natural climate variability on Earth as well as contextualizing modern conditions. Paleoclimate studies often rely on records from ice sheets and glaciers, lake and ocean sediments, tree rings, and speleothems to reconstruct climate and pollution over past centuries to millennia. Over the past tens or hundreds of thousands of years, polar ice cores and deep sediment cores document global-scale oscillations between glacial and interglacial conditions.[1-4] Over past centuries to millennia, lake sediments, glacial ice, and tree rings document natural climate variability as well as anthropogenic pollution.[5-9] The most recent period of Earth history, known as the Holocene epoch, spans the 11,600 years since the end of the last ice age, when ice sheets covered much of North America, Europe, and Asia.

Holocene-length climate reconstructions in the Rocky Mountains are largely dominated by lake sediment records, one of the few natural archives that consistently record and preserve climate information over the past 10,000 years at the mid-latitudes. Although polar ice cores can extend back in time for many millennia, the only existing ice-core records from this region are from the Upper Fremont Glacier (UFG) in the Wind River Range, Wyoming,[6, 7, 10] which only document the past 250 years as potentially older glacial ice is lost to flow and thinning or basal melt in these, and other, glacial ice cores. The length of tree ring records is generally on the order of the lifespan of trees, typically a few centuries but up to a few millennia for certain species, though some records can be extended farther back in time by sampling of fossil wood or well-preserved dead trees.[11]

The overarching goal of this dissertation is to combine perspectives on Holocene climate and pollution from lake sediments, glacial ice, and tree rings in the northern Rocky Mountains. By developing records from geographically co-located archives, it was possible to use the strengths of one archive to address shortcomings of another, and therefore develop paired records

that provide a more complete understanding of environmental processes than otherwise could be gained by records limited to a single archive. The paired ice-core and tree-ring records in Chapters 1 and 2 used the absolute dating of the tree chronology to constrain the difficult-to-date UFG ice-core records. In turn, the pollutant records from the ice core were used to assess trees as bioindicators of atmospheric pollution. The paired ice-core and lake-sediment core records in Chapters 3 and 4 were used to develop an enhanced understanding of hydroclimatic changes over the Holocene, including changes in fire history and wintertime temperature and precipitation.

Holocene Climate in Wyoming

Preceding the transition from the Pleistocene to the Holocene epoch, northern North America was covered by the Cordilleran and Laurentide ice sheets at a time known as the Last Glacial Maximum (LGM). These two massive ice sheets began to retreat between 20,000 and 19,000 years before present (ybp; defined here as years before 1950 CE), marking the end of the LGM, the deglaciation into the Holocene, and the transition to a climate more resembling that of present.[12] The maximum extent of the Cordilleran and Laurentide ice sheets reached south across the modern U.S.-Canada border,[13] but did not cover the mountainous areas of Wyoming. Both the Greater Yellowstone Area (GYA) and the Wind River Range were covered in separate, smaller ice caps. The deglaciation of the Wind River Range began around 15,000 ybp, and glaciers rapidly retreated into high-elevation cirques by 12,100 ybp.[14] Similarly, the glacial system covering the GYA, which was ~1 km thick at its maximum, began to retreat between 15,000 and 14,000 ybp because of rain-shadow-driven stagnation at its northern extent and overall warming temperatures, with glaciers stabilizing in cirques by 13,000 ybp.[15]

Reconstructions of past climate in this region going back to the deglaciation are nearly exclusively based on lake sediment cores,[16-19] with a few speleothem records contributing to the overall understanding of hydroclimate.[20, 21] The Holocene is roughly divided into early (11,600 to

8,000 ybp), middle (8,000 to 4,000 ybp), and late (4,000 ybp to modern), with more recent work establishing formal divisions between early-middle and middle-late at 8,200 ybp and 4,200 ybp, respectively, based on globally-recorded stratigraphic events in numerous paleoclimate archives.[22] The early Holocene was thought to be characterized by overall warming[23, 24] leading to maximum mid-Holocene warmth around 5,000 to 6,000 ybp, sometimes referred to as the mid-Holocene climate optimum. There is conflicting evidence on the exact conditions during the mid-Holocene,[19, 25, 26] but most reconstructions support warm and dry conditions.[16, 19] Differences between interpretations of climate during this period may be attributed to variability on smaller spatial scales as well as uncertainties inherent to paleoclimate reconstructions, and points to the complexity of reconstructing a coherent picture of regional-scale climate. Broadly speaking, cooling following the mid-Holocene climate optimum generally coincided with increasing effective moisture in the region until modern.[23]

These trends generally continued through the late-Holocene. The cooler temperatures and increased moisture led to the so-called Neoglacial, which refers to the advance of alpine glaciers worldwide[27, 28] and Neopluvial, which refers specifically to highstands of many Great Basin lakes as a result of increased moisture.[29, 30] Notable late-Holocene temperature fluctuations include the Medieval Warm Period, characterized by relatively warm conditions lasting from ~1100 to 800 ybp, and the Little Ice Age, characterized by relatively cool conditions lasting from ~600 to 300 ybp.[31, 32] These climate anomalies are apparent in many proxy records from the Northern Rocky Mountains and western US.[17, 18, 33, 34]

Water isotopes in mid-latitude snow and ice

Measurements and interpretation of stable water isotopes in snow and ice are fundamental to two chapters of this dissertation. The stable isotopes of the water molecule refer to minute differences in the weight of water molecules resulting from natural differences in the

masses of hydrogen and oxygen atoms. Atoms of the same element can have slightly different masses resulting from having different numbers of neutrons in their nucleus. On earth, the natural abundance of the stable isotopes of oxygen are ^{16}O (99.76%), ^{17}O (0.04%), and ^{18}O (0.20%), and for hydrogen are ^{1}H (99.985%) and ^{2}H (0.015%), and water molecules can have any combination of these isotopes resulting in water molecules with slightly different masses. As a result of having different masses, water molecules with different isotopic compositions, known as isotopologues behave differently in physical processes, namely heavier water isotopes prefer to be in phases with lower energy and stronger bonds.

The preference of heavier water isotopes to remain in more stable phases results in fractionation, or separation of water isotopes, during physical processes, namely evaporation and condensation.[35] During evaporation, heavier water isotopes will prefer to remain as a liquid, leading to preferential isotopic depletion of water vapor in non-equilibrium situations. As air masses laden with water vapor move inland from the oceans, the air mass cools and condenses, thereby creating precipitation. During condensation, the heavier isotopes again prefer the liquid phase and condense first, isotopically depleting the remaining water vapor. Thus, as storms move inland, precipitation becomes increasingly isotopically depleted.[36] Furthermore, the amount of fractionation during condensation is controlled by the ambient temperature and humidity. Therefore, the falling precipitation is not only affected by the isotopic signature of the initial water and the degree of rainout to the point of deposition, but also the temperature at which the precipitation condensed. The isotopic imprint left by temperature is of great interest to paleoclimate studies, as measurements of water isotopes in snow and ice are directly representative of the isotopic signature of the original precipitation and therefore can be used to estimate the temperature at which that precipitation fell.[2, 37]

Water isotopes are reported as the ratio of the measured ratio of the heavier to lighter isotope in an environmental sample to that of a reference standard, generally Vienna Standard

Mean Ocean Water (VSMOW) for water isotopic measurements. Results are reported in delta notation with units of per mil, or per thousand (‰). The two commonly reported values for the isotopes of water are $\delta^{18}O$ and $\delta^{2}H$ (also referred to as δD) and for studies within this dissertation, isotopic measurements were made with a Picarro instrument (L2130-i; Picarro, Inc.). The Picarro uses a technique known as laser adsorption spectroscopy, which is a type of cavity ring-down spectroscopy, that measures the decay of a laser pulsed through a chamber containing water vapor to determine the vapor's hydrogen and oxygen isotopic composition.[38, 39] Laser adsorption-based instruments are affordable, precise, and small and have been used extensively for isotopic measurements in snow and ice;[40, 41] one limitation is that they can be subject to interferences from organic compounds or other chemicals.[42]

Mercury in natural systems

Two chapters of this dissertation relate to reconstructing past atmospheric concentrations of mercury (Hg). As a persistent and toxic pollutant, quantifying past emissions and releases of Hg is important for understanding the Hg budget and cycle at present. Hg occurs in numerous forms in the environment and is stored in atmospheric (~5 Mg), terrestrial (~250-300 Gg), and oceanic (~270-450 Gg) reservoirs.[43, 44] Hg can take the form of elemental mercury (Hg^{0}) or divalent mercury (Hg^{II}) that exists in gaseous, particulate, and aqueous forms, as well as numerous other organic and inorganic compounds. While all forms of Hg are toxic, methylmercury, the most common organic form of Hg, is the most toxic and can bioaccumulate in food chains.[45] The transformation of elemental or divalent mercury to methylmercury can occur as a result of biotic processes facilitated by microbes or abiotic reactions. Mercury has a long residence time in the environment, thus, Hg can accumulate in ecosystems over time so understanding current Hg budgets and cycling requires accurate quantification of past deposition.[43, 44]

Atmospheric Hg deposition is a crucial pathway for Hg to enter both terrestrial and aquatic ecosystems.[43] While Hg can be emitted from natural sources, such as volcanic emissions or weathering, anthropogenic emissions from industrial and mining activities over the past few centuries have significantly altered Earth's mercury budget, with anthropogenic emissions resulting in a ~300% increase in Hg deposition worldwide.[43, 46] Reconstructions of atmospheric concentrations of Hg rely on lake sediment cores,[47, 48] tree rings,[49, 50] and ice cores.[6, 9, 51] Chapters 1 and 2 of this dissertation use both ice-core and tree-ring records of mercury to better quantify atmospheric Hg trends since 1750 CE. The dominant pathway for tree uptake of Hg is direct assimilation of gaseous elemental mercury through the stomata and into the tree's tissues.[52-54] While other pathways such as via the roots or diffusion through the bark have been noted,[55] they are thought to be insignificant. Hg in ice cores is deposited via wet and dry deposition representing both particulate and gaseous forms of Hg in the atmosphere.[56]

Mercury measurements in this dissertation were performed on tree-ring samples using a Direct Mercury Analyzer instrument (DMA-80; Milestone). This instrument measures total mercury by combusting the samples, thereby releasing Hg as a combustion byproduct. All combustion byproducts are passed through a furnace that catalyzes removal of interfering compounds, after which Hg vapor is selectively trapped by gold amalgamation. After all other byproducts are flushed though the system, Hg is released from the gold amalgamator and measured by atomic adsorption spectroscopy.

Black carbon in ice cores and lake sediments

Black carbon (BC) is another natural proxy used in Chapters 1 and 4 of this dissertation. BC, which consists of microscopic soot particles less than a micron in diameter, is emitted as a result of incomplete combustion of fossil fuels or biomass. Since BC is a small, dark particle, it is an important driver of Earth's energy budget because of its radiative forcing. BC decreases

Earth's albedo when deposited on bright surfaces such as snow[57, 58] or transported through the atmosphere.[59] This decreased albedo translates to increased radiation absorption which can drive warmer atmospheric temperatures and enhanced snowmelt.[57, 60, 61] BC is also important in natural archives such as ice cores and lake sediment cores as a proxy for past burning. Over recent centuries, measurements of BC in polar and alpine ice cores indicate pervasive pollution from coal combustion during the Industrial Revolution.[58] Over longer timescales, prior to industrial BC emissions, BC records from Arctic and Antarctic ice cores have been used to infer trends in natural wildfires related to continental hydroclimate.[62-64]

BC measurements presented in this dissertation were made using the Single Particle Soot Photometer (SP2; Droplet Measurement Technologies). The SP2 is a highly-sensitive instrument specifically designed for measuring individual particles of soot in environmental samples. BC is introduced to the SP2 as a dry aerosol, either directly from the atmosphere or after nebulization of an aqueous sample. The aerosol passes through a laser cavity, where a 1064 nm Nd:YAG laser heats BC particles to their boiling point. The radiation emitted from the BC particles as they pass through the laser is directly proportional to the particle's mass and is detected on two photomultiplier tubes. When first introduced, this method reduced the sample size for BC measurements in ice cores by three orders of magnitude,[58] and it has since been adapted for BC measurements in lake sediment cores.[65] The SP2 has also been used extensively for BC measurements in the atmosphere[66, 67] and snow.[60, 68]

Overview of chapters

This dissertation examines proxy records from tree rings, lake sediments, and ice cores on two different timescales. Chapters 1 and 2 focus on climate and anthropogenic pollution records from ice cores and tree rings in the Wind River Range that extend back ~250 to 300 ybp,

while Chapters 3 and 4 focus on climate records from lake sediments and ice on the Beartooth Plateau that extend back ~10,000 ybp. Locations of study sites are shown in Figure 1.

The goal of Chapter 1 was to develop well-dated, high-resolution pollution and climate records from the Upper Fremont Glacier (UFG) ice core collected by the USGS in 1998. The United States Geological Survey (USGS) recovered two ~160 m-long cores from UFG, the UFG91 and UFG98 cores, collected in 1991 and 1998, respectively. These unique ice cores are the only continental, alpine ice cores recovered from the contiguous U.S. known to document regional climate and pollution. These cores were initially dated using tritium concentrations in the upper 50 m to constrain the past 50 years and a radiocarbon-dated grasshopper leg to date the bottom of the core to between 190 and 130 ybp.[10] The dating was subsequently further refined in a later publication by attempted volcanic synchronization of electrical conductivity data to known volcanic eruptions.[69] These early depth-age models were used to support interpretations that the UFG water isotope profile documented the end of the Little Ice Age[10] and that mid-19th century Gold Rush-era mining contributed significant mercury pollution.[6] The temporal trend of mercury pollution, however, was not corroborated by trends observed in other nearby lake sediment records[5] or an ice core from Alaska,[9] calling into question the accuracy of the UFG mercury records.

To develop new chemical records and reassess the UFG chronology, the archived UFG98 ice core was analyzed on the continuous flow analysis ice core system at DRI and the new high-resolution measurements were used to develop a revised chronology for the ice core while still maintaining the unambiguous age control points from the original depth-age scale,[7] such as fallout from atmospheric nuclear weapons testing and radiocarbon dating. The dating between these sparse control points was refined by synchronizing the water isotope record to an absolutely-dated, nearby tree ring chronology, both hypothesized to be temperature-sensitive proxies. This approach did not incorporate volcanic synchronization, which is known to be

imprecise in alpine ice cores like UFG with high impurity concentrations. The new depth-age scale indicated that heavy metal pollution at UFG paralleled industrial pollution in southern Greenland ice cores, and that the mercury record from the UFG ice core was initially misinterpreted because of the original, inaccurate dating. Mercury increases previously associated with Gold Rush-era mining on the original chronology were shifted to coincide with 20th century industrial emissions on the new depth-age scale.

Chapter 2 builds upon the improved understanding of mercury deposition at UFG with the new depth-age scale by complementing the ice core record with mercury records from precisely-dated tree rings. The goal of this study was to develop a mercury record from trees co-located with the UFG to evaluate if tree rings can be used to develop a valid record of atmospheric mercury concentration. Tree rings are emerging as a potential archive for long-term reconstructions of atmospheric mercury concentrations,[49, 50] as they are ubiquitous on the landscape and mercury in tree rings has been shown to be largely controlled by ambient atmospheric concentrations.[52] However, few studies have thoroughly evaluated long-term tree ring mercury profiles with direct atmospheric measurements or temporal trends evident in other proxy records.[52, 70] This project leveraged the unique situation that the trees and ice core records are effectively co-located at this field site, allowing direct comparison of the mercury records from each archive. The tree mercury record parallels the ice core mercury profile, but appears to be impacted by radial translocation between tree rings leading to a smoothed and temporally-shifted signal.

Chapter 3 transitions to a field site in northern Wyoming on the Beartooth Plateau to evaluate semi-permanent ice patches as climate archives. Semi-permanent ice patches are unique features, never growing big enough to develop into a flowing glacier yet persisting on the landscape for thousands of years. Ice patches have been recognized as important archaeological archives,[71, 72] as they preserve fragile artefacts that otherwise would rapidly decompose. To

explore their potential as a climate archive, a ~6 m core was recovered from an ice patch in 2016. The chronology of the core, developed using numerous radiocarbon dates of organic material preserved within the core, showed that the ice patch record was ~10,000 years long and that ice accreted sporadically but consistently throughout the entire period. Water isotope measurements in the ice units showed large changes that parallel changes observed in regional lake sediment core and speleothem records.[20] The ice cores recovered from the ice patch represent some of the oldest ice recovered from the mid-latitudes and the water isotope and ice accumulation records are, to our knowledge, the first paleoclimate records developed from this natural archive.

Chapter 4 applies a new method for measuring BC,[65] a proxy for biomass and fossil fuel combustion, to two lake sediment cores, one extending back 2,000 years from North Lake, located near the Upper Fremont Glacier, and one extending back 10,000 years from Island Lake, located near the ice patch on the Beartooth Plateau. The two lakes represent contrasting depositional environments, with Island Lake having a comparatively larger, more complex, and vegetated watershed than North Lake. Thus, the Island Lake BC record, which had higher BC deposition than expected from solely atmospheric deposition, was interpreted to be more representative of local burning with influences from secondary deposition processes such as fluvial transport, whereas BC deposition at North Lake seemed to be predominantly atmospheric and therefore representative of a more regional signal.

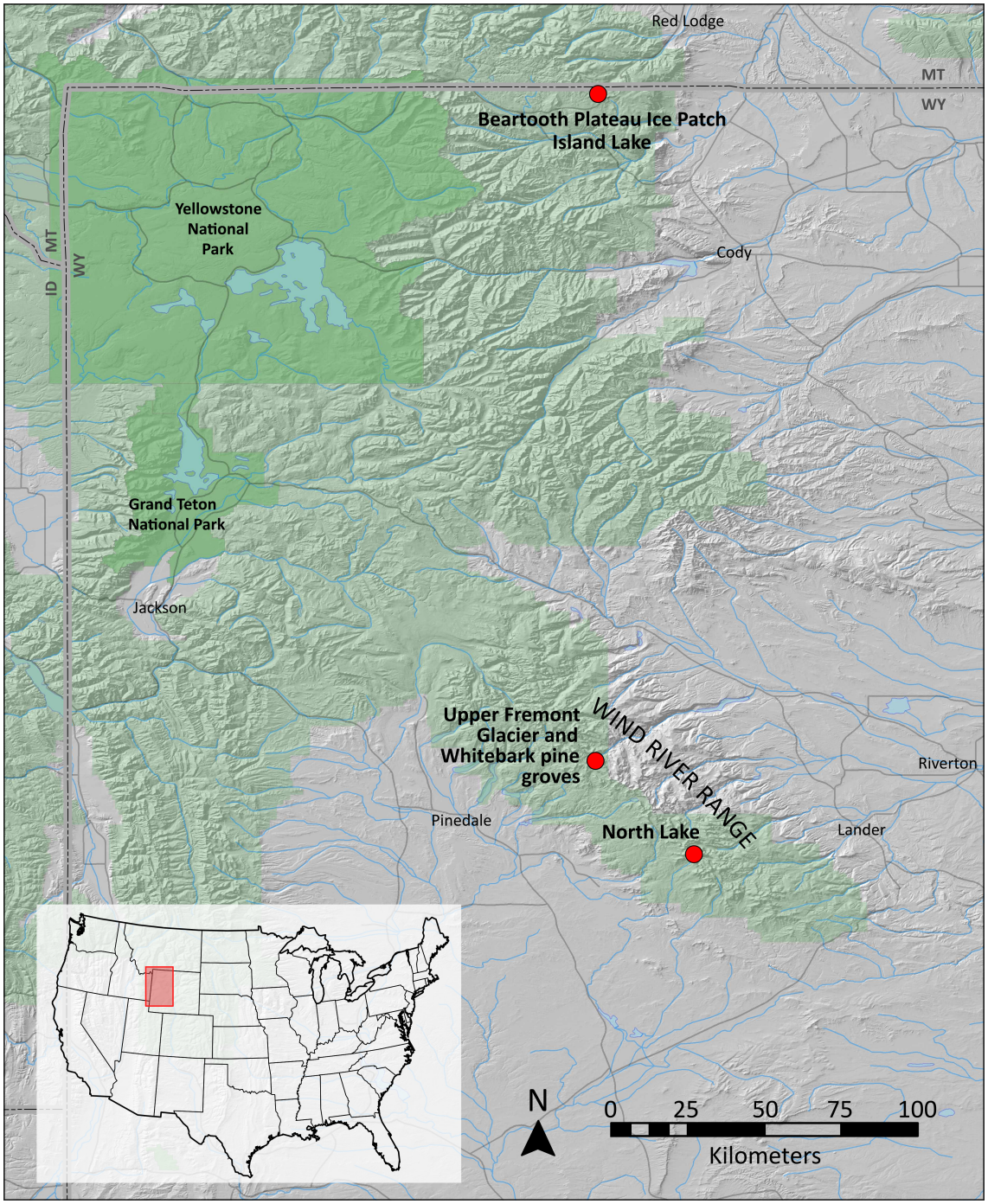

Figure 1. Location of dissertation study sites. Chapter 1 and 2: Upper Fremont Glacier and Whitebark pine groves. Chapter 3: Beartooth Plateau ice patch and Island Lake. Chapter 4: Island Lake and North Lake.

References

1. EPICA Community Members, Eight glacial cycles from an Antarctic ice core. *Nature* **2004,** *429*, (6992), 623-628.
2. Dansgaard, W.; Johnsen, S. J.; Clausen, H. B.; Dahl-Jensen, D.; Gundestrup, N. S.; Hammer, C. U.; Hvidberg, C. S.; Steffensen, J. P.; Sveinbjornsdottir, A. E.; Jouzel, J.; Bond, G., Evidence for general instability of past cliate from a 250-kyr ice core record. *Nature* **1993,** *364*, (6434), 218-220.
3. Melles, M. et al., 2.8 Million Years of Arctic Climate Change from Lake El'gygytgyn, NE Russia. *Science* **2012,** *337*, (6092), 315-320.
4. Brigham-Grette, J. et al., Pliocene Warmth, Polar Amplification, and Stepped Pleistocene Cooling Recorded in NE Arctic Russia. *Science* **2013,** *340*, (6139), 1421-1427.
5. Engstrom, D. R.; Fitzgerald, W. F.; Cooke, C. A.; Lamborg, C. H.; Drevnick, P. E.; Swain, E. B.; Balogh, S. J.; Balcom, P. H., Atmospheric Hg Emissions from Preindustrial Gold and Silver Extraction in the Americas: A Reevaluation from Lake-Sediment Archives. *Environ. Sci. Tech.* **2014,** *48*, (12), 6533-6543.
6. Schuster, P. F.; Krabbenhoft, D. P.; Naftz, D. L.; Cecil, L. D.; Olson, M. L.; Dewild, J. F.; Susong, D. D.; Green, J. R.; Abbott, M. L., Atmospheric mercury deposition during the last 270 years: A glacial ice core record of natural and anthropogenic sources. *Environ. Sci. Tech.* **2002,** *36*, (11), 2303-2310.
7. Chellman, N.; McConnell, J. R.; Arienzo, M.; Pederson, G. T.; Aarons, S. M.; Csank, A., Reassessment of the Upper Fremont Glacier Ice-Core Chronologies by Synchronizing of Ice-Core-Water Isotopes to a Nearby Tree-Ring Chronology. *Environ. Sci. Tech.* **2017,** *51*, (8), 4230-4238.
8. Pederson, G. T.; Gray, S. T.; Woodhouse, C. A.; Betancourt, J. L.; Fagre, D. B.; Littell, J. S.; Watson, E.; Luckman, B. H.; Graumlich, L. J., The Unusual Nature of Recent Snowpack Declines in the North American Cordillera. *Science* **2011,** *333*, (6040), 332-335.
9. Beal, S. A.; Osterberg, E. C.; Zdanowicz, C. M.; Fisher, D. A., Ice Core Perspective on Mercury Pollution during the Past 600 Years. *Environ. Sci. Tech.* **2015,** *49*, (13), 7641-7647.
10. Naftz, D. L.; Klusman, R. W.; Michel, R. L.; Schuster, P. F.; Reddy, M. M.; Taylor, H. E.; Yanosky, T. M.; McConnaughey, E. A., Little ice age evidence from a south-central North America ice core, USA. *Arctic Alpine Res.* **1996,** *28*, (1), 35-41.
11. Salzer, M. W.; Bunn, A. G.; Graham, N. E.; Hughes, M. K., Five millennia of paleotemperature from tree-rings in the Great Basin, USA. *Clim. Dynam.* **2014,** *42*, (5-6), 1517-1526.
12. Clark, P. U.; Dyke, A. S.; Shakun, J. D.; Carlson, A. E.; Clark, J.; Wohlfarth, B.; Mitrovica, J. X.; Hostetler, S. W.; McCabe, A. M., The Last Glacial Maximum. *Science* **2009,** *325*, (5941), 710-714.
13. Peltier, W. R., Ice-age paleotopography. *Science* **1994,** *265*, (5169), 195-201.
14. Gosse, J. C.; Klein, J.; Evenson, E. B.; Lawn, B.; Middleton, R., Be-10 dating of the duration and retreat of the last pinedale glacial sequence. *Science* **1995,** *268*, (5215), 1329-1333.
15. Licciardi, J. M.; Pierce, K. L., History and dynamics of the Greater Yellowstone Glacial System during the last two glaciations. *Quaternary Sci. Rev.* **2018,** *200*, 1-33.

16. Shuman, B. N.; Serravezza, M., Patterns of hydroclimatic change in the Rocky Mountains and surrounding regions since the last glacial maximum. *Quaternary Sci. Rev.* **2017,** *173*, 58-77.

17. Anderson, L.; Berkelhammer, M.; Barron, J. A.; Steinman, B. A.; Finney, B. P.; Abbott, M. B., Lake oxygen isotopes as recorders of North American Rocky Mountain hydroclimate: Holocene patterns and variability at multi-decadal to millennial time scales. *Global Planet. Change* **2016,** *137*, 131-148.

18. Whitlock, C.; Dean, W. E.; Fritz, S. C.; Stevens, L. R.; Stone, J. R.; Power, M. J.; Rosenbaum, J. R.; Pierce, K. L.; Bracht-Flyr, B. B., Holocene seasonal variability inferred from multiple proxy records from Crevice Lake, Yellowstone National Park, USA. *Palaeogeogr. Palaeocl.* **2012,** *331*, 90-103.

19. Mensing, S.; Korfmacher, J.; Minckley, T.; Musselman, R., A 15,000 year record of vegetation and climate change from a treeline lake in the Rocky Mountains, Wyoming, USA. *Holocene* **2012,** *22*, (7), 739-748.

20. Lundeen, Z.; Brunelle, A.; Burns, S. J.; Polyak, V.; Asmerom, Y., A speleothem record of Holocene paleoclimate from the northern Wasatch Mountains, southeast Idaho, USA. *Quatern. Int.* **2013,** *310*, 83-95.

21. Ersek, V.; Clark, P. U.; Mix, A. C.; Cheng, H.; Edwards, R. L., Holocene winter climate variability in mid-latitude western North America. *Nat. Comm.* **2012,** *3,* 1219.

22. Walker, M. J. C.; Berkelhammer, M.; Bjorck, S.; Cwynar, L. C.; Fisher, D. A.; Long, A. J.; Lowe, J. J.; Newnham, R. M.; Rasmussen, S. O.; Weiss, H., Formal subdivision of the Holocene Series/Epoch: a Discussion Paper by a Working Group of INTIMATE (Integration of ice-core, marine and terrestrial records) and the Subcommission on Quaternary Stratigraphy (International Commission on Stratigraphy). *J. Quaternary Sci.* **2012,** *27*, (7), 649-659.

23. Shuman, B. N.; Marsicek, J., The structure of Holocene climate change in mid-latitude North America. *Quaternary Sci. Rev.* **2016,** *141*, 38-51.

24. Marsicek, J.; Shuman, B. N.; Bartlein, P. J.; Shafer, S. L.; Brewer, S., Reconciling divergent trends and millennial variations in Holocene temperatures. *Nature* **2018,** *554*, (7690), 92-96.

25. Minckley, T. A.; Shriver, R. K.; Shuman, B., Resilience and regime change in a southern Rocky Mountain ecosystem during the past 17 000 years. *Ecol. Monogr.* **2012,** *82*, (1), 49-68.

26. Moir, W. H.; Rochelle, S. G.; Schoettle, A. W., Microscale patterns of tree establishment near upper treeline, Snowy Range, Wyoming, USA. *Arct Antarct Alp. Res.* **1999,** *31*, (4), 379-388.

27. Denton, G. H.; Porter, S. C., Neoglaciation. *Scientific American* **1970,** *222*, (6), 100-111.

28. Luckman, B. H.; Holdsworth, G.; Osborn, G. D., Neoglacial glacier fluctuations in the canadian rockies. *Quaternary Res.* **1993,** *39*, (2), 144-153.

29. Currey, D. R., Quaternary palaeolakes in the evolution of semidesert basins, with special emphasis on Lake Bonneville and the Great-Basin, USA. *Palaeogeogr. Palaeocl.* **1990,** *76*, (3-4), 189-214.

30. Yuan, F. S.; Koran, M. R.; Valdez, A., Late Glacial and Holocene record of climatic change in the southern Rocky Mountains from sediments in San Luis Lake, Colorado, USA. *Palaeogeogr. Palaeocl.* **2013,** *392*, 146-160.

31. Mann, M. E.; Zhang, Z.; Rutherford, S.; Bradley, R. S.; Hughes, M. K.; Shindell, D.; Ammann, C.; Faluvegi, G.; Ni, F., Global Signatures and Dynamical Origins of the Little Ice Age and Medieval Climate Anomaly. *Science* **2009,** *326*, (5957), 1256-1260.

32. Ljungqvist, F. C.; Krusic, P. J.; Brattstrom, G.; Sundqvist, H. S., Northern Hemisphere temperature patterns in the last 12 centuries. *Clim. Past* **2012,** *8*, (1), 227-249.

33. Calder, W. J.; Parker, D.; Stopka, C. J.; Jimenez-Moreno, G.; Shuman, B. N., Medieval warming initiated exceptionally large wildfire outbreaks in the Rocky Mountains. *P. Natl. Acad. Sci. USA* **2015,** *112*, (43), 13261-13266.

34. Meko, D. M.; Woodhouse, C. A.; Baisan, C. A.; Knight, T.; Lukas, J. J.; Hughes, M. K.; Salzer, M. W., Medieval drought in the upper Colorado River Basin. *Geophys. Res. Lett.* **2007,** *34*, (10), L10705.

35. IAEA, *Environmental Isotopes in the Hydrological Cycle: Principles and Applications*, vol. 2. **2001**.

36. Terzer, S.; Wassenaar, L. I.; Araguas-Araguas, L. J.; Aggarwal, P. K., Global isoscapes for delta O-18 and delta H-2 in precipitation: improved prediction using regionalized climatic regression models. *Hydrol. Earth Syst. Sc.* **2013,** *17*, (11), 4713-4728.

37. Jouzel, J.; Lorius, C.; Petit, J. R.; Genthon, C.; Barkov, N. I.; Kotlyakov, V. M.; Petrov, V. M., Vostok ice core - a continuous isotope temperature record over the last climatic cycle (160,000 years). *Nature* **1987,** *329*, (6138), 403-408.

38. Iannone, R. Q.; Kassi, S.; Jost, H. J.; Chenevier, M.; Romanini, D.; Meijer, H. A. J.; Dhaniyala, S.; Snels, M.; Kerstel, E. R. T., Development and airborne operation of a compact water isotope ratio infrared spectrometer. *Isot. Environ. Heal. S.* **2009,** *45*, (4), 303-320.

39. Kerstel, E. R. T.; van Trigt, R.; Dam, N.; Reuss, J.; Meijer, H. A. J., Simultaneous determination of the H-2/H-1, O-17/O-16, and O-18/O-16 isotope abundance ratios in water by means of laser spectrometry. *Anal. Chem.* **1999,** *71*, (23), 5297-5303.

40. Maselli, O. J.; Fritzsche, D.; Layman, L.; McConnell, J. R.; Meyer, H., Comparison of water isotope-ratio determinations using two cavity ring-down instruments and classical mass spectrometry in continuous ice-core analysis. *Isot. Environ. Heal. S.* **2013,** *49*, (3), 387-398.

41. Gkinis, V.; Popp, T. J.; Blunier, T.; Bigler, M.; Schupbach, S.; Kettner, E.; Johnsen, S. J., Water isotopic ratios from a continuously melted ice core sample. *Atmos. Meas. Tech.* **2011,** *4*, (11), 2531-2542.

42. Wassenaar, L. I.; Terzer-Wassmuth, S.; Douence, C.; Araguas-Araguas, L.; Aggarwal, P. K.; Coplen, T. B., Seeking excellence: An evaluation of 235 international laboratories conducting water isotope analyses by isotope-ratio and laser-absorption spectrometry. *Rapid Commun. Mass Sp.* **2018,** *32*, (5), 393-406.

43. Outridge, P. M.; Mason, R. P.; Wang, F.; Guerrero, S.; Heimburger-Boavida, L. E., Updated Global and Oceanic Mercury Budgets for the United Nations Global Mercury Assessment 2018. *Environ. Sci. Tech.* **2018,** *52*, (20), 11466-11477.

44. Obrist, D.; Kirk, J. L.; Zhang, L.; Sunderland, E. M.; Jiskra, M.; Selin, N. E., A review of global environmental mercury processes in response to human and natural perturbations: Changes of emissions, climate, and land use. *Ambio* **2018,** *47*, (2), 116-140.

45. Morel, F. M. M.; Kraepiel, A. M. L.; Amyot, M., The chemical cycle and bioaccumulation of mercury. *Annu. Rev. Ecol. and Syst.* **1998,** *29*, 543-566.

46. Streets, D. G.; Horowitz, H. M.; Jacob, D.; Lu, Z. F.; Levin, L.; ter Schure, A. F. H.; Sunderland, E. M., Total Mercury Released to the Environment by Human Activities. *Environ. Sci. Tech.* **2017,** *51*, (11), 5969-5977.

47. Heyvaert, A. C.; Reuter, J. E.; Slotton, D. G.; Goldman, C. R., Paleolimnological reconstruction of historical atmospheric lead and mercury deposition at Lake Tahoe, California-Nevada. *Environ. Sci. Tech.* **2000,** *34*, (17), 3588-3597.

48. Drevnick, P. E. et al., Spatiotemporal patterns of mercury accumulation in lake sediments of western North America. *Sci. Total Environ.* **2016,** *568*, 1157-1170.

49. Wright, G.; Woodward, C.; Peri, L.; Weisberg, P. J.; Gustin, M. S., Application of tree rings dendrochemistry for detecting historical trends in air Hg concentrations across multiple scales. *Biogeochemistry* **2014,** *120*, (1-3), 149-162.

50. Clackett, S. P.; Porter, T. J.; Lehnherr, I., 400-Year Record of Atmospheric Mercury from Tree-Rings in Northwestern Canada. *Environ. Sci. Tech.* **2018,** *52*, (17), 9625-9633.

51. Eyrikh, S.; Eichler, A.; Tobler, L.; Malygina, N.; Papina, T.; Schwikowski, M., A 320 Year Ice-Core Record of Atmospheric Hg Pollution in the Altai, Central Asia. *Environ. Sci. Tech.* **2017,** *51*, (20), 11597-11606.

52. Arnold, J.; Gustin, M. S.; Weisberg, P. J., Evidence for Nonstomatal Uptake of Hg by Aspen and Translocation of Hg from Foliage to Tree Rings in Austrian Pine. *Environ. Sci. Tech.* **2018,** *52*, (3), 1174-1182.

53. Fleck, J. A.; Grigal, D. F.; Nater, E. A., Mercury uptake by trees: An observational experiment. *Water Air Soil Poll.* **1999,** *115*, (1-4), 513-523.

54. Siwik, E. I. H.; Campbell, L. M.; Mierle, G., Distribution and trends of mercury in deciduous tree cores. *Environ. Pollut.* **2010,** *158*, (6), 2067-2073.

55. Abreu, S. N.; Soares, A.; Nogueira, A. J. A.; Morgado, F., Tree rings, Populus nigra L., as mercury data logger in aquatic environments: Case study of an historically contaminated environment. *B. Environ. Contam. Tox.* **2008,** *80*, (3), 294-299.

56. Durnford, D.; Dastoor, A., The behavior of mercury in the cryosphere: A review of what we know from observations. *J. Geophys. Res.-Atmos.* **2011,** *116*, D06305.

57. Bond, T. C. et al., Bounding the role of black carbon in the climate system: A scientific assessment. *J. Geophys. Res.-Atmos.* **2013,** *118*, (11), 5380-5552.

58. McConnell, J. R.; Edwards, R.; Kok, G. L.; Flanner, M. G.; Zender, C. S.; Saltzman, E. S.; Banta, J. R.; Pasteris, D. R.; Carter, M. M.; Kahl, J. D. W., 20th-century industrial black carbon emissions altered arctic climate forcing. *Science* **2007,** *317*, (5843), 1381-1384.

59. Jacobson, M. Z., Effects of externally-through-internally-mixed soot inclusions within clouds and precipitation on global climate. *J. Phys. Chem. A* **2006,** *110*, (21), 6860-6873.

60. Gleason, K. E.; McConnell, J. R.; Arienzo, M. M.; Chellman, N.; Calvin, W. M., Four-fold increase in solar forcing on snow in western U.S. burned forests since 1999. *Nat. Comm.* **2019,** *10*, 2026.

61. Painter, T. H.; Flanner, M. G.; Kaser, G.; Marzeion, B.; VanCuren, R. A.; Abdalati, W., End of the Little Ice Age in the Alps forced by industrial black carbon. *P. Natl. Acad. Sci. USA* **2013,** *110*, (38), 15216-15221.

62. Zennaro, P.; Kehrwald, N.; McConnell, J. R.; Schuepbach, S.; Maselli, O. J.; Marlon, J.; Vallelonga, P.; Leuenberger, D.; Zangrando, R.; Spolaor, A.; Borrotti, M.; Barbaro, E.; Gambaro, A.; Barbante, C., Fire in ice: two millennia of boreal forest fire history from the Greenland NEEM ice core. *Clim. Past* **2014,** *10*, (5), 1905-1924.

63. Arienzo, M. M.; McConnell, J. R.; Murphy, L. N.; Chellman, N.; Das, S.; Kipfstuhl, S.; Mulvaney, R., Holocene black carbon in Antarctica paralleled Southern Hemisphere climate. *J. Geophys. Res.-Atmos.* **2017,** *122*, (13), 6713-6728.

64. Bisiaux, M. M.; Edwards, R.; McConnell, J. R.; Albert, M. R.; Anschutz, H.; Neumann, T. A.; Isaksson, E.; Penner, J. E., Variability of black carbon deposition to the East Antarctic Plateau, 1800-2000 AD. *Atmos. Chem. Phys.* **2012,** *12*, (8), 3799-3808.

65. Chellman, N. J.; McConnell, J. R.; Heyvaert, A.; Vanniere, B.; Arienzo, M. M.; Wennrich, V., Incandescence-based single-particle method for black carbon quantification in lake sediment cores. *Limnol. Oceanogr.-Meth.* **2018,** *16*, (11), 711-721.

66. Schwarz, J. P. et al., Single-particle measurements of midlatitude black carbon and light-scattering aerosols from the boundary layer to the lower stratosphere. *J. Geophys. Res.-Atmos.* **2006,** *111*, D16207.

67. Moteki, N.; Kondo, Y.; Miyazaki, Y.; Takegawa, N.; Komazaki, Y.; Kurata, G.; Shirai, T.; Blake, D. R.; Miyakawa, T.; Koike, M., Evolution of mixing state of black carbon particles: Aircraft measurements over the western Pacific in March 2004. *Geophys. Res. Lett.* **2007,** *34*, L11803.

68. Schwarz, J. P.; Gao, R. S.; Perring, A. E.; Spackman, J. R.; Fahey, D. W., Black carbon aerosol size in snow. *Sci. Rep.-UK* **2013,** *3*, 1356.

69. Schuster, P. F.; White, D. E.; Naftz, D. L.; Cecil, L. D., Chronological refinement of an ice core record at Upper Fremont Glacier in south central North America. *J. Geophys. Res.-Atmos.* **2000,** *105*, (D4), 4657-4666.

70. Navratíl, T.; Nováková, T.; Shanley, J. B.; Rohovec, J.; Matoušková, S.; Vaňková, M.; Norton, S. A., Larch Tree Rings as a Tool for Reconstructing 20th Century Central European Atmospheric Mercury Trends. *Environ. Sci. Tech.* **2018,** *52*, (19), 11060-11068.

71. Lee, C. M., Withering Snow and Ice in the Mid-latitudes: A New Archaeological and Paleobiological Record for the Rocky Mountain Region. *Arctic* **2012,** *65*, 165-177.

72. Hare, P. G.; Thomas, C. D.; Topper, T. N.; Gotthardt, R. M., The Archaeology of Yukon Ice Patches: New Artifacts, Observations, and Insights. *Arctic* **2012,** *65*, 118-135.

Chapter 1

Reassessment of the Upper Fremont Glacier ice core chronologies by synchronizing ice core water isotopes to a nearby tree-ring chronology

Nathan Chellman[1,2], Joseph R. McConnell[1], Monica Arienzo[1], Gregory Pederson[3], Sarah Aarons[4], Adam Csank[5]

[1]Desert Research Institute, Division of Hydrologic Sciences, Reno, NV
[2]Graduate Program of Hydrologic Sciences, University of Nevada, Reno, NV
[3]U.S. Geological Survey, Northern Rocky Mountain Science Center, Bozeman, MT
[4]Department of Earth System Science, University of California, Irvine, CA
[5]Department of Geography, University of Nevada, Reno, NV

Reproduced with permission from:
Chellman, N.; McConnell, J. R.; Arienzo, M.; Pederson, G. T.; Aarons, S. M.; Csank, A., Reassessment of the Upper Fremont Glacier Ice-Core Chronologies by Synchronizing of Ice-Core-Water Isotopes to a Nearby Tree-Ring Chronology. *Environ. Sci. Technol.* **2017**, 51 (8), 4230-4238. doi: 10.1021/acs.est.6b06574.

Abstract

The Upper Fremont Glacier (UFG), Wyoming, is one of the few continental glaciers in the contiguous United States known to preserve environmental and climate records spanning recent centuries. Two ice cores taken from UFG have been studied extensively to document changes in climate and industrial pollution—most notably mid-19th century increases in mercury pollution. Fundamental to these studies is the chronology used to map ice core depth to age. Here we present a revised chronology for the UFG ice cores based on new measurements and using a novel dating approach of synchronizing continuous water isotope measurements to a nearby tree-ring chronology. While consistent with the few unambiguous age controls underpinning the previous UFG chronologies, the new interpretation suggests a very different timescale for the UFG cores with changes of up to 80 years. Mercury increases previously associated with the mid-19th century Gold Rush now coincide with early-20th century industrial emissions, aligning the UFG record with other North American mercury records from ice and lake sediment cores. Additionally, new UFG records of industrial pollutants parallel changes documented in ice cores from southern Greenland, further validating the new UFG chronologies while documenting the extent of late 19th and early 20th century pollution in remote North America.

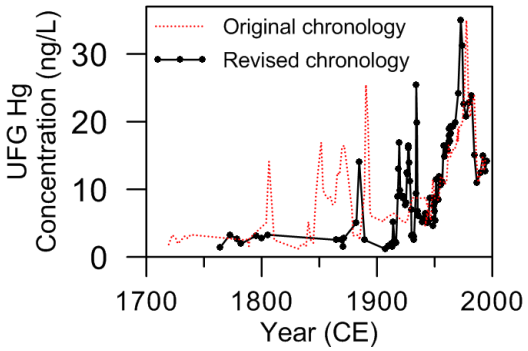

Abstract Art

1. Introduction

The Upper Fremont Glacier (UFG), located in the Wind Rivers Range of Wyoming, is one of the few interior continental glaciers in North America and perhaps the only one in the contiguous United States from which century-scale ice core records can be obtained. Two ice cores, both approximately 165 m in length and located 220 m apart, were collected from UFG in two drilling seasons in 1991 and 1998, and are hereafter referred to as UFG91 and UFG98, respectively. Despite the high surface melt observed at UFG, previous studies show that valid records of climate and anthropogenic pollution can be obtained from the UFG ice cores.[1-5] For example, the concentrations and stable isotope ratios of nitrate and sulfate over the past 50 years at UFG are consistent with United States industrial emissions trends,[4] and the UFG91 water isotope ratio record reflects the end Little Ice Age, suggesting that the UFG record is representative of large-scale climate.[2]

Perhaps the most important record produced from the UFG cores to date is the record of mercury (Hg) deposition, which has become a benchmark study for understanding North American pollution. Schuster et al.[5] posited that an initial 5-fold increase Hg deposition at UFG first coincided with the American Gold Rush during the 1850s before dropping to near pre-industrial levels until the early 1900s when industrial activity resulted in a 20-fold increase of Hg between 1930 and 1990 CE. However, other archives of Hg from lake sediment cores[6-10] and a western Canadian ice core[11] reflect proportionally lower increases during the Gold Rush-era and largely do not capture the distinct mid-19th century Hg peak found by Schuster et al.[5] Thus, some interpretations of these other archives[7,11] suggest that reconstructed North American Hg emissions[12,13] overestimate Hg releases from mining activities between 1850 and 1900 CE.

The interpretation of the UFG ice cores hinges on accurate chronologies used to map from ice core depth to age. The UFG91 chronology in previous work was based on fallout from mid-20th century nuclear bomb testing evident in tritium and chlorine-36, as well as an insect leg

found near the bottom of the core that was carbon-14-dated to 1729±95 CE, with a smooth, nearly linear interpolation of the depth-age relationship between these few age control points.[2] This initial age scale subsequently was refined using measurements of sulfate and electrical conductivity (ECM) to synchronize the ice core record to known volcanic eruptions.[2,14] A slightly modified depth-age scale was determined for the UFG98 core to account for additional snowfall accumulation between 1991 and 1998 CE, though this modified profile has been published only for the upper 50 m of the UFG98 core.[3,4] However, the prevalence of surface melt and percolation on Fremont glacier, as well as the relatively high level of locally sourced impurities, hinder the identification of specific eruptions based on sulfate and ECM, particularly without confirmation using geochemically fingerprinted volcanic tephra.[15]

Because of the importance of accurate ice chronologies for the interpretation of the climate and environmental records contained in the UFG ice cores, we revisit and improve upon the original dating of these ice cores. The new chronologies for the UFG ice cores are constrained by five primary age control points, then tuned by synchronization of the UFG water isotope ratio records to a nearby, calendar-year dated tree-ring chronology. Using new, state-of-the-art chemical measurements of archived UFG ice core samples and comparisons to lake sediment and ice core records from North America and Greenland, we then evaluate the new chronologies as well as the timing and extent of North American industrial pollution.

2. Methods

2.1 Laboratory analysis

The UFG98 ice core was collected in 1998 CE at UFG (43.1°N, 109.6°W), approximately 220 m from the original UFG91 core along the same ~4100 m elevation contour (Figure 1). The 86 mm diameter core was drilled using a 100 mm diameter thermal drill. The remaining archive of the UFG98 ice core, stored at the National Ice Core Laboratory (NICL) in

Golden, CO, included continuous samples from 9.5 to 161 m depth and an additional 20 cm section from 6.2 to 6.4 m depth. Longitudinal samples approximately 3 cm by 3 cm in cross-section and 1 m in length were collected from the remaining archive at NICL in 2014. The majority of the archive was from the outer edge of the ice core. The samples were transported frozen to the Desert Research Institute (DRI), Reno, NV where they were analyzed in February 2015 on a continuous flow analysis (CFA) system for more than 20 chemical species including water isotopes, black carbon (BC), a range of heavy metals, and other aerosols.[16-18] $\delta^{18}O$ was measured using a Picarro 2130i (Picarro Inc., Santa Clara, USA) calibrated to Vienna Standard Mean Ocean Water (VSMOW) using methods described by Maselli et al.[18] BC was measured using an Apex-Q nebulizer (Elemental Scientific Inc., Omaha, USA) coupled to a Single Particle Soot Photometer (SP2; Droplet Measurement Technologies, Boulder, USA) adapted from the method described by McConnell et al.[16] Trace elements were measured using two Thermo-Finnigan Element2 Inductively Coupled Plasma Mass Spectrometers (ICP-MS) (Thermo Scientific, Bremen, Germany) based on methods described by McConnell et al.[17,19] The ICP-MS sample line was acidified inline to 1% nitric acid just after the melter head for the four-minute transport time to the instrument, and further acidified to 2% nitric acid immediately prior to injection to the instrument. Plutonium (^{239}Pu) also was measured continuously by ICP-MS using methods described by Arienzo et al.[20] between 9.5 m and 44 m to capture fallout from nuclear weapons testing in the 1950s and 1960s.[20] Continuous measurements were averaged to a depth resolution of 1.5 cm for interpretation.

Analyses of four Greenland ice cores (ACT11d, ACT2, D4, and D5) were conducted on the CFA system as described above with the goal of comparing pollutants between UFG and Greenland. The four cores (Figure 1) were dated with annual layer counting constrained by volcanic synchronization.[21] Estimated dating uncertainty in each of the Greenland cores is less than 1 year. The ACT11d (66.5°N, 46.3°W; elevation 2296 m) and ACT2 (66.0°N, 45.2°W;

elevation 2410 m)[17] ice cores were collected in 2011 and 2004, respectively. The D4 (71.4°N, 43.9°W; elevation 2766 m) [16] and D5 (68.5°N, 42.9°W; elevation 2519 m) ice cores were collected in 2003. Annual-averaged concentrations from these cores were then log-averaged to create a composite record representative of southern Greenland.

2.2 Whitebark pine ring-width chronology

Samples used to develop a Fremont whitebark pine (*Pinus albicaulis*) ring-width chronology were collected in the summer of 2001 CE at a site near the Fremont Glacier, approximately 4.8 km from the ice core sites (Figure 1; 43.15°N, 109.55°W; elevation 3180 m). The trees were growing in a granite talus field on a 30° slope with an aspect spanning 180-200°. The annually-resolved, ring-width chronology was constructed from a mix of living and fossil wood containing 32 individual ring-width series from 22 individual trees with individual growth rings each accurately dated (i.e. cross dated) to the calendar year in which the growth occurred. The ring-width chronology spans 1227 to 2001 CE, with the record attaining a maximum sample depth of 30 series in 1802 CE, with 25 series at 1750 CE— the approximate basal date on the UFG98 ice core. All samples were first visually cross dated[22] then statistically checked for dating errors in dplR[23] in the analytical program R, [24] ensuring accurate calendar year dating of each growth ring across all series.

To retain as much low-frequency climate information as possible in the final growth chronology, the individual ring-width records were detrended to remove the non-climatic, biological growth curve in the program "RCSsigFree45_v2b.app"[25] using an age-dependent spline required to retain a zero or negative slope with initial spine stiffness set to 50-years.[26] This individual-series detrending method is designed to preserve low-frequency climate signals and positive monotonic growth trends, if present, in a similar fashion to using a negative exponential curve, but with some advantages during the juvenile growth years. Regional Curve

Standardization was not used on this chronology since the record did not meet the assumptions and sample depth requirements for this method.[27,28] The final composite ring-width chronology was constructed by calculating a bi-weight robust mean from the power-transformed residuals of the individually detrended ring-width series. These methods reduced potential trend distortion from end effects that can result from the ratio method of chronology calculation on non-transformed ring-width series. To correct for artificial increases in variance due to decreasing number of ring-width series through time, variance stabilization was performed using the Rbar method with correction of trend in variance provided by an age-dependent spline. The final composite ring-width chronology exhibits significant ($p \leq 0.001$) and positive correlation ($r = 0.423$) with summer (JJA) temperature when compared against the 0.5° gridded temperature dataset CRU TS3.2[29] over the 1900-2001 CE interval.

2.3 UFG98 and UFG91 revised chronologies

To enable consistent interpretation of both the UFG91 and UFG98 glaciochemical measurements, the new high-resolution $\delta^{18}O$ record from the UFG98 core was synchronized visually at 24 depths to the previously published $\delta^{18}O$ record[2,30] from the UFG91 core (Figure 2a). An additional four depth tie points were obtained by synchronizing the tritium measurements[31,32] in the shallow sections of both cores (Figure 2c).

To develop a revised UFG chronology, five primary age control points first were used to create a low frequency estimate of the depth-age scale, which subsequently was refined by visually synchronizing the ice core $\delta^{18}O$ record to the composite tree-ring width chronology from the nearby grove of whitebark pines. Of the five primary tie points, four were unambiguous and also served as age constraints in the original chronology. These four points included 1998 CE at the glacier's surface when the UFG98 core was collected, ^{239}Pu and tritium peaks at 24.2 m (1963 CE) and 36.6 m (1954 CE) coinciding with the beginning and end of nuclear weapons testing,[20]

and a radiocarbon dated insect leg encased in the ice.[14] The radiocarbon-dated grasshopper leg found in the UFG91 ice core at a depth of 152 m (corresponding to a UFG98 depth of 150.5 m) was dated by Schuster et al. [14] to 1729±95 CE. The fifth primary point was largest observed BC peak (113.3 m) tied to the nearby Great Fire of 1910 CE, which burned over 3 million acres in Montana, Idaho, and Washington and is evident in charcoal records from lakes in Montana and Oregon.[33,34] This point is the only new primary age control compared to the original dating and the BC spike assigned to the fire reaches 26 ppb, a factor of 2-5 higher than the industrial background and a factor of 5-10 higher than the pre-industrial background.

The depth-age scale defined by these primary control points was refined using a total of 21 tie points visually identified between the ice core $\delta^{18}O$ record and the absolutely-dated tree-ring width chronology (Figure 3). Both ice core water isotope ratios and tree-ring widths are thought to be local temperature proxies.[2,3,35,36] Ties between the $\delta^{18}O$ and tree rings used here generally are limited to extreme high or low points evident in both records, assuming for example that an extremely cold year is represented both by depleted $\delta^{18}O$ in the ice and by lower tree growth.

3. Results and Discussion

3.1 UFG91 to UFG98 depth synchronization

Linking the two cores in depth is critical for mapping previous measurements from the UFG91 ice core on to the new UFG98 depth-age scale (Figure 2). The synchronized $\delta^{18}O$ records agree well, including the increase in variability at depths greater than 100 m and enriched $\delta^{18}O$ between 140 and 160 m. The tritium records provide four tie points in the shallower sections of the cores where the water isotope records are not as similar and thus more difficult to link. The depth offset between the two cores follows a 1:1 line (Figure 2b), indicating there are no major ice flow differences between the two sites. Lack of ice and data shallower than 6 m for the

UFG98 core prevents precise synchronization of the UFG91 surface to the UFG98 core. On average, the UFG91 core is offset 1.2 m deeper relative to the UFG98 core indicating a lower net snow accumulation rate at the UFG98 site.

3.2 UFG98 chronology

The new depth-age scale for the UFG98 ice core is very different than the original chronology, yet still consistent with the age control points from nuclear fallout and radiocarbon dating used to develop the original UFG91 chronology. Here we discuss annual layer thickness rather than annual net snow accumulation because no correction for density or ice flow thinning has been made. Such corrections would require modeling based on a thorough understanding of ice stratigraphy, ice flow, accumulation variability, and the bedrock and glacier geometry. This data is poorly constrained or non-existent at UFG. The new chronology indicates relatively small annual layer thicknesses (i.e., lower net snow accumulation) from the surface to 35 m, a period of larger annual layer thicknesses from 35 to 85 m (corresponding to 1955 to 1930 CE), and smaller annual layers below 85 m (Figure 4). The new age at 160 m depth near the bottom of the UFG98 core is 1747 CE compared to 1712 CE in the original dating.[14] The final correlation (Pearson's r) between $\delta^{18}O$ on the new depth-age scale and the tree-ring width index is $r=0.39$ ($p<0.001$), compared to $r=0.08$ ($p=0.11$) when correlating $\delta^{18}O$ using the original dating to the tree-ring width record.

Compared to the original chronology, the revised depth-age scale is older at depths above 41 m by an average of 7.5 years and younger at depths below 41 meters by an average of 53 years. The maximum difference between the original and new dating is between depths 126 and 130 m, where the original dating is on average 80 years older than the new chronology. Despite these large differences, the new chronology maintains consistency with the original unambiguous age constraints of nuclear weapons testing in the 1950s and 1960s and the carbon-14-dated

grasshopper leg that was dated to 1729±95 CE. The new chronology dates the depth of the grasshopper leg to 1803 CE, well within the uncertainty of the radiocarbon date.

This chronology incorporates effects from densification, spatial and temporal snow accumulation rate changes, and ice flow thinning. It is unclear whether this decadal to century scale variability in annual layer thickness is driven by long-term changes in regional climate, such as changes in overall net snow accumulation, as opposed to changes in upstream accumulation that affect ice flow to the coring site. Previous work from other alpine glaciers has shown that large spatial changes in net accumulation from processes such as drifting and shading are likely near the headwall of a glacier such as UFG.[37,38] There also is evidence supporting significant changes in snow accumulation at UFG during the 20th century. Tree ring-based snow-water equivalent (SWE) reconstructions and observed SWE from the Bighorn Basin, which contains UFG, indicate a greater than 50% increase of April 1 SWE between 1950 to 1970 CE compared to the preceding time period from 1900 to 1940 CE (Figure 5).[39] These decades of increased SWE also are apparent in larger-scale SWE reconstructions for the Greater Yellowstone Region and Northern Rockies.[39,40] Further support for increased accumulation at UFG is the slowing of retreat, and in some cases even advance, of glaciers in Glacier National Park, MT from the 1940s to 1970s as a result of climatic conditions favoring positive glacier mass balance.[41,42]

Our method for synchronizing the ice core and tree-ring records assumes that in an extreme cold year, represented by depleted $\delta^{18}O$ in the ice, there also is slower tree growth, and vice versa. By limiting tie points to extremes, we minimize uncertainties inherent to each proxy, such as potential effects from changes in snow accumulation and atmospheric circulation, as well as diffusion of water isotopes in snow and ice. Naftz et al.[3] showed that during an average winter, there is a strong relationship between temperature and $\delta^{18}O$ at UFG, and although this relationship was not as robust for a high precipitation El Niño winter, the $\delta^{18}O$ deposited that winter was not anomalous. The ability to date the core using two local temperature proxies, $\delta^{18}O$

of ice and the high-elevation tree-ring chronology, implies that these two parameters record a similar climate signal via two different, but not necessarily unrelated, mechanisms. The water isotope ratios at UFG are representative of local temperature as recorded by snow deposited in winter storms,[2,3] while variations in the tree-ring chronology largely are controlled by growing season temperature and to a lesser extent, winter and spring precipitation.[35,36]

Schuster et al.[14] refined the original depth-age scale by volcanic synchronization of ECM and sulfate measurements to known volcanic eruptions within the absolute constraints of the bomb pulses and carbon-14-dated grasshopper leg. However, the ECM record used for volcanic synchronization was noisy, allowing for ambiguity in what ECM spikes could be concretely defined as volcanic without influence from other parameters such as melt layers, organic acids from forest fires, industrial pollution, or continental dust, which has increased at UFG during the past two centuries due to industrial and agricultural activities in the American West.[1] Additionally, due to the high sulfur loading from terrestrial and industrial sources, it is difficult in non-polar ice cores to attribute sulfur peaks to specific volcanic eruptions without other evidence such as chemically fingerprinted volcanic tephra.[15] Compared to the sulfur data from the Mt. Logan and Eclipse ice cores in the Canadian Yukon or polar ice cores, where volcanic fallout has been well-studied and attributed to specific eruptions using tephra,[21,43,44] it is clear that the poor fidelity of the UFG records does not permit unambiguous volcanic synchronization using sulfur and ECM alone.

High concentrations of bismuth (Bi) previously have been linked to fallout in ice cores from the 1912 CE Katmai eruption in Alaska.[43] The largest spike in Bi in the UFG98 record occurs between 1908 and 1912 CE on the new chronology (Figure 6c). However, this peak occurs at the height of industrial Bi pollution and we have no tephra geochemistry to support a conclusive link to Katmai.

3.3 UFG pollution records

The UFG ice core records have been of particular interest because they preserve an interior continental record of pollution. On the new chronology, trends observed in the pollutants Bi, thallium (Tl), and BC in the new high-resolution UFG98 measurements are surprisingly similar to those observed in an array of southern Greenland ice cores during the past 200 years (Figure 6b,c,d). Despite significant differences between UFG and Greenland – UFG is a high-melt, mid-latitude alpine glacier influenced by completely different air masses than the low-melt, high-latitude southern Greenland ice sheet – the similarities between the pollution records from these sites indicates that heavy metal and other Industrial pollution from late 19th and early 20th century coal combustion was pervasive on a regional-to-hemispheric scale. The strong covariance of these pollutants between UFG and Greenland, especially the synchronous increases observed in the late 1800s, is additional evidence supporting the new UFG98 chronology. Both the UFG98 ice core and the southern Greenland array record sharp increases in Tl, Bi, and BC beginning in 1870 CE and peaking in 1900 CE before declining to present. While Bi concentrations are consistently greater by a factor of five at UFG compared to southern Greenland, both sites show more than 40-fold increases from the pre-industrial to the early 20th-century. Over the same time period, Tl and BC concentrations at UFG both increased by a factor of three. These trends are consistent with previously reported coal tracer emissions of BC and Tl during the Industrial Revolution from the ACT2 core.[17]

The lead (Pb) records from UFG and southern Greenland do not agree (Figure 6e), as UFG98 Pb increases in 1810 CE and gradually diminishes to present with a brief, smaller increase around 1900 CE whereas Pb in southern Greenland exhibits two peaks, one in 1900 CE and a second larger peak in the 1975 CE. The Pb record from the Eclipse ice core[45] from the Canadian Yukon parallels the changes observed in Greenland although increases in the first half of the 20th century relative to those in second half are substantially larger in Greenland than at

Eclipse. The anomalous Pb record from UFG could be a result of more localized pollution transported to the site or contamination of the ice samples used for measurements, since Pb is contaminated easily and the remaining archive available for our analysis was from the outer edge of the ice core where contamination is most likely.

The new chronology significantly changes the interpretation of the Hg record from UFG. The record based on the original chronology indicated a large Hg increase in the mid-1800s which was attributed to mining activities during the Gold Rush, with a second large increase beginning in 1950 CE linked to industrialization (Figure 7).[5] This interpretation of UFG Hg has been used in reconstructions of Hg emissions and to evaluate Hg deposition in North America.[13,46,47] A perplexing feature of the original UFG record was the Hg increase in 1850 CE attributed to mining (Figure 7b) that was not represented to the same extent in other records from North American ice cores[11] and sediment cores,[6-10] or in more regional-to-hemispheric records from Greenland, Arctic Canada, the Alps, and the Himalayas.[48-51] In general, these archives document large Hg deposition increases limited to the 20th century without any preceding increases in the 19th century, leading to doubts of the regional-representativeness of the original UFG Hg record.

The new depth-age scale reconciles the UFG Hg record with these regionally-representative archives, including Hg concentrations in firn air at Summit, Greenland (Figure 7a,c).[49,52] The new UFG chronology largely shifts the ice age to younger years, thus moving Hg concentration increases at UFG into the 20th century. The absence of Hg increases in the late 19th century at UFG despite major increases in coal burning tracers Bi, Tl, and BC is consistent with low Hg emissions from coal combustion before 1900 CE as reconstructed by Streets et al.[13] However, this new interpretation is at odds with pre-1930 CE reconstructed Hg emissions from mining activities, which argued for peak anthropogenic Hg emissions in 1890 CE.[12,13] As noted by Engstrom et al.,[7] it seems unlikely that such large Hg emissions would not be recorded by any

North American archives of Hg in sediments or ice. If the reconstructed Hg emissions increases associated with mining were significantly reduced, the emissions profile from Horowitz et al.[12] would be very similar to Hg observed at UFG – low Hg loading until 1900 with increasing Hg until the 1940s, followed by a small dip and subsequent increase to a maximum in the 1970s. Previously the only archive to record a 5-fold Hg increase during the Gold Rush Era, the UFG record, when dated using the new chronology, no longer provides evidence for significant influence from early North American mining activities on atmospheric Hg.

The revised chronology and new measurements from the UFG98 ice core document the pervasiveness of heavy metal and BC pollution emitted during the Industrial Revolution, with the UFG Bi, Tl, and BC records paralleling patterns observed in southern Greenland. The new chronology also reconciles the previously-anomalous UFG Hg record with data from lake sediment cores and other ice cores, and calls for a reassessment of Hg emissions from 19th century North American mining activities.

Acknowledgements

We thank the Sulo and Aileen Maki Endowment at the Desert Research Institute for largely funding this research, the USGS for collecting the UFG ice cores, the National Ice Core Laboratory for curating the ice cores, and those who assisted in sampling, packing, and analyzing the samples. We also thank NASA's Cryospheric Processes Program and NSF's Arctic Natural Sciences program for supporting collection and analysis of the Greenland ice cores. The authors thank the three anonymous reviewers for their insightful comments. Any use of trade, firm, or product names is for descriptive purposes only and does not imply endorsement by the U.S. Government.

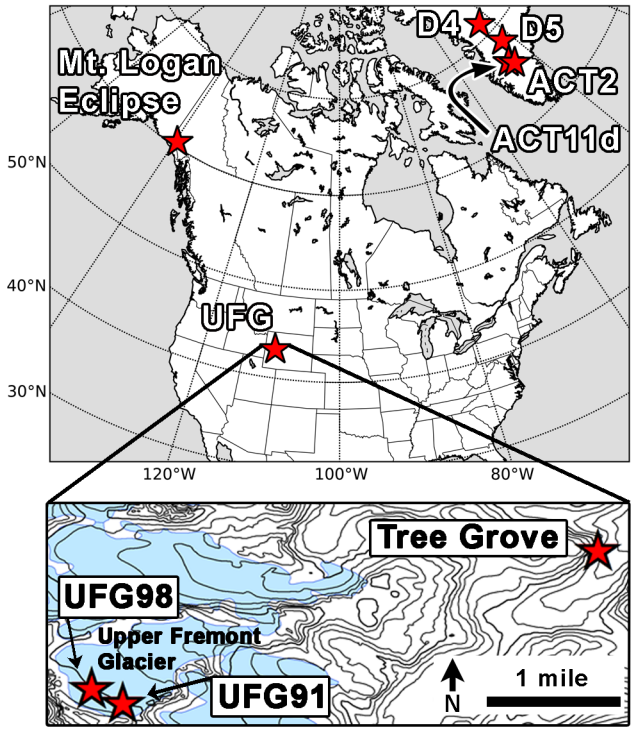

Figure 1. Map showing relevant research sites.

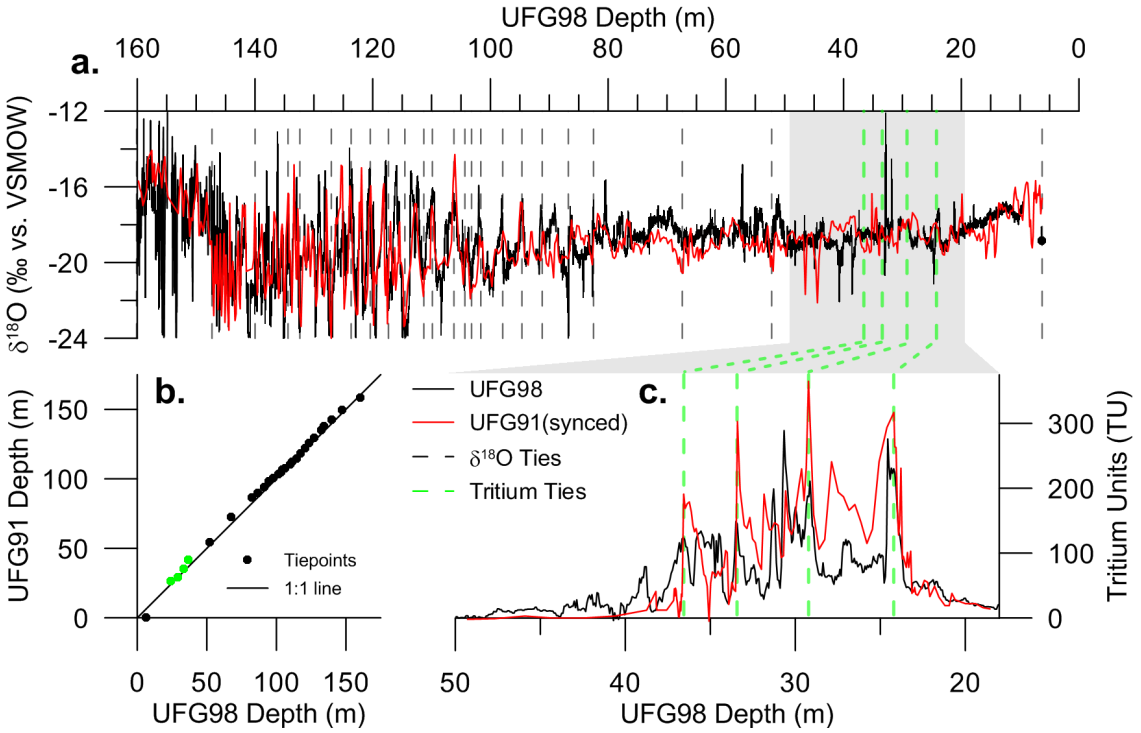

Figure 2. Depth synchronization between $\delta^{18}O$ (a; single point is discontinuous ice from 6.2 to 6.4 m depth).[30] Relationship between UFG98 and UFG91 depth ties with 1:1 line for reference (b). Tritium (c) measured in the UFG91 and UFG98 ice cores.[31,32]

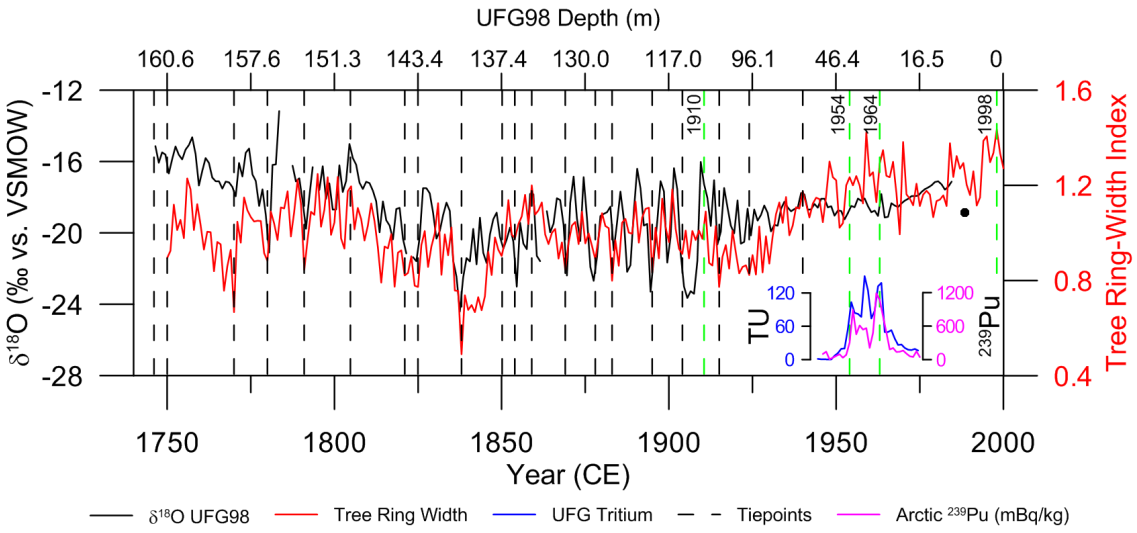

Figure 3. Synchronization tie points between UFG98 ice core $\delta^{18}O$ (black; annual averages; single point is discontinuous ice from 6.2 to 6.4 m depth) and the Fremont whitebark pine tree-ring chronology (red). Dashed green vertical bars represent primary age constraints. Dashed black vertical bars show tie points between ice core $\delta^{18}O$ and the tree ring-width index. Inset shows UFG98 tritium[31] (Tritium Units [TU]; annual averages) compared to a composite record of Arctic ^{239}Pu.[20]

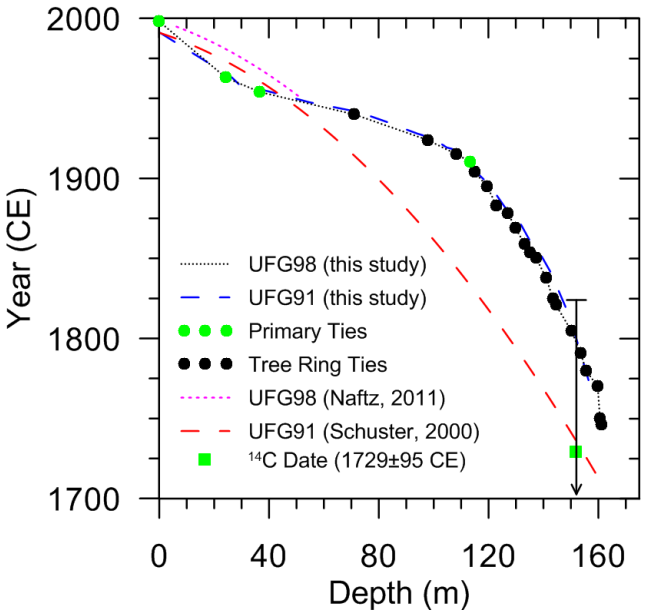

Figure 4. New depth-age scale for the UFG91 (blue dashed) and UFG98 (black dotted with points) ice cores compared to original depth age scales for UFG91[14] (red dashed) and UFG98[4] (magenta dotted).

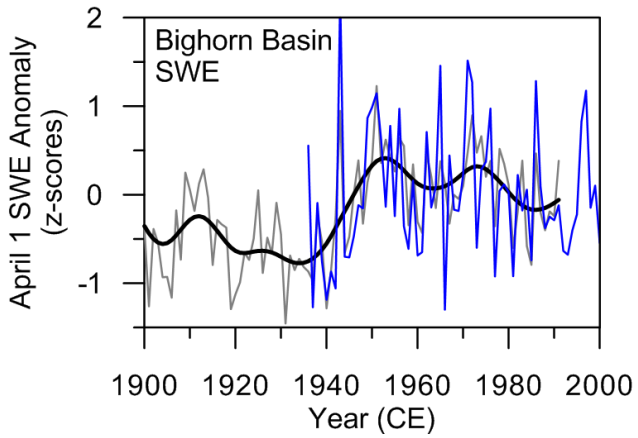

Figure 5. Reconstructed (grey) and observed (blue) April 1 SWE (z-scores) in the Bighorn Basin, MT and WY. 20-year spline fit to reconstructed SWE shown in black. Note elevated SWE from 1950 to 1970 CE. Data from Pederson et al.[39]

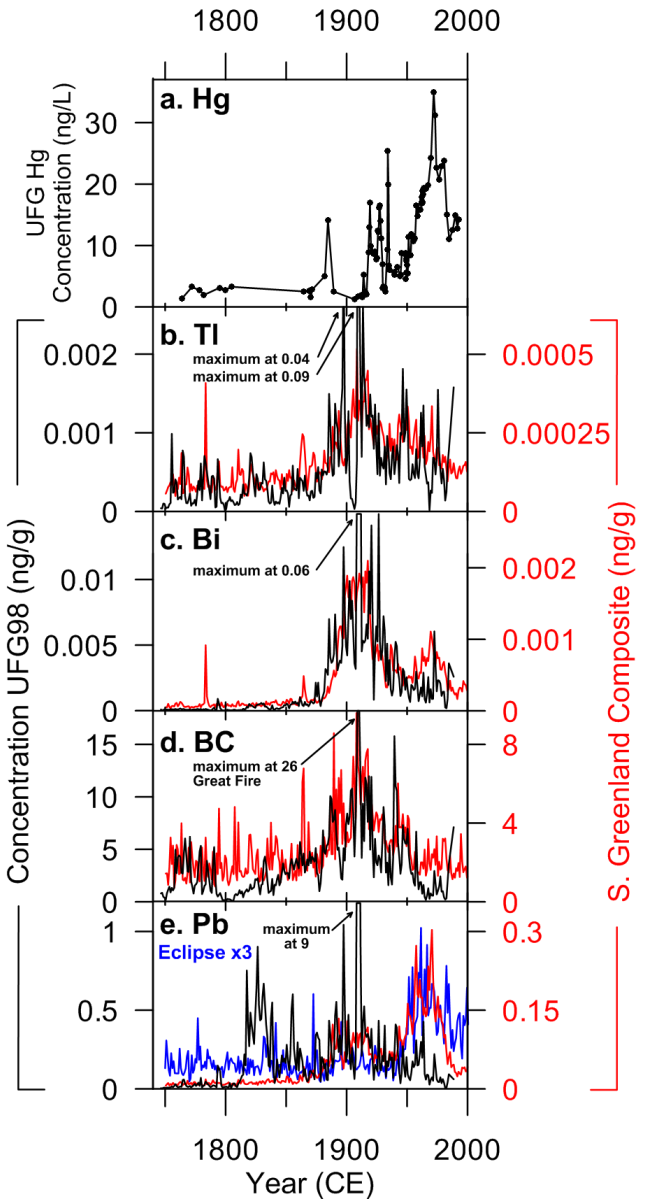

Figure 6. (a) UFG mercury record[5] on the new chronology. (b-e) Chemical tracers (Tl (thallium), Bi (bismuth), BC (black carbon), Pb (lead)) at UFG (black) compared to measurements in a southern Greenland array which consists of four precisely-dated ice core records (red). Pb measured in the northwestern Canada Eclipse ice core[45] (blue) scaled by 3 on right Y axis. Annotations denote maximum for off-scale peaks.

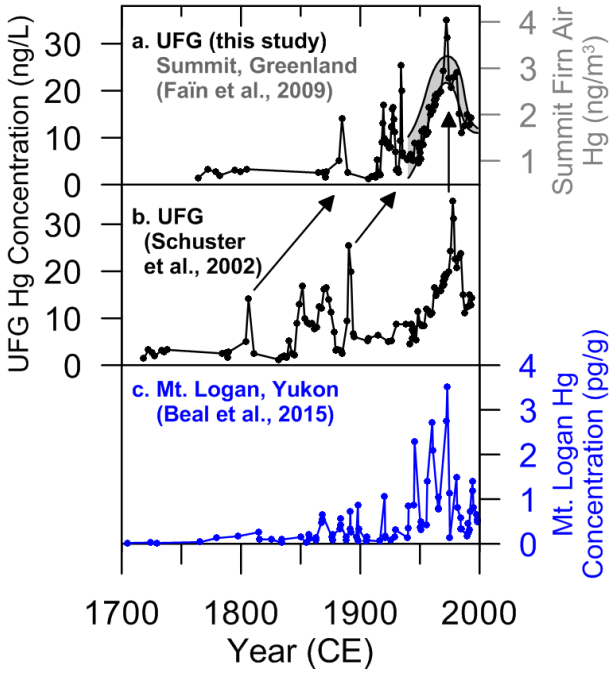

Figure 7. (a) UFG mercury record[5] on the new chronology, with firn air Hg measurements from Summit, Greenland in grey shading.[49] (b) UFG mercury record on original depth-age scale[4,5], arrows indicate the shift in age between the new and old chronologies. (c) Mt. Logan mercury record.[11]

References

1. Aarons, S. M.; Aciego, S. M.; Gabrielli, P.; Delmonte, B.; Koornneef, J. M.; Uglietti, C.; Wegner, A.; Blakowski, M. A.; Bouman, C. Ice core record of dust sources in the western United States over the last 300 years. *Chem. Geol.* **2016**, *442,* 160-173; DOI 10.1016/j.chemgeo.2016.09.006.
2. Naftz, D. L.; Klusman, R. W.; Michel, R. L.; Schuster, P. F.; Reddy, M. M.; Taylor, H. E.; Yanosky, T. M.; McConnaughey, E. A. A. Little ice age evidence from a south-central North America ice core, USA. *Arctic Alpine Res.* **1996**, *28* (1), 35-41; DOI 10.2307/1552083.
3. Naftz, D. L.; Susong, D. D.; Schuster, P. F.; Cecil, L. D.; Dettinger, M. D.; Michel, R. L.; Kendall, C. Ice core evidence of rapid air temperature increases since 1960 in alpine areas of the Wind River Range, Wyoming, United States. *J. Geophys. Res-Atmos.* **2002**, *107* (D13), 1-16; DOI 10.1029/2001jd000621.
4. Naftz, D. L.; Schuster, P. F.; Johnson, C. A. A 50-year record of NOx and SO2 sources in precipitation in the Northern Rocky Mountains, USA. *Geochem. T.* **2011**, *12,* 1-10; DOI 10.1186/1467-4866-12-4.
5. Schuster, P. F.; Krabbenhoft, D. P.; Naftz, D. L.; Cecil, L. D.; Olson, M. L.; Dewild, J. F.; Susong, D. D.; Green, J. R.; Abbott, M. L. Atmospheric mercury deposition during the last 270 years: A glacial ice core record of natural and anthropogenic sources. *Environ. Sci. Tech.* **2002**, *36* (11), 2303-2310; DOI 10.1021/es0157503.
6. Drevnick, P. E. et al., Spatiotemporal patterns of mercury accumulation in lake sediments of western North America. *Sci. Total Environ.* **2016**, *568*, 1157-1170; DOI 10.1016/j.scitotenv.2016.03.167.
7. Engstrom, D. R.; Fitzgerald, W. F.; Cooke, C. A.; Lamborg, C. H.; Drevnick, P. E.; Swain, E. B.; Balogh, S. J.; Balcom, P. H. Atmospheric Hg Emissions from Preindustrial Gold and Silver Extraction in the Americas: A Reevaluation from Lake-Sediment Archives. *Environ. Sci. Tech.* **2014**, *48* (12), 6533-6543; DOI 10.1021/es405558e.
8. Fitzgerald, W. F.; Engstrom, D. R.; Lamborg, C. H.; Tseng, C. M.; Balcom, P. H.; Hammerschmidt, C. R. Modern and historic atmospheric mercury fluxes in northern Alaska: Global sources and Arctic depletion. *Environ. Sci. Tech.* **2005**, *39* (2), 557-568; DOI 10.1021/es049128x.
9. Drevnick, P. E.; Shinneman, A. L. C.; Lamborg, C. H.; Engstrom, D. R.; Bothner, M. H.; Oris, J. T. Mercury flux to sediments of Lake Tahoe, California-Nevada. *Water Air Soil Poll.* **2010**, *210* (1-4), 399-407; DOI 10.1007/s11270-009-0262-y.
10. Pirrone, N.; Allegrini, I.; Keeler, G. J.; Nriagu, J. O.; Rossmann, R.; Robbins, J. A. Historical atmospheric mercury emissions and depositions in North America compared to mercury accumulations in sedimentary records. *Atmos. Environ.* **1998**, *32* (5), 929-940; DOI 10.1016/s1352-2310(97)00353-1.
11. Beal, S. A.; Osterberg, E. C.; Zdanowicz, C. M.; Fisher, D. A. Ice Core Perspective on Mercury Pollution during the Past 600 Years. *Environ. Sci. Tech.* **2015**, *49* (13), 7641-7647; DOI 10.1021/acs.est.5b01033.
12. Horowitz, H. M.; Jacob, D. J.; Amos, H. M.; Streets, D. G.; Sunderland, E. M. Historical Mercury Releases from Commercial Products: Global Environmental Implications. *Environ. Sci. Tech.* **2014**, *48* (17), 10242-10250; DOI 10.1021/es501337j.

13. Streets, D. G.; Devane, M. K.; Lu, Z. F.; Bond, T. C.; Sunderland, E. M.; Jacob, D. J. All-Time Releases of Mercury to the Atmosphere from Human Activities. *Environ. Sci. Tech.* **2011**, *45* (24), 10485-10491; DOI 10.1021/es202765m.

14. Schuster, P. F.; White, D. E.; Naftz, D. L.; Cecil, L. D. Chronological refinement of an ice core record at Upper Fremont Glacier in south central North America. *J. Geophys. Res-Atmos.* **2000**, *105* (D4), 4657-4666; DOI 10.1029/1999jd901095.

15. Moore, J. C.; Beaudon, E.; Kang, S. C.; Divine, D.; Isaksson, E.; Pohjola, V. A.; van de Wal, R. S. W. Statistical extraction of volcanic sulphate from nonpolar ice cores. *J. Geophys. Res-Atmos.* **2012**, *117*, D03306; DOI 10.1029/2011jd016592.

16. McConnell, J. R.; Edwards, R.; Kok, G. L.; Flanner, M. G.; Zender, C. S.; Saltzman, E. S.; Banta, J. R.; Pasteris, D. R.; Carter, M. M.; Kahl, J. D. W. 20th-century industrial black carbon emissions altered arctic climate forcing. *Science* **2007**, *317* (5843), 1381-1384; DOI 10.1126/science.1144856.

17. McConnell, J. R.; Edwards, R. Coal burning leaves toxic heavy metal legacy in the Arctic. *Proc. Natl. Acad. Sci. USA* **2008**, *105* (34), 12140-12144; DOI 10.1073/pnas.0803564105.

18. Maselli, O. J.; Fritzsche, D.; Layman, L.; McConnell, J. R.; Meyer, H. Comparison of water isotope-ratio determinations using two cavity ring-down instruments and classical mass spectrometry in continuous ice-core analysis. *Isot. Environ. Health S.* **2013**, *49* (3), 387-398; DOI 10.1080/10256016.2013.781598.

19. McConnell, J. R. Continuous ice-core chemical analyses using inductively Coupled Plasma Mass Spectrometry. *Environ. Sci. Tech.* **2002**, *36* (1), 7-11; DOI 10.1021/es011088z.

20. Arienzo, M. M.; McConnell, J. R.; Chellman, N.; Criscitiello, A. S.; Curran, M.; Fritzsche, D.; Kipfstuhl, S.; Mulvaney, R.; Nolan, M.; Opel, T.; Sigl, M.; Steffensen, J. P. A Method for Continuous (PU)-P-239 Determinations in Arctic and Antarctic Ice Cores. *Environ. Sci. Tech.* **2016**, *50* (13), 7066-7073; DOI 10.1021/acs.est.6b01108.

21. Sigl, M.; McConnell, J. R.; Layman, L.; Maselli, O.; McGwire, K.; Pasteris, D.; Dahl-Jensen, D.; Steffensen, J. P.; Vinther, B.; Edwards, R.; Mulvaney, R.; Kipfstuhl, S. A new bipolar ice core record of volcanism from WAIS Divide and NEEM and implications for climate forcing of the last 2000 years. *J. Geophys. Res-Atmos.* **2013**, *118* (3), 1151-1169; DOI 10.1029/2012jd018603.

22. Stokes, M. A.; Smiley, T. L. *An introduction to tree-ring dating*; The University of Arizona Press: Tucson, USA, 1968.

23. Bunn, A. G., Korpela, M., Biondi, F., Campelo, F., Mérian, P., Qeadan, F., and Zang, C. *dplR: Dendrochronology Program Library* in R. [R package version 1.6.2]. 2015.

24. R Core Team. A language and environment for statistical computing. 2013. Vienna, Austria, R Foundation for Statistical Computing.

25. Cook, E. R., Krusic, P. J., and Melvin, T. RCS signal free program: version 45 (2b). 2014.

26. Melvin, T. M.; Briffa, K. R.; Nivolussi, K.; Grabner, M. Time-varying-response smoothing. *Dendrochronologia* **2007**, *25* (1), 65-69; DOI 10.1016/j.dendro.2007.01.004.

27. Briffa, K. R. and Melvin, T. M. A Closer Look at Regional Curve Standardization of Tree-Ring Records: Justification of the Need, a Warning of Some Pitfalls, and Suggested Improvements in Its Application. In *Dendroclimatology;* Hughes, M. K.; Swetnam, T. W.; Diaz, H. F. Eds.; Springer Netherlands: Dordrecht, 2011; pp 113-145.

28. Cook, E. R., Briffa, K., Shiyatov, S. G., and Mazepa, V. S. Tree-ring standardization and grow-trend estimation. In *Methods of dendrochronology: Applications in environmental sciences*, Cook, E. R.; Kairiukstis, L. A. Eds.; Kluwer Acadmic, Springer Netherlands: Dordrecht, 1990. pp 104-123.

29. Harris, I.; Jones, P. D.; Osborn, T. J.; Lister, D. H. Updated high-resolution grids of monthly climactic observations- the CRU TS3.10 dataset. *Int. J. Climatol.* **2014**, *34* 623-642; DOI 10.1002/joc.3711.

30. Schuster, P. F. et al. Fremont Glacier 1991 Core Oxygen Isotope Data. *NOAA/NGDC Paleoclimatology Program,* 2004. IGBP PAGES/World Data Center for Paleoclimatology Data Contribution Series # 2004-079. https://www1.ncdc.noaa.gov/pub/data/paleo/icecore/trop/fremont (accessed August 10, 2016).

31. Schuster, P. F. et al. Fremont Glacier 1998 Core Tritium Data. *NOAA/NGDC Paleoclimatology Program,* 2004. IGBP PAGES/World Data Center for Paleoclimatology Data Contribution Series # 2004-079. https://www1.ncdc.noaa.gov/pub/data/paleo/icecore/trop/fremont (accessed August 10, 2016).

32. Schuster, P. F. et al. Fremont Glacier 1991 Core Tritium Data. *NOAA/NGDC Paleoclimatology Program,* 2004. IGBP PAGES/World Data Center for Paleoclimatology Data Contribution Series # 2004-079. https://www1.ncdc.noaa.gov/pub/data/paleo/icecore/trop/fremont (accessed August 10, 2016).

33. Long, C. J.; Whitlock, C.; Bartlein, P. J.; Millspaugh, S. H. A 9000-year fire history from the Oregon Coast Range, based on a high-resolution charcoal study. *Can. J. Forest Res.* **1998**, *28* (5), 774-787; DOI 10.1139/cjfr-28-5-774.

34. Power, M. J.; Whitlock, C.; Bartlein, P.; Stevens, L. R. Fire and vegetation history during the last 3800 years in northwestern Montana. *Geomorphology* **2006**, *75* (3-4), 420-436; DOI 10.1016/j.geomorph.2005.07.025.

35. Kipfmueller, K. F.; Salzer, M. W. Linear trend and climate response of five-needle pines in the western United States related to treeline proximity. *Can. J. Forest Res.* **2010**, *40* (1), 134-142; DOI 10.1139/x09-187.

36. Perkins, D. L.; Swetnam, T. W. A dendroecological assessment of whitebark pine in the Sawtooth-Salmon River region, Idaho. *Can. J. Forest Res.* **1996**, *26* (12), 2123-2133; DOI 10.1139/x26-241.

37. Hoffman, M. J.; Fountain, A. G.; Achuff, J. M. 20th-century variations in area of cirque glaciers and glacierets, Rocky Mountain National Park, Rocky Mountains, Colorado, USA. *Ann. Glaciol.* **2007**, *46,* 349-354.

38. Machguth, H.; Eisen, O.; Paul, F.; Hoelzle, M. Strong spatial variability of snow accumulation observed with helicopter-borne GPR on two adjacent Alpine glaciers. *Geophys. Res. Lett.* **2006**, *33* (13), L13503; DOI 10.1029/2006gl026576.

39. Pederson, G. T.; Gray, S. T.; Woodhouse, C. A.; Betancourt, J. L.; Fagre, D. B.; Littell, J. S.; Watson, E.; Luckman, B. H.; Graumlich, L. J. The unusual nature of recent snowpack declines in the North American Cordillera. *Science*. **2011**, *333* (6040), 332-335; DOI 10.1126/science.1201570.

40. Pederson, G. T.; Betancourt, J. L.; McCabe, G. J. Regional patterns and proximal causes of the recent snowpack decline in the Rocky Mountains, U.S. *Geophys. Res. Lett.* **2013**, *40* (9), 1811-1816; DOI 10.1002/grl.50424.

41. Carrara, P. E.; McGimsey, R. G. The late-neoglacial histories of the Agassiz and Jackson Glaciers, Glacier National Park, Montana. *Arctic Alpine Res.* **1981**, *13* (2), 183-196; DOI 10.2307/1551194.

42. Pederson, G. T.; Fagre, D. B.; Gray, S. T.; Graumlich, L. J. Decadal-scale climate drivers for glacial dynamics in Glacier National Park, Montana, USA. *Geophys. Res. Lett.* **2004**, *31* (12), L12203; DOI 10.1029/2004gl019770.

43. Osterberg, E. C.; Mayewski, P. A.; Fisher, D. A.; Kreutz, K. J.; Maasch, K. A.; Sneed, S. B.; Kelsey, E. Mount Logan ice core record of tropical and solar influences on Aleutian Low variability: 500-1998 AD. *J. Geophys. Res-Atmos.* **2014**, *119* (19), 11189-11204; DOI 10.1002/2014jd021847.

44. Yalcin, K.; Wake, C. P.; Kreutz, K. J.; Germani, M. S.; Whitlow, S. I. Ice core paleovolcanic records from the St. Elias Mountains, Yukon, Canada. *J. Geophys. Res-Atmos.* **2007**, *112* (D8), D08102; DOI 10.1029/2006jd007497.

45. Gross, B. H.; Kreutz, K. J.; Osterberg, E. C.; McConnell, J. R.; Handley, M.; Wake, C. P.; Yalcin, K. Constraining recent lead pollution sources in the North Pacific using ice core stable lead isotopes. *J. Geophys. Res-Atmos.* **2012**, *117*, D16307; DOI 10.1029/2011jd017270.

46. Strode, S.; Jaegle, L.; Selin, N. E. Impact of mercury emissions from historic gold and silver mining: Global modeling. *Atmos. Environ.* **2009**, *43* (12), 2012-2017; DOI 10.1016/j.atmosenv.2009.01.006.

47. UNEP *Global Mercury Assessment 2013: Sources, Emissions, Releases, and Environmental Transport*; UNEP Chemicals Branch: Geneva, Switzerland, 2013.

48. Zheng, J. C. Archives of total mercury reconstructed with ice and snow from Greenland and the Canadian High Arctic. *Sci. Total Environ.* **2015**, *509,* 133-144; DOI 10.1016/j.scitotenv.2014.05.078.

49. Fain, X.; Ferrari, C. P.; Dommergue, A.; Albert, M. R.; Battle, M.; Severinghaus, J.; Arnaud, L.; Barnola, J. M.; Cairns, W.; Barbante, C.; Boutron, C. Polar firn air reveals large-scale impact of anthropogenic mercury emissions during the 1970s. *Proc. Natl. Acad. Sci. USA* **2009**, *106* (38), 16114-16119; DOI 10.1073/pnas.0905117106.

50. Jitaru, P.; Infante, H. G.; Ferrari, C. P.; Dommergue, A.; Boutron, C. F.; Adams, F. C. Present century record of mercury species pollution in high altitude alpine snow and ice. *J. Phys. IV*. **2003**, *107*, 683-686; DOI 10.1051/jp4:20030395.

51. Kang, S. C.; Huang, J.; Wang, F. Y.; Zhang, Q. G.; Zhang, Y. L.; Li, C. L.; Wang, L.; Chen, P. F.; Sharma, C. M.; Li, Q.; Sillanpaa, M.; Hou, J. Z.; Xu, B. Q.; Guo, J. M. Atmospheric mercury depositional chronology reconstructed from lake sediments and ice core in the Himalayas and Tibetan Plateau. *Environ. Sci. Tech.* **2016**, *50* (6), 2859-2869; DOI 10.1021/acs.est.5b04172.

52. Dommergue, A.; Martinerie, P.; Courteaud, J.; Witrant, E.; Etheridge, D. M. A new reconstruction of atmospheric gaseous elemental mercury trend over the last 60 years from Greenland firn records. *Atmos. Environ.* **2016**, *136,* 156-164; DOI 10.1016/j.atmosenv.2016.04.012.

Chapter 2

Comparison of co-located ice-core and tree-ring mercury records indicates radial translocation of mercury in whitebark pine

Nathan Chellman[1,2], Adam Csank[3], Joseph R. McConnell[1], Mae Sexauer Gustin[4], Monica Arienzo[1], and Margarita Vargas Estrada[4]

[1]Desert Research Institute, Division of Hydrologic Sciences, Reno, Nevada 89512, United States
[2]Graduate Program of Hydrologic Sciences, University of Nevada, Reno, Nevada 89557, United States
[3]Department of Geography, University of Nevada, Reno, Nevada 89557, United States
[4]Department of Natural Resources and Environmental Science, University of Nevada, Reno, Nevada 89557, United States

Abstract

Tree ring records are a potential archive for reconstructing long-term historical trends in atmospheric mercury (Hg) concentrations. Although Hg preserved in tree rings has been shown to be largely derived from the atmosphere, quantitative relationships linking atmospheric concentrations to those in tree rings are limited. In addition, few tree-ring-based Hg records have been evaluated against co-located proxies of atmospheric Hg or direct atmospheric measurements. Here we develop long-term Hg records extending from 1800 to 2018 CE using cores collected from two whitebark pine stands co-located with the Upper Fremont Glacier in the Wind River Range, Wyoming, where a long-term record of atmospheric Hg previously was developed from an ice core. The tree ring record shows that Hg concentrations increased beginning in 1800 CE to a peak at ~1950 CE, before decreasing to present, generally paralleling the co-located ice-core record of Hg deposition. The exact timing and magnitude of the Hg increases in the trees, however, is offset relative to the ice-core record. Results from an advection-diffusion model indicate that these differences are consistent with radial movement of Hg within the trees, indicating that while whitebark pine can be used to document hemispheric-scale Hg pollution at remote field sites, interpretation of temporal trends observed in these trees must account for potential influences from biotic processes that may impact Hg uptake and preservation.

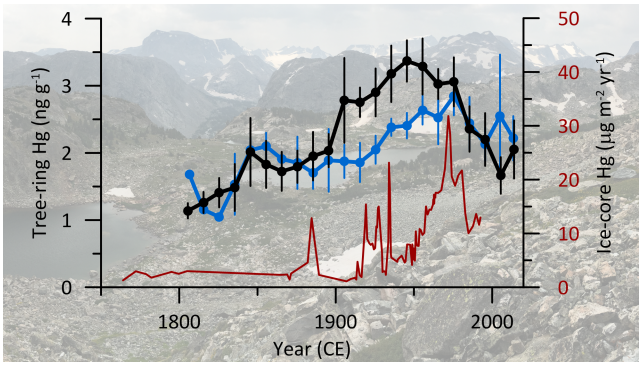

Abstract Art

1. Introduction

Tree-ring records are well-established proxies for past climatic change and have been used extensively to reconstruct temperature, precipitation, streamflow, and other environmental parameters during past centuries to millennia.[1-4] Because of the widespread availability of trees across the landscape, studies also have attempted with varying degrees of success to infer past changes in environmental and atmospheric pollution at local and regional scales using dendrochemical analyses of trace metals.[5-11] Of particular interest has been the potential for trees to serve as indicators of atmospheric mercury (Hg) concentrations. There are now a number of long-term tree-ring Hg records from North America and Europe that have been interpreted to reflect changes in regional Hg emissions.[7, 8, 12] Tree rings directly record atmospheric Hg concentrations in contrast to other archives that record Hg deposition such as lake sediment cores,[13-15] peat cores,[16, 17] and ice cores.[18-20] Firn air measurements from Greenland have been used to directly reconstruct atmospheric Hg concentration.[21]

Previous research has shown that Hg preserved in wood tissue primarily is assimilated from the ambient atmosphere,[22-24] and Hg concentrations in foliage, bark, and wood have been shown to increase with proximity to known point sources of contamination.[25, 26] Additional work has explored whether temporal trends of Hg measured in tree cores can be attributed to past local- or regional-scale emissions.[11, 27-29] Current understanding of Hg pathways and preservation within trees, while improving, is still limited.[23, 24] For example, radial translocation of Hg within trees has been observed but remains poorly quantified[23, 25] and high variability of intra-tree and intra-grove Hg measurements requires a large number of samples from the same time period for confidence in mean trends.[7, 8, 25, 30] Furthermore, the absence of long-term atmospheric Hg measurements makes quantitative assessment of tree-ring Hg records difficult or impossible, with few studies directly linking modern atmospheric Hg measurements to a tree Hg record.[7, 23]

Here, we developed long-term Hg records extending from 1800 to 2018 CE from two high-elevation whitebark pine (*Pinus albicaulis)* stands in the Wind River Range, Wyoming. We evaluated these records as indicators of past atmospheric Hg concentration using the recently revised, nearby Upper Fremont Glacier (UFG) ice-core record of Hg deposition extending from 1760 to 1991 CE. This ice-core record previously was used to document hemispheric-scale industrial pollution and climate.[19, 20, 31]

2. Methods

2.1 Tree sampling and Hg analysis

Living trees from two whitebark pine stands in the Wind River Range, hereafter the Fremont (FRE; 43.158 °N, 109.558 °W; 3410 masl) and the Rock Lake stands (RLK; 43.188 °N, 109.542 °W; 3290 masl), were sampled in July 2018 (Figure 1). Five cores from four individual trees were recovered at the FRE stand, and four cores from four individual trees were recovered at the RLK stand. While a recent study recommended sampling 10 trees for Hg studies,[30] the number of cores in this study was limited by permitting constraints in wilderness areas and unanticipated field conditions. The FRE stand was located on the south-facing aspect of a ridge. The area had a surface slope of 30–35° and largely was composed of bedrock with shallow, patchy soil and no upstream catchment or drainage. The RLK stand also was located on a south-facing aspect with little to no upstream catchment, but on a less steep slope (20–25°) with slightly more developed soil. The FRE and RLK tree stands were located 4 km apart and 7 and 10 km from the UFG ice-core sites, respectively (Figure 1). Tree core sample collection and analysis were based on methods described by Peckham et al.[30] Tree cores were collected using a new, 12-mm Haglöf increment borer and handled with nitrile gloves. Cores were transferred directly from the increment borer to sealed Teflon™ tubes, frozen within 48 hours of collection, and stored at -20 °C until further processing.

Prior to subsampling, cores were dried at room temperature with clean air using a Tekran Model 1100 zero air generator for at least 72 hours. To facilitate dating, a flat surface was milled into one side of each core using a drill and clean carbide bit. If necessary, cores were polished with 800-grit sandpaper to better visualize individual rings. Cores were subsampled at decadal resolution using a stainless steel blade, freeze-dried to remove remaining moisture, and stored frozen until analysis. Cores were visually cross-dated against a master chronology from a previous collection from the area in 2001 CE[20] using the list method of cross-dating.[32] The program COFECHA[33] was used to verify the accuracy of the visual cross-dating, leading to an estimated age uncertainty in certain cores of 1 to 3 years at 1800 CE from missing rings. This age uncertainty has an insignificant effect on final average Hg profiles because of the decadal resolution of subsampling. Samples represented the time period between 1800 and 2018 CE to facilitate comparison with the nearby UFG record that extends from 1760 to 1991 CE.

A Milestone DMA-80 instrument was used for mercury analysis. The instrument was calibrated using aqueous standards with a daily adjustment based on the recovery of National Institute of Standards and Technology (NIST) Pine Needle Standard 1575a quality control standards. The detection limit, calculated as three times the standard deviation of the blank, was 0.08 ng g^{-1} (n=50) and the average standard deviation of triplicate measurements of the same sample was 0.28 ng g^{-1} (n=12). Measured concentration (39.2±0.9 ng g^{-1}) of quality control standard NIST 1575a analyzed periodically during each day was consistent with the certified value (39.9±0.7 ng g^{-1}). The DMA-80 was set to a 10 s drying time at 300 °C, a 120 s decomposition time at 850 °C, and a 60 s dwell time.

2.2 Diffusion and advection modeling

We used the one-dimensional advection-diffusion equation (Equation 1) to simulate how spatial movement from diffusion (diffusion coefficient *D*) and advection (advection coefficient *u*) can result in concentration changes through time. This equation, defined as:

$$\frac{\partial C}{\partial t} = D\frac{\partial^2 C}{\partial x^2} - u\frac{\partial C}{\partial x} \qquad (1)$$

was used to model two simulations to investigate (1) how an atmospheric Hg signal could be altered by advection or diffusion within tree rings and (2) if such movement is plausible, how a valid atmospheric record could be reconstructed from the tree Hg profiles. This model included a finite-volume partial differential equation solver in Python.[34]

First, we used this equation to evaluate how changes in atmospheric Hg uptake could be smoothed or distorted by diffusion or radial movement of Hg within tree rings. The Hg record from the nearby UFG was assumed to be representative of atmospheric Hg deposition at the site and used to drive a simple model of diffusion alone and of combined advection and diffusion processes. The tree cores were idealized as a series of equal-sized cells with widths equivalent to the average annual ring-widths of the FRE (0.57 mm) or RLK (0.80 mm) samples. The model was run from 1765 to 1991 CE in 1-year time steps with a fixed concentration at the inner boundary (1765 CE) and a no-flux condition at the outer edge of the most recently added cell. At each time-step, the domain was extended by one cell, representing one year of growth, with the initial concentration derived from the normalized and annually-interpolated UFG Hg flux record.

Second, we used only the advection-term of Equation 1 to inverse-model atmospheric Hg concentrations from the tree ring profiles assuming, based on the forward model results, that diffusion processes were negligible, although loss of temporal resolution is inherent in the inverse advection model. This inverse model was run from 2015 to 1805 CE in decadal time steps with tree cores idealized as cells with a length representing the decadal resolution of the Hg measurements (5.7 and 8.0 mm for FRE and RLK, respectively). Boundary conditions were a

fixed concentration at the inner boundary (1805 CE) and a no-flux condition on the outer boundary. At each time-step, the outer-most cell was removed from the model domain and its concentration remained unchanged for all remaining solutions.

2.3 UFG Ice Core Flux Calculations

Hg flux was calculated for the UFG ice cores by multiplying Hg concentrations by the water equivalent accumulation rate at the site of 0.91 m yr^{-1} (ice accumulation of 1 m yr^{-1} [19]). The depth-age relationship predicted by an ice flow model[35] run using this constant accumulation rate, a basal melt rate of 0.05 m yr^{-1}, and the glacier's surface and bed topography[31] along a flow line intersecting the ice-core site agrees well with the revised chronology from Chellman et al.[20] This suggests that the ice-core depth-age scale largely is determined by the basin and glacier geometry, not by large temporal changes in accumulation rate or along the glacier flow line, and therefore it is reasonable to assume a constant accumulation rate through time.

3. Results and Discussion

Average decadal Hg concentrations in individual trees ranged from 0.8 to 5.3 ng g^{-1} between 1800 and 2018 CE (Figure 2). These concentrations are similar to previously reported measurements from other remote tree records.[7, 8, 12, 30] Hg profiles—both within a single tree and between trees within each stand—were variable, also consistent with observations from previous studies.[8, 12, 30] The average relative percent difference (RPD; calculated as the absolute value of the difference between two measurements divided by their average) for two cores taken from a single tree was 39±24% (n=22) for tree FRE005. Within each stand, the standard deviation (SD) for decadal measurements ranged between 0.06 and 1.8 ng g^{-1}, with an average SD of 0.65 and 0.56 ng g^{-1} for the FRE and RLK stands, respectively. The SD of the decadal data represents on

average 25–30% of the overall magnitude of the average Hg concentration, reinforcing the need for multiple cores to have confidence in long-term trends.

The source of variability between nearby tree Hg profiles is poorly understood, but hypothesized to derive from site- and tree-specific factors that influence atmospheric Hg uptake—including but not limited to asymmetrical growth, stomatal conductance, prevailing winds, and hill slope.[8, 30] At the FRE and RLK stands, some of the differences in site physical characteristics are minimized, with all trees growing on a steep, fractured bedrock slope with little soil. The trees likely access similar, shallow water sources derived predominately from some combination of each year's seasonal snowmelt and summer monsoonal rainfall, with little to no contributions from groundwater sources. Furthermore, these trees probably all have similar growing seasons controlled by mid-summer snow disappearance and the arrival of cold temperatures in fall. Although the physical characteristics of each site are similar, the variability of Hg measurements supports that there are other tree-specific biotic factors that influence atmospheric Hg uptake and preservation by these trees.

Despite observed Hg variability between trees, the average composite Hg profiles from both sites show significant increases during the past 200 years (Figure 2). At the FRE stand, the average Hg concentration increased from 1.3 ng g^{-1} between 1800 and 1840 CE to a small peak of 1.9 ng g^{-1} in 1850 CE before subsequently increasing to 3.4 ng g^{-1} in 1950 CE and declining to 1.8 ng g^{-1} in the 2000s. All individual FRE records that extend from 1800 CE to modern (n=4) document increasing Hg concentrations from 1850 CE to the mid-20th century, and all individual FRE records (n=5) document declines between 1950 CE and modern. The coherence of all the individual Hg records within this stand leads to high confidence in the observed mean profile. At the RLK stand, the average Hg concentration ranged from 1.1 to 2.0 ng g^{-1} between 1800 and 1850 CE with an increase to 2.8 ng g^{-1} in 1975 CE before declining to 2.4 ng g^{-1} in the 2000s. This trend agrees well with that observed at the FRE stand, but the mean Hg profile at RLK is

heavily influenced by a single profile from tree RLK002—the only record from this site to extend to 1800 CE. Without this record, the average trend at RLK still shows an industrial increase exceeding the standard error of the mean measurements, but the magnitude of the increase is lower. The two profiles are strongly related with a near-zero intercept (FRE = 1.07*RLK + 0.06, r^2=0.49, p <0.01), suggesting there is no significant concentration offset between the two records despite the slight differences in temporal trends.

The decadal Hg concentrations showed no significant correlation to the amount of decadal growth at either stand (r=-0.09, p=0.37 for FRE; r=-0.18, p=0.15 for RLK). No trends in Hg concentration with respect to age were observed despite a large span of tree ages, with tree ages at RLK ranging from 125 to 224 years old and at FRE ranging from 272 to 439 years old.

Previous Hg studies based on tree rings and lake sediment cores have calculated the ratio between modern and preindustrial Hg deposition to quantify how each archive has responded to increased atmospheric Hg concentrations originating from anthropogenic emissions.[8, 13, 36] For FRE and RLK, the observed Hg increases correspond to a ratio of 1.7 for both stands, calculated here as between modern (1950 CE to present) to pre-industrial (1800 to 1850 CE) Hg concentrations. When calculated as the ratio of the highest modern Hg value to lowest pre-1850 CE value, the ratio increases to 3.0 and 2.7, respectively. These are similar to ratios reported for another North American tree record[8] (1.9 from NW Canada), but lower than values observed in lake sediments[13] (5.6 for Wyoming, 3.2 for Western US) or ice cores[19, 20] (6.2 for the UFG ice core).

The FRE and RLK stands are in close proximity to UFG, allowing for direct comparison of the tree-derived Hg profiles to the long-term atmospheric Hg record from the UFG ice cores (Figure 3). On the recently revised chronology, these ice cores document hemispheric-scale industrial pollution, with trends in black carbon and the pollution-related heavy metals thallium and bismuth paralleling those observed in Greenland ice cores.[20] The Hg record from UFG shows

significant 20th century Hg increases peaking in 1970 CE that were attributed to industrial emissions, with potentially smaller contributions in the late 1800s from Gold Rush-era mining. The magnitude of Hg deposition at UFG, generally ranging from 1 to 22 μg m^{-2} yr^{-1}, is comparable to fluxes from a nearby lake sediment core,[37] and modern flux at UFG, between 10 and 12 μg m^{-2} yr^{-1} from 1980 to 1990 CE, is in good agreement with estimated modern wet Hg deposition for the Wind River Range.[38] From 2008 to 2017 CE, the only time period with available data for this region, Hg deposition ranged from 7.4 and 15 μg m^{-2} yr^{-1} (average 10.6 μg m^{-2} yr^{-1}) based on precipitation-weighted, interpolated deposition data from the National Atmospheric Deposition Program Mercury Deposition Network.[38] Although in agreement with these modern observations, the UFG ice core fluxes are approximately an order of magnitude higher than Hg fluxes observed at other alpine ice core sites.[18, 39] We hypothesize the higher fluxes at UFG can be attributed to significant melt and refreezing processes that form ice layers, thereby enhancing preservation by preventing reemission of volatile Hg species.[40]

The water isotope record from the UFG cores previously has been linked to a tree-ring width chronology from another nearby stand of whitebark pine (Figure 1), suggesting the ice and tree archives document a common climate signal.[20] Here we compared the tree-based Hg profile to the UFG ice cores, assuming both archives are exposed to the same air masses, to assess if these tree Hg records reflect long-term changes in atmospheric Hg concentration. Compared to the UFG Hg record—that showed a short-lived increase in 1880 CE (inferred from a single measurement) followed by a rapid ~6-fold increase from 1900 to 1970 CE (Figure 3c)—the FRE Hg profile was smoother with a more gradual, sustained increase between 1800 CE and 1950 CE and a short-lived peak at ~1850 CE. After 1950 CE, the FRE Hg decreased by a factor of 2 until modern, similar to declines observed in the ice core since 1970 CE. The decadal resolution of the FRE Hg data likely contributes to the overall smoother trend, but there is also smoothing inherent to the UFG Hg measurements that were made on discrete, non-contiguous 7 cm sections of ice.[19]

The overall parallel trend between the trees and ice core suggests that the tree Hg signal is linked to atmospheric Hg concentrations, but there are important differences in timing—namely Hg increases in the trees began a century earlier and peak Hg pollution during the 20th century occurred approximately 20 years earlier than in the ice-core record.

Radial movement of Hg is a mechanism that potentially could explain the temporal discrepancies between the tree and ice core Hg profiles. Though the radial movement of lead and other species within wood, either by movement through ray cells or diffusion, has been observed in various tree species,[41-46] previous studies have reached mixed conclusions regarding the role of radial movement of Hg. Radial Hg translocation has been suggested in a dose-response experiment,[23] a study of Hg pollution near a chlor-alkali plant,[25] and an investigation of volcanic Hg preservation in trees.[9] Other studies, however, have suggested minimal to no influence from radial movement,[7, 8, 12, 24] primarily based on synchronous timing of Hg peaks across multiple individual records or correlation of sharp changes in Hg concentration to known historical emissions sources.

Using an advection-diffusion model (Equation 1) driven by the UFG Hg profile, assumed here to be directly representative of local to regional atmospheric loading, we investigated how diffusion and inward Hg movement could alter the Hg signal preserved by the trees as they grow and incorporate atmospheric Hg. These model results should be taken only as a qualitative evaluation of the tree-ring Hg trends, as the current process-level understanding of how Hg is incorporated, moved, and preserved within trees is limited, resulting in few constraints on modeling. Radial movement by ray cells in trees is thought to be largely limited to sapwood, although movement of chemical species in the heartwood, largely by diffusion, has also been observed.[44, 47] Such movement implies that large temporal shifts in the Hg profile are plausible.

Forward model results that do not include advection suggest that diffusion alone, which results in a smoother simulated Hg signal preserved in the trees without significant translation in

time (Figure 3d), is not a sufficient explanation for the observed temporal differences. When the model also includes inward radial movement as simulated by advection, the combined effect of smoothing and migration of Hg results in a temporal shift of the tree-ring Hg profile. These model simulations shift peak Hg concentrations to 1955 and 1935 CE (Figure 3e), respectively, in agreement with the observed FRE peak between 1930 and 1960 CE and the RLK peak between 1950 and 1980 CE. Additionally, the simulation run with diffusion coefficient D=0.001 and advection coefficient u=0.5 shifts the early 1900s-era atmospheric increase to ~1860 CE, in agreement with an observed secondary peak at both FRE and RLK. The translocation of Hg over these timescales seems plausible since the median radial distance represented by the 1950 to 1980 CE timespan was 11.7 and 24.2 mm for the FRE and RLK cores, respectively. Furthermore, the sapwood, in which most radial movement is thought to occur, approximately represents the outmost 50 to 100 rings in the FRE and RLK samples. The greater inward shift observed in the FRE Hg profile, compared to that of RLK, may be a result of the smaller median radial distance represented by this time period in the FRE trees, suggesting the same amount of radial translocation at FRE results in a larger temporal shift because of the overall smaller ring widths.

The inward advection of the Hg profile results in dispersing the sharp increases observed in the ice-core flux record during the 20th century into a more gradual increase beginning as early as the mid-18th century—more consistent with the tree Hg profile. This smoothing may also help to explain the relatively low modern-to-preindustrial Hg ratio observed in tree-based Hg records relative to lake sediments or the UFG ice core. The decadal resolution further contributes to the low observed ratios, since the lower resolution would lead to an underestimate of the industrial-era Hg peak.

This advection-diffusion model provides a mechanism to reconcile temporal differences between the co-located ice core and tree-ring Hg records at this site and suggests that the tree Hg record has been altered by post-depositional radial movement of Hg with little influence from

diffusion. Assuming advection is the dominant process affecting the tree Hg profiles, we used an inverse model incorporating only the advection term of Equation 1 to determine if a plausible atmospheric signal could be recovered from the tree-ring Hg data.

After applying the inverse model with advection rates of 2 and 4 mm per decade, the reconstructed atmospheric Hg profiles are in better agreement with the UFG ice core Hg data than the untransformed data (Figure 4). The industrial-to-preindustrial Hg ratio increases to 2.3 for the FRE profile for these simulations from the original value of 1.7. Furthermore, the reconstructed profiles better parallel measurements of gaseous Hg in the interstitial air of firn from Greenland,[21] suggesting a valid, albeit smoothed, atmospheric signal can be recovered provided that any radial translocation in the tree-based records is inverted. After application to records from these two stands, the inverse model is able to reconstruct the timing of atmospheric changes, but is unable to reconstruct high-frequency variability in part because of limitations inherent to the inverse model, but also because of the decadal resolution of the Hg measurements. Higher-resolution tree Hg measurements would allow for better estimation of high-frequency variability after application of an inverse model, although some high-frequency detail would still be lost in the advection making it difficult to reconstruct rapid transitions or sharp spikes. Also note that the earlier part of the inverse-modeled record is controlled by the innermost boundary condition, as Hg concentrations in the tree representative of this timeframe were translocated to rings older than 1800 CE, the oldest rings measured in this study. While radial movement of Hg seems likely in these stands of whitebark pine, further work is needed to assess its importance for other tree species and in other environmental situations.

Radial translocation also may help explain overall why another long-term tree record from Canada[8] showed Hg increases ~100 years earlier than observed in nearby sediment records[13] or in the Mt. Logan ice core located upwind ~530 km to the southwest.[18] Although the Hg increases observed in Clackett et al. as early as 1750 CE were attributed to anthropogenic

emissions, potentially from colonial mining in South America,[8] radial movement of Hg could be an alternative explanation. Preliminary application of the inverse advection model to this dataset results in shifting the timing of observed increases in the tree record to better agreement with the Mt. Logan ice core.

The Hg profiles from the FRE and RLK trees, like other long-term Hg records from other North American proxies, can be used to inform current understanding of the global Hg budget. The largest discrepancy between the most recent perspectives on the historical Hg budgets is the magnitude of mining in the Americas from the 16th to 19th century relative to modern industrial emissions. Some reconstructions argue that as a result of the widespread use of Hg in early gold mining, Hg emissions to the atmosphere during the 19th century equaled or exceeded 20th century industrial emissions.[36, 48, 49] Hg profiles from North American trees, lakes, and ice cores, however, generally do not show significant concentration increases during this time period, leading to alternative Hg budgets with lower estimated emissions from mining activities.[50, 51] The FRE and RLK tree records, as well as the recently revised UFG ice-core, document peak Hg concentrations during the 20th century with relatively much smaller increases during the mining eras, supporting the lower mining emissions scenario. These tree samples were collected at a high-elevation site within 10 km of UFG. The ice core records from UFG have been shown to be downwind of western U.S. mining regions[52] and to document a large-scale atmospheric pollution signal similar to Greenland ice cores,[20] where pollution trends were driven primarily by 19th and 20th century emissions from North America and Europe.[53] It seems unlikely that emissions of the magnitude suggested by high-mining emissions scenarios would not be reflected either in the ice or tree-ring records unless these postulated mining emissions were overestimated or they were not transported to these sites.

Acknowledgements

We thank the Sulo and Aileen Maki Endowment at the Desert Research Institute and the University of Nevada, Reno Graduate Student Association for funding this research. We thank the U.S. Forest Service for allowing sample collection in the Fitzpatrick Wilderness within the Shoshone National Forest.

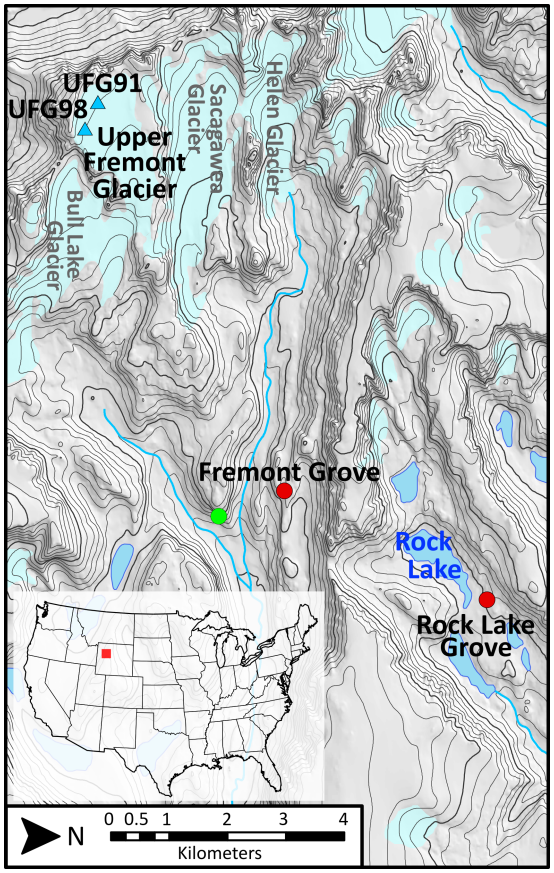

Figure 1. Location of tree stands for this study (red dots), the UFG91 and UFG98 ice cores (blue triangles), and the location of the tree stand used to develop the revised UFG ice-core chronologies from Chellman et al.[20] (green dot).

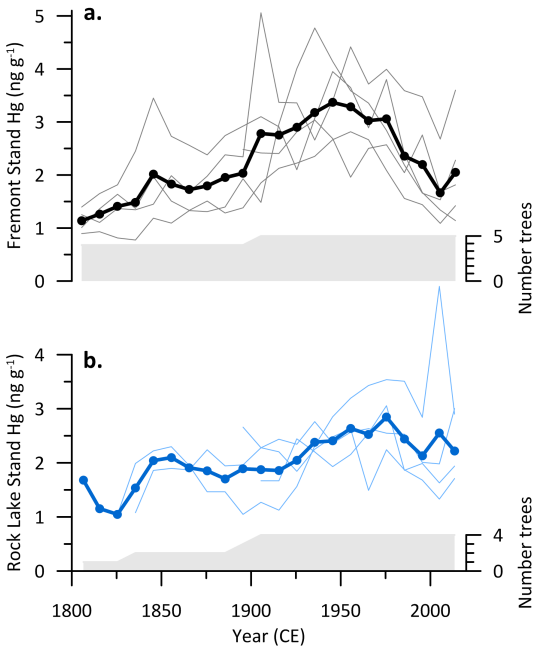

Figure 2. Tree Hg profiles (a) Fremont stand (FRE) individual tree Hg profiles (grey lines) with site average (black line) and number of contributing records (grey bar). (b) Rock Lake stand (RLK) individual tree Hg profiles (light blue lines) with site average (dark blue line) and number of contributing records (grey bar).

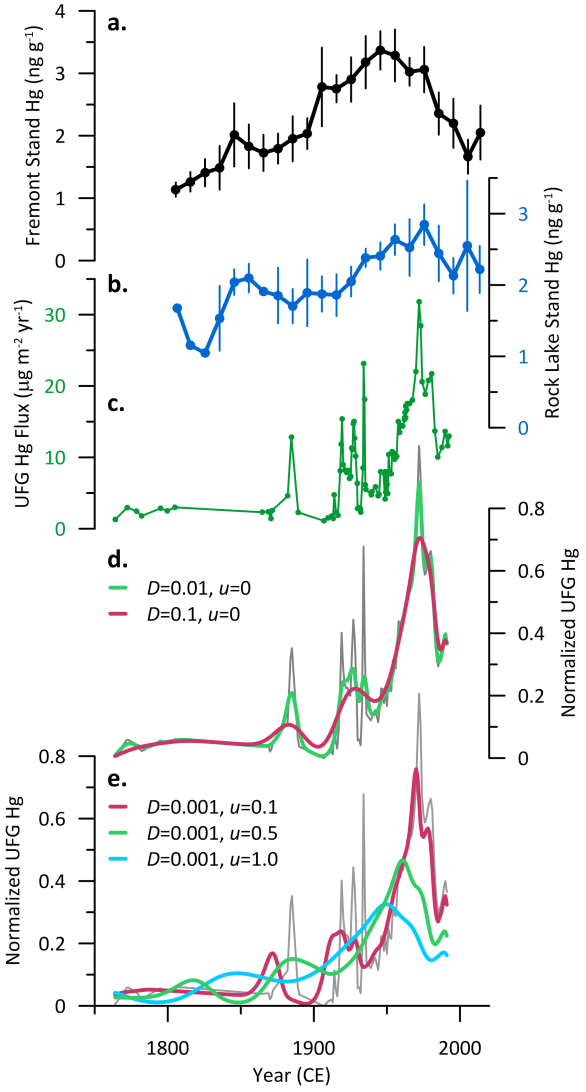

Figure 3. Results for advection-diffusion model. (a) FRE average Hg. (b) RLK average Hg. Error bars for both (a) and (b) represent standard error of the mean. (c) UFG ice core Hg.[19,20] (d) Results for diffusion-only model. (e) Results for advection-diffusion model.

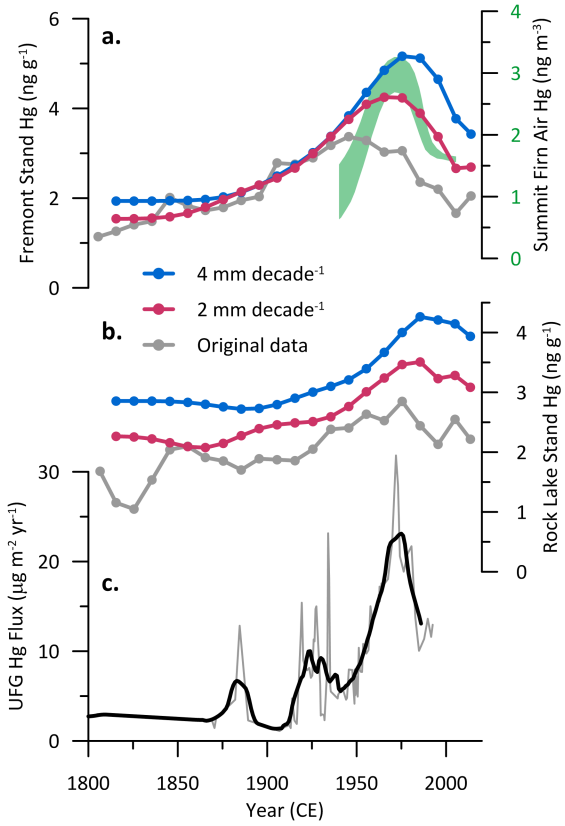

Figure 4. Results for inverse diffusion-advection model. (a) and (b) inverse advection-modeled decadal Hg profiles for the FRE and RLK stands, respectively. Green shading in (a) represents Hg measurements in firn air from Summit, Greenland.[21] (c) UFG Hg flux (grey) with 10-yr moving average (black).[19,20]

References

1. Büntgen, U.; Tegel, W.; Nicolussi, K.; McCormick, M.; Frank, D.; Trouet, V.; Kaplan, J. O.; Herzig, F.; Heussner, K. U.; Wanner, H.; Luterbacher, J.; Esper, J., 2500 Years of European Climate Variability and Human Susceptibility. *Science* **2011,** *331* (6017), 578-582.
2. Meko, D. M.; Woodhouse, C. A.; Baisan, C. A.; Knight, T.; Lukas, J. J.; Hughes, M. K.; Salzer, M. W., Medieval drought in the upper Colorado River Basin. *Geophys. Res. Lett.* **2007,** *34* (10), L10705.
3. Salzer, M. W.; Hughes, M. K.; Bunn, A. G.; Kipfmueller, K. F., Recent unprecedented tree-ring growth in bristlecone pine at the highest elevations and possible causes. *P. Natl. Acad. Sci. USA* **2009,** *106* (48), 20348-20353.
4. Pederson, G. T.; Gray, S. T.; Woodhouse, C. A.; Betancourt, J. L.; Fagre, D. B.; Littell, J. S.; Watson, E.; Luckman, B. H.; Graumlich, L. J., The Unusual Nature of Recent Snowpack Declines in the North American Cordillera. *Science* **2011,** *333* (6040), 332-335.
5. Bindler, R.; Renberg, I.; Klaminder, J.; Emteryd, O., Tree rings as Pb pollution archives? A comparison of Pb-206/Pb-207 isotope ratios in pine and other environmental media. *Sci. Total Environ.* **2004,** *319* (1-3), 173-183.
6. Watmough, S. A., Monitoring historical changes in soil and atmospheric trace metal levels by dendrochemical analysis. *Environ. Pollut.* **1999,** *106* (3), 391-403.
7. Navrátil, T.; Nováková, T.; Shanley, J. B.; Rohovec, J.; Matoušková, S.; Vaňková, M.; Norton, S. A., Larch Tree Rings as a Tool for Reconstructing 20th Century Central European Atmospheric Mercury Trends. *Environ. Sci. Technol.* **2018,** *52* (19), 11060-11068.
8. Clackett, S. P.; Porter, T. J.; Lehnherr, I., 400-Year Record of Atmospheric Mercury from Tree-Rings in Northwestern Canada. *Environ. Sci. Technol.* **2018,** *52* (17), 9625-9633.
9. Martín, J. A. R.; Nanos, N.; Miranda, J. C.; Carbonell, G.; Gil Sánchez, L., Volcanic mercury in Pinus canariensis. *Naturwissenschaften* **2013,** *100* (8), 739-747.
10. Nabais, C.; Freitas, H.; Hagemeyer, J., Dendroanalysis: a tool for biomonitoring environmental pollution? *Sci. Total Environ.* **1999,** *232* (1-2), 33-37.
11. Martín, J. A. R.; Gutiérrez, C.; Torrijos, M.; Nanos, N., Wood and bark of Pinus halepensis as archives of heavy metal pollution in the Mediterranean Region. *Environ. Pollut.* **2018,** *239*, 438-447.
12. Wright, G.; Woodward, C.; Peri, L.; Weisberg, P. J.; Gustin, M. S., Application of tree rings dendrochemistry for detecting historical trends in air Hg concentrations across multiple scales. *Biogeochemistry* **2014,** *120* (1-3), 149-162.
13. Engstrom, D. R.; Fitzgerald, W. F.; Cooke, C. A.; Lamborg, C. H.; Drevnick, P. E.; Swain, E. B.; Balogh, S. J.; Balcom, P. H., Atmospheric Hg Emissions from Preindustrial Gold and Silver Extraction in the Americas: A Reevaluation from Lake-Sediment Archives. *Environ. Sci. Technol.* **2014,** *48* (12), 6533-6543.
14. Drevnick, P. E. et al., Spatiotemporal patterns of mercury accumulation in lake sediments of western North America. *Sci. Total Environ.* **2016,** *568*, 1157-1170.
15. Fitzgerald, W. F.; Engstrom, D. R.; Lamborg, C. H.; Tseng, C. M.; Balcom, P. H.; Hammerschmidt, C. R., Modern and historic atmospheric mercury fluxes in northern Alaska: Global sources and Arctic depletion. *Environ. Sci. Technol.* **2005,** *39* (2), 557-568.

16. Enrico, M.; Le Roux, G.; Heimburger, L. E.; Van Beek, P.; Souhaut, M.; Chmeleff, J.; Sonke, J. E., Holocene Atmospheric Mercury Levels Reconstructed from Peat Bog Mercury Stable Isotopes. *Environ. Sci. Technol.* **2017,** *51* (11), 5899-5906.

17. Martínez-Cortizas, A.; Pontevedra-Pombal, X.; Garcia-Rodeja, E.; Novoa-Muñoz, J. C.; Shotyk, W., Mercury in a Spanish peat bog: Archive of climate change and atmospheric metal deposition. *Science* **1999,** *284* (5416), 939-942.

18. Beal, S. A.; Osterberg, E. C.; Zdanowicz, C. M.; Fisher, D. A., Ice Core Perspective on Mercury Pollution during the Past 600 Years. *Environ. Sci. Technol.* **2015,** *49* (13), 7641-7647.

19. Schuster, P. F.; Krabbenhoft, D. P.; Naftz, D. L.; Cecil, L. D.; Olson, M. L.; Dewild, J. F.; Susong, D. D.; Green, J. R.; Abbott, M. L., Atmospheric mercury deposition during the last 270 years: A glacial ice core record of natural and anthropogenic sources. *Environ. Sci. Technol.* **2002,** *36* (11), 2303-2310.

20. Chellman, N.; McConnell, J. R.; Arienzo, M.; Pederson, G. T.; Aarons, S. M.; Csank, A., Reassessment of the Upper Fremont Glacier Ice-Core Chronologies by Synchronizing of Ice-Core-Water Isotopes to a Nearby Tree-Ring Chronology. *Environ. Sci. Technol.* **2017,** *51* (8), 4230-4238.

21. Faïn, X.; Ferrari, C. P.; Dommergue, A.; Albert, M. R.; Battle, M.; Severinghaus, J.; Arnaud, L.; Barnola, J. M.; Cairns, W.; Barbante, C.; Boutron, C., Polar firn air reveals large-scale impact of anthropogenic mercury emissions during the 1970s. *P. Natl. Acad. Sci. USA* **2009,** *106* (38), 16114-16119.

22. Becnel, J.; Falgeust, C.; Cavalier, T.; Gauthreaux, K.; Landry, F.; Blanchard, M.; Beck, M. J.; Beck, J. N., Correlation of mercury concentrations in tree core and lichen samples in southeastern Louisiana. *Microchem. J.* **2004,** *78* (2) 205-210.

23. Arnold, J.; Gustin, M. S.; Weisberg, P. J., Evidence for Nonstomatal Uptake of Hg by Aspen and Translocation of Hg from Foliage to Tree Rings in Austrian Pine. *Environ. Sci. Technol.* **2018,** *52* (3), 1174-1182.

24. Peckham, M. A.; Gustin, M. S.; Weisberg, P. J.; Weiss-Penzias, P., Results of a controlled field experiment to assess the use of tree tissue concentrations as bioindicators of air Hg. *Biogeochemistry* **2019,** *142* (2), 265-279.

25. Navratíl, T.; Šimeček, M.; Shanley, J. B.; Rohovec, J.; Hojdová, M.; Houška, J., The history of mercury pollution near the Spolana chlor-alkali plant (Neratovice, Czech Republic) as recorded by Scots pine tree rings and other bioindicators. *Sci. Total Environ.* **2017,** *586*, 1182-1192.

26. Abreu, S. N.; Soares, A.; Nogueira, A. J. A.; Morgado, F., Tree rings, Populus nigra L., as mercury data logger in aquatic environments: Case study of an historically contaminated environment. *B. Environ. Contam. Tox.* **2008,** *80* (3), 294-299.

27. Hojdová, M.; Navratíl, T.; Rohovec, J.; Žák, K.; Vaněk, A.; Chrastný, V.; Bače, R.; Svoboda, M., Changes in Mercury Deposition in a Mining and Smelting Region as Recorded in Tree Rings. *Water Air Soil Poll.* **2011,** *216* (1-4), 73-82.

28. Siwik, E. I. H.; Campbell, L. M.; Mierle, G., Distribution and trends of mercury in deciduous tree cores. *Environ. Pollut.* **2010,** *158* (6), 2067-2073.

29. Maillard, F.; Girardclos, O.; Assad, M.; Zappelini, C.; Mena, J. M. P.; Yung, L.; Guyeux, C.; Chretien, S.; Bigham, G.; Cosio, C.; Chalot, M., Dendrochemical assessment of mercury releases from a pond and dredged-sediment landfill impacted by a chlor-alkali plant. *Environ. Res.* **2016,** *148*, 122-126.

30. Peckham, M. A.; Sexauer Gustin, M.; Weisberg, P. J., Assessment of the Suitability of Tree Rings as Archives of Global and Regional Atmospheric Mercury Pollution. *Environ. Sci. Technol.* **2019,** *53* (7), 3663-3671.

31. Naftz, D. L.; Klusman, R. W.; Michel, R. L.; Schuster, P. F.; Reddy, M. M.; Taylor, H. E.; Yanosky, T. M.; McConnaughey, E. A., Little ice age evidence from a south-central North America ice core, USA. *Arctic Alpine Res.* **1996,** *28* (1), 35-41.

32. Yamaguchi, D. K., A simple method for cross-dating increment cores from living trees. *Can. J. Forest Res.* **1991,** *21*, (3), 414-416.

33. Holmes, R., Computer-assisted quality control in tree-ring data and measurement. *Tree-Ring Bulletin* **1983,** *43*, 69-75.

34. Guyer, J. E.; Wheeler, D.; Warren, J.A., FiPy: Partial Differential Equations with Python. *Comput. Sci. Eng.* **2009,** *11* (3), 6-15.

35. Pattyn, F., Antarctic subglacial conditions inferred from a hybrid ice sheet/ice stream model. *Earth Planet. Sc. Lett.* **2010,** *295* (3-4), 451-461.

36. Amos, H. M.; Sonke, J. E.; Obrist, D.; Robins, N.; Hagan, N.; Horowitz, H. M.; Mason, R. P.; Witt, M.; Hedgecock, I. M.; Corbitt, E. S.; Sunderland, E. M., Observational and Modeling Constraints on Global Anthropogenic Enrichment of Mercury. *Environ. Sci. Technol.* **2015,** *49* (7), 4036-4047.

37. Van Metre, P. C.; Fuller, C. C., Dual-Core Mass-Balance Approach for Evaluating Mercury and Pb-210 Atmospheric Fallout and Focusing to Lakes. *Environ. Sci. Technol.* **2009,** *43* (1), 26-32.

38. National Atmospheric Deposition Program (NRSP-3). **2019**. NADP Program Office, Wisconsin State Laboratory of Hygeine, 465 Henry Mall, Madison, WI 53706.

39. Eyrikh, S.; Eichler, A.; Tobler, L.; Malygina, N.; Papina, T.; Schwikowski, M., A 320 Year Ice-Core Record of Atmospheric Hg Pollution in the Altai, Central Asia. *Environ. Sci. Technol.* **2017,** *51* (20), 11597-11606.

40. Durnford, D.; Dastoor, A., The behavior of mercury in the cryosphere: A review of what we know from observations. *J. Geophys. Res.-Atmos.* **2011,** *116,* D06305.

41. Edmands, J. D.; Brabander, D. J.; Coleman, D. S., Uptake and mobility of uranium in black oaks: implications for biomonitoring depleted uranium-contaminated groundwater. *Chemosphere* **2001,** *44* (4), 789-795.

42. Watmough, S. A.; Hutchinson, T. C., Historical changes in lead concentrations in tree-rings of sycamore, oak and Scots pine in north-west England. *Sci. Total Environ.* **2002,** *293* (1-3), 85-96.

43. Lageard, J. G. A.; Howell, J. A.; Rothwell, J. J.; Drew, I. B., The utility of Pinus sylvestris L. in dendrochemical investigations: Pollution impact of lead mining and smelting in Darley Dale, Derbyshire, UK. *Environ. Pollut.* **2008,** *153* (2), 284-294.

44. Okada, N.; Hirakawa, Y.; Katayama, Y., Radial movement of sapwood-injected rubidium into heartwood of Japanese cedar (Cryptomeria japonica) in the growing period. *J. Wood Sci.* **2012,** *58* (1), 1-8.

45. Cheng, Z. Q.; Buckley, B. M.; Katz, B.; Wright, W.; Bailey, R.; Smith, K. T.; Li, J. B.; Curtis, A.; van Geen, A., Arsenic in tree rings at a highly contaminated site. *Sci. Total Environ.* **2007,** *376* (1-3), 324-334.

46. Bunn, A. G.; Helfield, J. M.; Gerdts, J. R.; Gleaves, D. A.; Drake, D. C.; Sheppard, P. R., A solvent-based extraction fails to remove mobile nitrogen from western redcedar (Thuja plicata). *Dendrochronologia* **2017,** *44*, 19-21.

47. Okada, N.; Hirakawa, Y.; Katayama, Y., Application of activable tracers to investigate radial movement of minerals in the stem of Japanese cedar (Cryptomeria japonica). *J. Wood Sci.* **2011,** *57* (5), 421-428.

48. Streets, D. G.; Horowitz, H. M.; Jacob, D.; Lu, Z. F.; Levin, L.; ter Schure, A. F. H.; Sunderland, E. M., Total Mercury Released to the Environment by Human Activities. *Environ. Sci. Technol.* **2017,** *51* (11), 5969-5977.

49. Horowitz, H. M.; Jacob, D. J.; Amos, H. M.; Streets, D. G.; Sunderland, E. M., Historical Mercury Releases from Commercial Products: Global Environmental Implications. *Environ. Sci. Technol.***2014,** *48* (17), 10242-10250.

50. Zhang, Y. X.; Jaegle, L.; Thompson, L.; Streets, D. G., Six centuries of changing oceanic mercury. *Global Biogeochem. Cy.* **2014,** *28* (11), 1251-1261.

51. Outridge, P. M.; Mason, R. P.; Wang, F.; Guerrero, S.; Heimburger-Boavida, L. E., Updated Global and Oceanic Mercury Budgets for the United Nations Global Mercury Assessment 2018. *Environ. Sci. Technol.* **2018,** *52* (20), 11466-11477.

52. Aarons, S. M.; Aciego, S. M.; Gabrielli, P.; Delmonte, B.; Koornneef, J. M.; Uglietti, C.; Wegner, A.; Blakowski, M. A.; Bouman, C., Ice core record of dust sources in the western United States over the last 300 years. *Chem. Geol.* **2016,** *442*, 160-173.

53. McConnell, J. R.; Edwards, R.; Kok, G. L.; Flanner, M. G.; Zender, C. S.; Saltzman, E. S.; Banta, J. R.; Pasteris, D. R.; Carter, M. M.; Kahl, J. D. W., 20th-century industrial black carbon emissions altered arctic climate forcing. *Science* **2007**, 317, (5843), 1381-1384.

Chapter 3

Wyoming ice patch record of rapid Holocene climate variability paralleled human activity

Nathan Chellman[1,2*], Gregory T. Pederson[3], Craig M. Lee[4], David B. McWethy[5], Joseph R. McConnell[1], Kathryn Puseman[6], Jeffery R. Stone[7], Sabrina R. Brown[8]

[1]Desert Research Institute, Division of Hydrologic Sciences, Reno, NV
[2]University of Nevada, Reno, Graduate Program of Hydrologic Sciences, Reno, NV
[3]U.S. Geological Survey, Northern Rocky Mountain Science Center, Bozeman, MT
[4]University of Colorado, Institute of Arctic and Alpine Research (INSTAAR), Boulder, CO
[5]Montana State University, Department of Earth Sciences, Bozeman, MT
[6]Paleoscapes Archaeobotanical Services Team, Bailey, CO
[7]Indiana State University, Department of Earth and Environmental Systems, Terra Haute, IN
[8]University of Nebraska-Lincoln, Earth and Atmospheric Sciences, Lincoln, NE

1. Introduction

Linking human history to paleoclimate changes requires well-dated climate proxies and historical data.[1-3] Within western North America, however, Holocene-length climate proxies are limited primarily to lake-sediment cores[4-6] because tree-ring chronologies document only recent millennia,[7, 8] speleothem records from caves[9] are rare and often incomplete, and glacial ice cores—generally considered to be the most direct records of environmental change—are limited to recent centuries.[10] Here, we present a 10,000-year, highly resolved ice-core record of wintertime climate for the northern Rocky Mountains, recovered from an ice patch on the Beartooth Plateau, Wyoming. Our findings indicate this small alpine ice patch preserved a regionally-representative climate record that documented a sustained 800-year period of peak Holocene warmth centered at 4,100 cal BP followed by a rapid cooling leading to a 1,500-year long period of cooler and wetter winters. The ice-patch record suggests rates of winter temperature change at the onset and termination of this cold period were as high as observed rates of modern warming. The well-dated ice-patch climate record closely paralleled human activity in western Wyoming[11] throughout the Holocene, with activity suppressed during both especially warm and cold climate periods.

Receding ice patches in the Rocky Mountains and worldwide are revealing archaeological materials—including wooden hunting shafts, basketry, leather objects, and the remains of hunted animals—reflecting human and animal behavior in alpine settings throughout the Holocene.[12, 13] Although their archaeological significance has been well-established, the potential for ice patches to provide paleoclimate records largely has been unexplored.[14] Here, we investigated the potential for ice patches to serve as paleoclimate archives by developing records of ice accumulation and water isotopes from a well-dated, 5.6 m-long ice core recovered from an ice patch on the Beartooth Plateau (Fig. 1). A 10,300-year-old artifact was previously identified along the melting edge of this ice patch, indicating the presence of early Holocene ice.[15]

2. Methods

2.1 Beartooth Ice Patch

Three ice cores were recovered from an ice patch on the Beartooth Plateau (elevation 3,145 masl, Shoshone National Forest, Wyoming) in late August 2016. The ice patch, referred to as ice patch TL1, faced northeast and was ellipsoidal in shape with a horizontally-oriented long-axis 215 m in length and short axis parallel to the underlying slope 120 m in length. The cores were recovered using a 4" electromechanical, two-barrel drill powered by a 2-kW generator.[16] The lengths of the three cores were 5.61 m, 2.88 m, and 1.69 m, and hereafter will be Core 1, Core 2, and Core 3, respectively (Fig. 4). Cores 1 and 2 were generally good quality, with most pieces longer than 30 cm. Core 2 was recovered as small pieces, however, less than 5 cm in length between depths 1.5 and 2.53 m, leading to uncertainty in the orientation and order of ice recovered in this section. Core 3 was poor quality, with many chips and re-drilled sections caused by partial recovery of previous drill runs that left ice in the borehole. Cores 1 and 2 were comprised of units of intact ice bisected by organic layers (Fig. 4). The organic layers were removed in the field using a hand saw and stored unfrozen in screw-cap plastic containers for further analysis. The intact ice units between organic layers were bagged, immediately stored in the field in foam-insulated ice core boxes with dry ice, and transported frozen to the Desert Research Institute (DRI), Reno, Nevada.

To develop a depth-age scale, organic material from each of the 29 organic layers from Core 1 was radiocarbon dated (Table 1). The R-package Bacon v2.2 was used to calculate the date of the radiocarbon age as calibrated year before present (cal BP) using IntCal13 and develop a depth-age model with an associated uncertainty for the core.[17-19] The net ice accumulation or accretion rate was calculated as the slope of the depth-age model.

All cores were subsampled for discrete analysis at DRI. On average, cores were subsampled at 5-cm depth resolution, although resolution in some sections was a high as 2 cm to

permit sampling between closely-spaced organic layers and as low as 8 cm in sections with poor ice quality. Frozen subsamples were rinsed with 18 MΩ ultrapure water, transferred to clean Whirlpak® bags, and melted at room temperature. The meltwater was transferred to 50 ml polypropelene vials, sonicated for 10 minutes, and subsequently analyzed for water isotopes ($\delta^{18}O$, δD). Water isotopes were measured using a Picarro 2130i (Picarro Inc., Santa Clara, CA) calibrated to Vienna Standard Mean Ocean Water (VSMOW). All samples were analyzed within eight hours of melting. A 20 μm stainless steel filter was installed inline prior to the instrumentation to prevent downstream clogging of sample flow lines.

Cores 2 and 3 were synchronized to an equivalent-Core 1 depth to facilitate comparisons of water isotope measurements. Assuming continuity in the organic layers through the ice patch, Core 2 was synchronized to Core 1 using the uppermost six organic layers as tie points. Because only one organic layer was recovered in the shallower Core 3 and overall ice quality was poor, Core 3 was visually synchronized to Core 1 using water isotope data.

To estimate the magnitude of temperature change, the $\delta^{18}O$ record was transformed to temperature using established $\delta^{18}O$-temperature relationships. Because no site-specific relationship exists for the ice-patch site, we used previously published values from the Fremont Glacier (47.127 °N 109.615 °W; 4,000 masl; $\delta^{18}O = 0.587 * °C - 12.6$) located approximately 200 km away in the Wind River Range, WY,[20] and the regional average $\delta^{18}O$-temperature relationship ($\delta^{18}O = 0.403 * °C - 17.698$) determined by modern snow pit studies across the Rocky Mountains,[21] These two relationships served as the maximum and minimum estimates, respectively, of the magnitude of temperature change. The magnitude of changes was calculated as the difference between the average value of three $\delta^{18}O$ measurements from either side of the transition. The magnitude of temperature change during the Holocene suggested by these relationships is within a factor of two compared to Minnetonka Cave, which may be attenuated by its sensitivity to rain and mean annual temperature within the cave.[9]

We used the 2σ ranges of the calibrated radiocarbon dates, which are absolute controls on the age of the adjacent ice and have less uncertainty than the modeled age scale, of the organic layers directly below each ice unit associated with the warm or cool isotopic values to estimate the duration of the temperature change. The ages of the preserved ice units may be biased toward the underlying organic layer because shallower ice would be preferentially lost during periods of melt. The maximum and minimum durations for the temperature change were calculated as the difference of the older-range of the 2σ uncertainty for the older date and the younger-range of the 2σ uncertainty for the younger date, and vice versa, respectively.

The maximum and minimum rate of temperature change were subsequently calculated using the maximum magnitude of temperature change divided by the minimum duration of temperature change, and vice versa, respectively. Note that, as calculated, the rates of change presented here are constraints on the maximum possible rate of change, as we neglect potential contributions from atmospheric variability or preservation biases to the $\delta^{18}O$ signal.

2.2 Island Lake

In July 2013, a 1.5 m-long lake sediment core was recovered from the central basin of Island Lake (46.949 °N 109.543 °W; 2,904 masl) using a Griffith corer.[35] A depth-age model was developed in the R-package Bacon v2.2 from eight extracted pollen samples radiocarbon dated at the Accelerator Mass Spectrometry Lab (directAMS, Bothell WA) (Fig. 7; Table 2) and calibrated using IntCal13.[17-19] The sediment accumulation rate was calculated as the slope of the depth-age model.

3. Results and Discussion

Unlike polar and alpine ice cores consisting of clean ice, the core recovered from the Beartooth Plateau ice patch was comprised of ice units bisected by organic layers containing plant

remains, animal dung, and soil. This stratigraphy indicated that ice accretion occurred during extended periods of positive mass balance interrupted sporadically by periods of negative mass balance that concentrated matter from melting snow and ice, along with windblown or animal-borne debris, on the ice-patch surface. Although the formation of such layers required a hiatus in ice accretion, therefore precluding preservation of a temporally-continuous ice record, the layers were crucial for developing a robust chronology.

A total of 29 organic layers were found in the ice core (Figs. 2, 4). Because traditional ice-core dating techniques such as volcanic synchronization or annual layer counting were not applicable, we constrained the ages of the ice units using ^{14}C-derived ages of intact organic material selected from each organic layers between them. The radiocarbon dates were used (Table 1) to develop an age model[18] with an average uncertainty of ±152 years (±2σ) (Fig. 2). Within their associated uncertainties, all but two of the 29 calibrated radiocarbon ages were in chronological order.

The deepest layer was radiocarbon dated to ca. 10,350 cal BP, implying the ice patch has persisted for more than 10,000 years, and the continuity of the radiocarbon dates suggests it consistently accreted ice throughout the Holocene. The chronology shows a marked change at 3,560 (3,880 to 3,410) cal BP (median and 95% confidence interval of modeled age scale; Fig. 2) when average net ice accretion more than doubled from 0.02–0.04 cm yr^{-1} to 0.04–0.12 cm yr^{-1} (Fig. 3). Organic layers formed at a frequency of 315±235 (±2σ) years with no consistent relationship to the centennial-scale climate records presented here, though layer formation may be related to extended warm, dry periods on finer time scales.

Ice accretion likely is controlled by a combination of temperature and precipitation—ice patches are too thin for ice to form through compaction and overburden pressure that are the mechanisms for ice formation in most polar and alpine glacial settings. Rather, it is possible that a small fraction of percolating surface meltwater accretes at the ice-snow interface by refreezing.[22]

Ice accretion appears to have been relatively continuous in the Beartooth Plateau ice patch, evidenced by parallel changes in $\delta^{18}O$ values during the past 800 years in the uppermost ice unit and in a well-dated speleothem from Minnetonka Cave[9] in southeastern Idaho (Fig. 5). We posit that ice accretion was more sensitive to temperature than precipitation, since the observed ice-accretion rates of less than 0.12 cm yr^{-1} required only minimal seasonal snow accumulation and the topographic setting of the ice patch at the edge of a plateau ensured sufficient accumulation from drifting even in drier winters.

Stable water isotope ($\delta^{18}O$, δD) measurements in the ice were used to develop a record of the isotopic composition of wintertime precipitation. The $\delta^{18}O$ record varied significantly during the Holocene, ranging from -24 to -16‰ (Fig. 3), and the recent $\delta^{18}O$ range was comparable to values from an ice core in the nearby Wind River Range.[20] Consistency of $\delta^{18}O$ values between three parallel cores from the ice patch indicated that records were spatially coherent. Comparisons of $\delta^{18}O$ and δD values to the Global Meteoric Water Line[23] suggested little impact from post-depositional processes such as evaporation (Fig. 6).

A number of physical processes may influence the $\delta^{18}O$ records preserved in the ice patch, including atmospheric circulation,[24] site temperature,[20] and seasonal biases in the preservation,[25] Large-scale atmospheric circulation patterns have been linked to water isotope variability in modern precipitation,[26] but model simulations show Holocene $\delta^{18}O$ changes of ~0.5 to 1‰,[27] much less than the observed ~4‰ variability, suggesting temperature and preservation biases are stronger contributors to the $\delta^{18}O$ signal.

We used the ice-accretion rate and $\delta^{18}O$ record, in conjunction with the precipitation-sensitive sediment accumulation rate from nearby Island Lake[28] (Figs. 3, 7), to develop a record of Holocene climate. We assumed that the ice-accretion rate was indicative of overall temperature, with cooler climates associated with increased ice accumulation, while the $\delta^{18}O$ was

a qualitative indicator of wintertime site temperature, with depleted isotopic compositions representing cooler winters.

Beginning 10,000 years ago, the $\delta^{18}O$ value was relatively stable until ca. 7,000 cal BP, suggesting little variation in wintertime temperatures. A brief increase in ice accumulation rate at 9,100 (9,280 to 9,040) cal BP reflected cooler overall temperatures. This coincided initially with higher sedimentation rates resulting from enhanced runoff in Island Lake—indicating wetter conditions—and a hiatus in speleothem growth in Minnetonka Cave, attributed to cooler or wetter conditions.[9] At 7,140 (7,250 to 6,960) cal BP, a short-lived cooling, evidenced by rapid depletion of $\delta^{18}O$ values to -21‰ and an increased ice-accretion rate, preceded gradual wintertime warming until 4,230 (4,380 to 4,060) cal BP when the $\delta^{18}O$ value reached a local maximum of -17‰, paralleling Northern Hemisphere pollen-derived temperature reconstructions that suggest a mid-Holocene warm period.[29] Between ca. 4,200 and 3,800 cal BP, high $\delta^{18}O$ values and low ice accretion indicated conditions in the region were the warmest of the Holocene prior to the last millennium. This warming coincided with widespread aridity at 4,200 cal BP recorded worldwide in a range of proxies, including from western North America,[30] as well as warm temperatures indicated by the Minnetonka Cave speleothem record.[9]

Between 3,930 (4,080 to 3,730) and 3,560 (3,880 to 3,410) cal BP, the ice-patch and Island Lake records showed a rapid transition to cooler and wetter conditions, evidenced by the synchronous decline in $\delta^{18}O$ values to between -21‰ and -24‰ and doubling of the net ice accretion rate in the ice patch, as well as a comparable increase in sedimentation rate in Island Lake (Fig. 3). Around this time, a hiatus attributed to cooler or wetter winters occurred in Minnetonka Cave[9] speleothem growth, and the Bison Lake calcite $\delta^{18}O$ record shifted from rain- to snow-dominated winter precipitation.[4] Furthermore, cooler temperatures were recorded in lakes in the Bighorn Mountains, Wyoming, and North Dakota ca. 3,000 cal BP.[5, 6] This cold and wet period coincided with glacial advances in the Canadian Rockies during the Neoglacial[31] and

the Neopluvial in the Great Basin characterized by highstands among many Utah and Nevada lakes.[32] Increased late Holocene moisture also has been noted in other lake-sediment records.[6]

The ice-patch $\delta^{18}O$ record remained depleted until 2,050 (2,240 to 1,970) cal BP, with relatively high ice- and sediment-accumulation rates in the ice patch and Island Lake, respectively, suggesting a prolonged era of cooler and wetter winters. This cool era is distinct in the ice-patch $\delta^{18}O$ record, with rapid transitions of greater than 3‰ bracketing 1,500-years of below-average values. The ice patch $\delta^{18}O$ record provided constraints on the rate of temperature change at the onset and termination of this Neoglacial period (see Methods), with a maximum rate of cooling at the onset of 0.08 to 0.15 °C per decade between ca. 3,930 and 3,560 cal BP, and a maximum rate of warming at the termination of 0.10 to 0.22 (between ca. 2,050 and 1,690 cal BP) °C per decade. Although many less-direct paleoclimate archives underestimate the rate of environmental change,[33] the rates from the ice-patch record are comparable to modern rates of observed warming and are some of the highest recorded among non-polar climate proxies, suggesting that the pace of regional-scale climate variability during the mid-Holocene may have been similar to present-day warming. The rate of temperature change suggested by the ice patch is an upper constraint as it excludes other factors that control the isotopic composition such as preservation bias or changing moisture sources and storm tracks.

The cool era ended with an abrupt $\delta^{18}O$ increase from -21‰ to -18‰ between 2,050 (1,970 to 2,240) and 1,690 (1,610 to 1,780) cal BP followed by a gradual increase to modern levels between -16‰ and -19‰, indicating a wintertime warming trend during the past millennium in close agreement with Minnetonka Cave[9] (Fig. 5). Although the cave calcite $\delta^{18}O$ value is driven largely by wintertime precipitation in the form of snow, it also is sensitive to rain and mean annual cave temperature,[9] resulting in overall lower variability than in the ice patch. The cave also is located at a lower elevation resulting in a more enriched $\delta^{18}O$ signal.

The climate variability preserved in the ice patch paralleled Native American activity as inferred from radiocarbon dates on archaeological materials in the nearby Bighorn Basin for most of the Holocene as reconstructed by ^{14}C-dated archaeological sites (Fig. 3).[11] A major decline in human activity in the region beginning between 4,500 and 4,000 cal BP,[11, 34] a trend not evident in other regions of North America,[35] coincided with the onset of the warmest winter temperatures indicated in the ice-patch record during the mid-Holocene (Fig. 3). Indicators of human activity remained low during the unusually cold, wet Neoglacial period suggesting that such conditions may have inhibited human activity in the Bighorn Basin, which is at odds with the previous interpretation that cool and wet periods fostered population growth.[11] Activity did not increase until ca. 2,000 cal BP when the ice-patch δ^{18}O record indicated a return to milder conditions. Human activity paralleled increasing δ^{18}O values until 1,100 cal BP, after which it again rapidly declined coeval with warm temperatures, as indicated by ice-patch δ^{18}O values and North American warmth associated with the Medieval Climate Anomaly.[36] Human activity since 1,100 cal BP remained low, coinciding with isotopic values exceeding -18‰ for much of the last millennia.

The rapid increases in human activity leading to maxima at ca. 1,200 and 4,500 cal BP each corresponded to δ^{18}O values between -18 and -19‰, but abruptly ended when δ^{18}O exceeded -18‰, suggesting conditions surpassed a climatic threshold that no longer supported high levels of human activity in the region. Although other factors such as social patterns and cultural preferences influenced human activity, the close parallels with climate during the past 10,000 years suggested that climate extremes were likely an important influence on human activity in the region.

Acknowledgments

We thank U. Wisconsin Ice Drilling Design and Operations, M. Jayred for assistance in drilling the cores, and all of the project field and laboratory assistants. This project was funded by Buffalo Bill Historical Center's Draper Natural History Museum, University of Wyoming's Biodiversity Institute, Prince Albert II of Monaco Foundation—Monaco and USA, NSF grant BCS 1832486, the U.S. Geological Survey Ecosystem Program and Climate Research and Development Program, and the Sulo and Aileen Maki Endowment at the Desert Research Institute. Any use of trade, firm, or product names is for descriptive purposes only and does not imply endorsement by the U.S. Government.

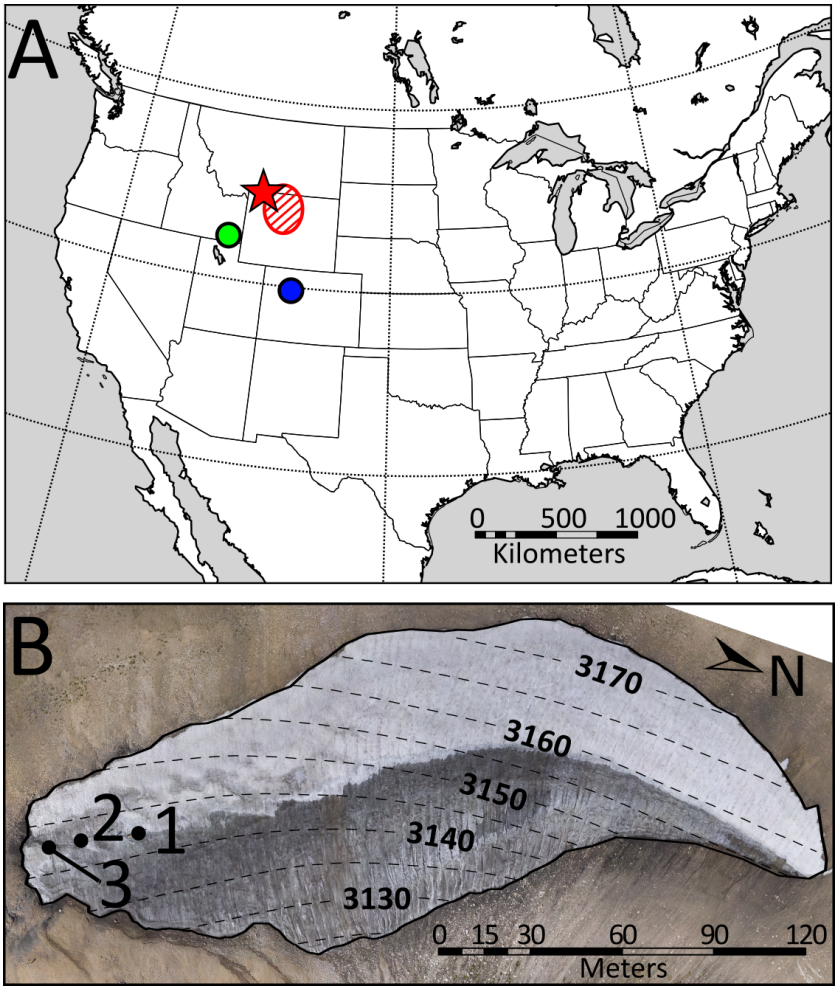

Figure 1. Location of archives. (A) Beartooth Plateau ice patch and Island Lake (red star), Minnetonka Cave[9] (green circle), Bison Lake[4] (blue circle), Bighorn Basin (red hatched oval). (B) Outline and aerial photo of the ice patch taken in August 2016, including coring locations (numbers correspond to cores as described in Methods) and elevation contours. [Aerial photo credit: J. Strait, Montana Department of Environmental Quality]

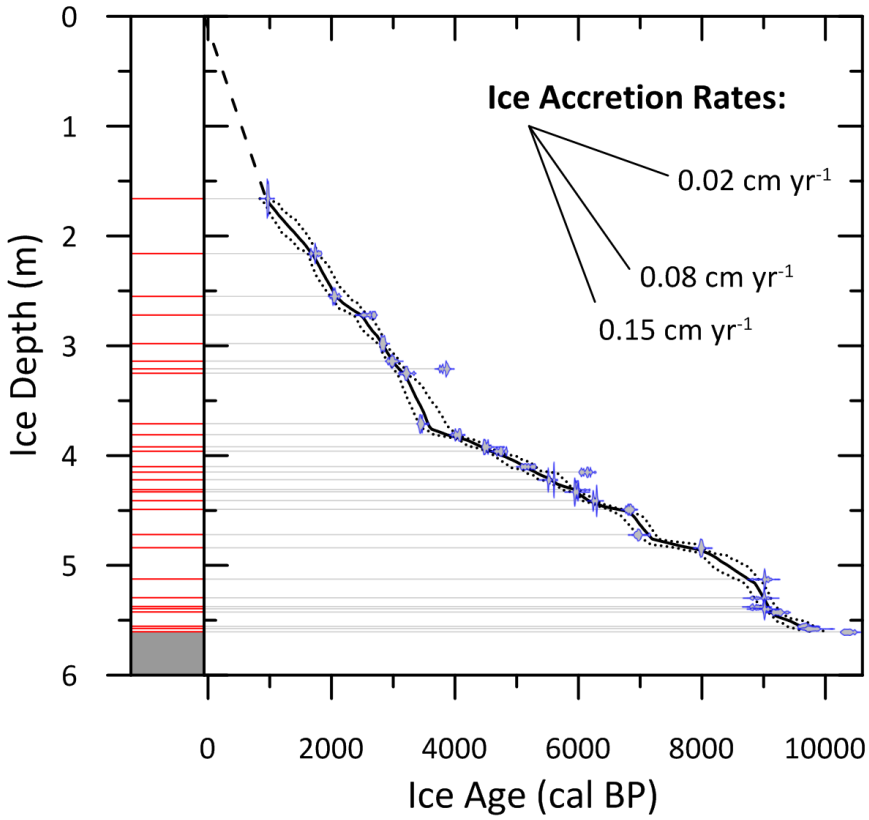

Figure 2. Beartooth Plateau ice-core profile and chronology. 29 organic layers (left, red) were identified in the 5.6 m-long core and their respective radiocarbon ages used to develop a chronology. At right, modeled age (black solid line) with 95% confidence intervals (black dotted lines). Dashed line indicates uncertainty in age from the uppermost organic layer (1.6 m) to the surface. Radiocarbon dates (blue) derived from Bayesian depth-age modeling[16] have ranges in calibrated age shown as horizontal extents and age probabilities shown as vertical extents.

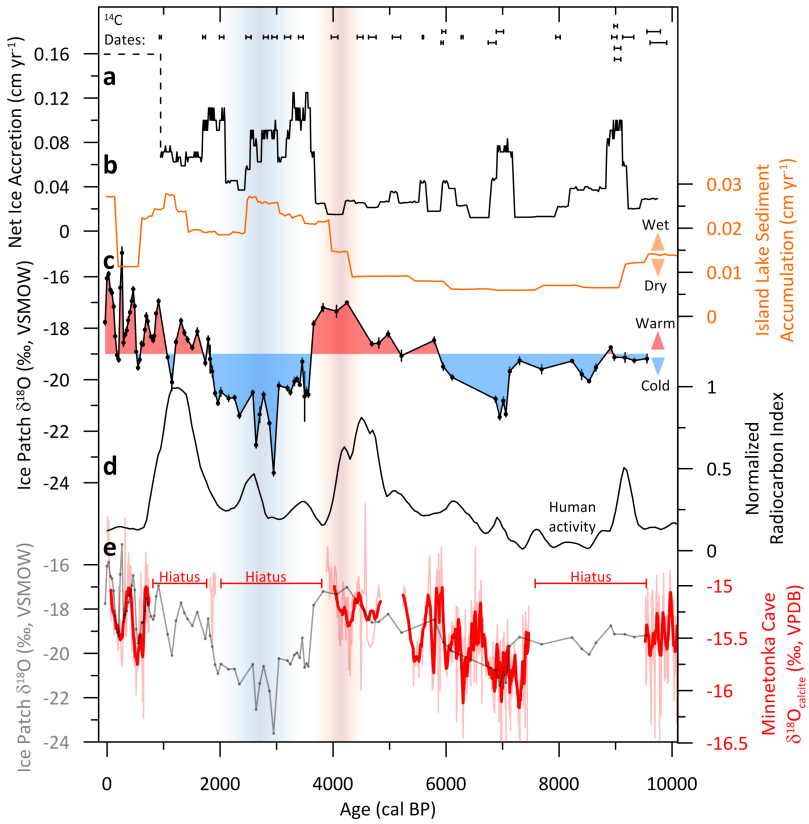

Figure 3. Paleoclimate data from the Beartooth Plateau ice patch and other archives. Red vertical shading indicates timing of maximum warmth recorded in the ice patch. Blue vertical shading indicates cooler and wetter climate from ca. 3,560 to 2,050 cal BP. (A) Ice-patch radiocarbon dates and net ice-accretion rate (black; dashed line to first age control point indicates uncertainty in current mass balance). (B) Island Lake[28] sediment-accumulation rate (orange). (C) Ice-patch $\delta^{18}O$ record (black) with shading relative to the record average. (D) Normalized radiocarbon index for the Bighorn Basin (black),[11] a proxy for human activity. (E) Minnetonka Cave speleothem $\delta^{18}O$ record[9] (red with 11-point running average), a proxy for wintertime temperature, and ice-patch $\delta^{18}O$ (grey). Hiatus in cave record indicate cold or wet periods.

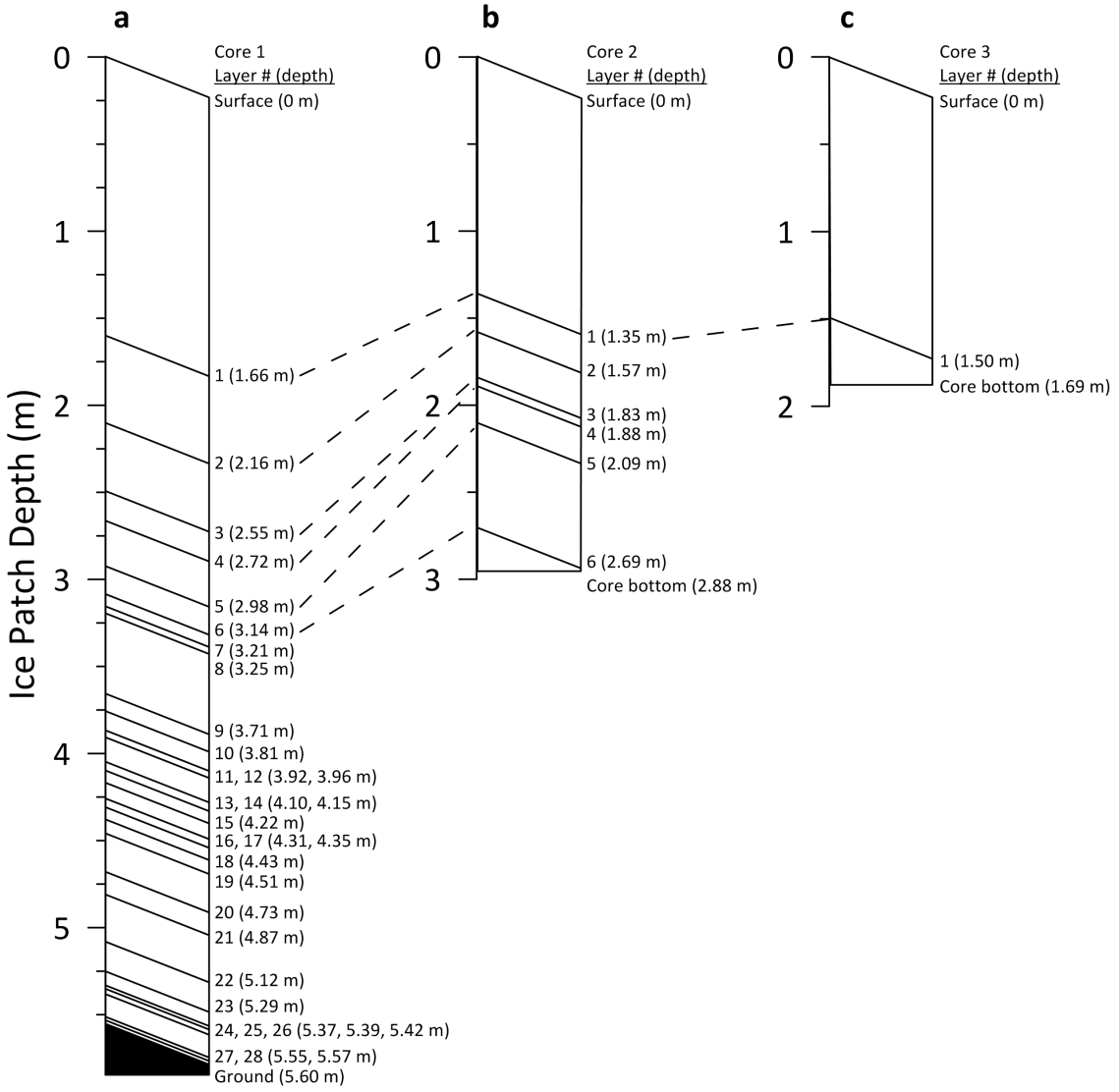

Figure 4. Schematics of ice patch cores. Profiles for (A) Core 1. (B) Core 2. (C) Core 3. Organic layers dipped at an angle approximately parallel to the surface slope of the ice patch. Relative patterns of organic layers between Cores 1 and 2 are similar, suggesting that the ice accretion rate as calculated from Core 1 also is representative of Core 2. The shallowest organic layer is at a similar depth in all three cores, suggesting relatively uniform ice accretion rates across the ice patch during the past ~900 years.

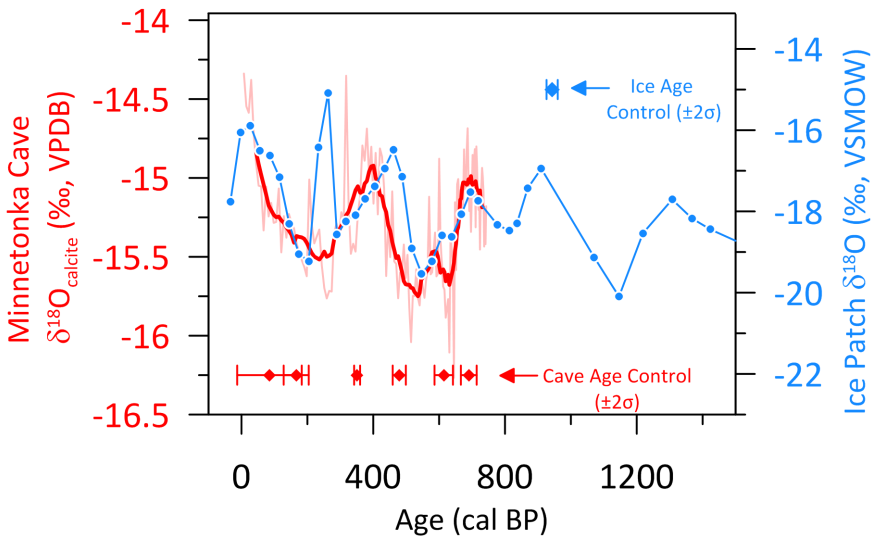

Figure 5. Comparison of $\delta^{18}O$ records from Minnetonka Cave (red with 11-point running average)[9] and ice patch Core 1 (blue) during the past 1400 years. Both $\delta^{18}O$ records are thought to be representative of wintertime meteoric precipitation. The chronology (red diamonds at bottom) for Minnetonka Cave suggests consistent accumulation at the cave during the past 800 years. The agreement between the ice patch, assuming constant accumulation between the surface at present and the first age control point (blue diamond at top), and cave calcite $\delta^{18}O$ implies that ice accretion is relatively continuous during this time period.

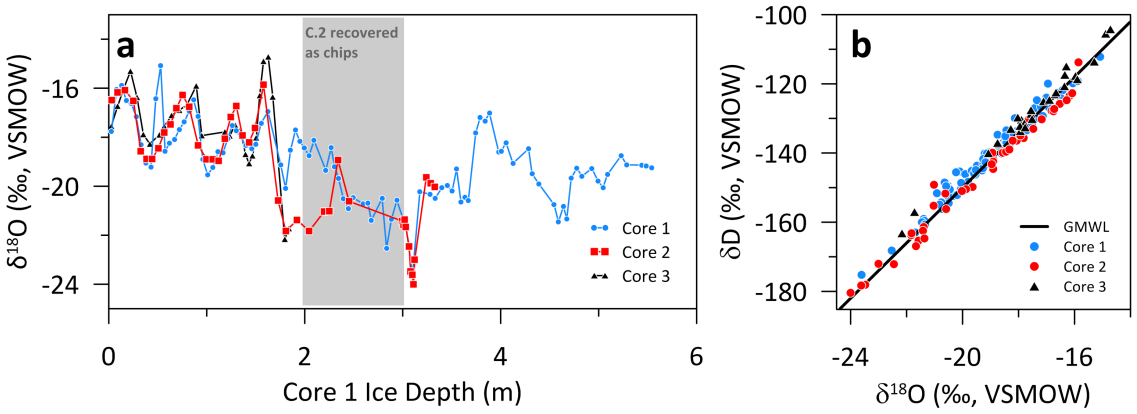

Figure 6. Water isotope measurements in three parallel cores recovered from the ice patch. (A) $\delta^{18}O$ measurements synchronized to equivalent Core 1 depth. Core 2 was synchronized to Core 1 solely using organic layers. Core 3 was synchronized to Core 1 by manual synchronization of $\delta^{18}O$ data. Shaded area indicates poor quality for recovered Core 2 ice, leading to uncertainty in orientation and sequence of samples. (B) $\delta^{18}O$ and δD measurements plot along the Global Meteoric Water Line (GMWL; defined as $\delta D = 8*\delta^{18}O + 10‰$),[23] suggesting minimal to no alteration from post-depositional processes such as evaporation.

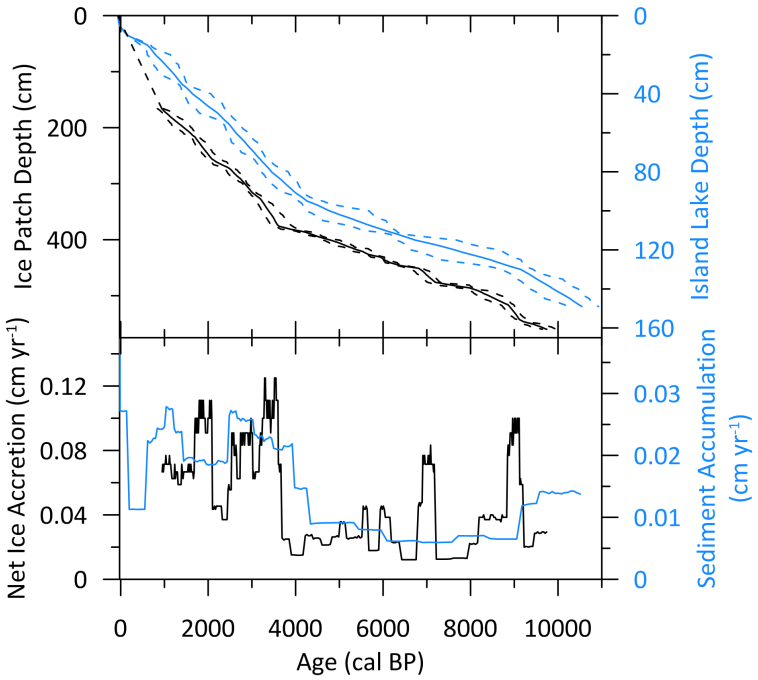

Figure 7. Comparison of chronologies (top), as well as net ice accretion and sediment accumulation rates (bottom) for the ice patch (black) and Island Lake[28] (blue), respectively.

Organic Layer	Depth (cm)	Material Selected	Uncalibrated Radiocarbon Age	Radiocarbon Age Stddev
1	166.0	Sagebrush stem	1,025	±15
2	216.0	Unidentified plant material/Digesta	1,790	±15
3	255.0	Grass stem and Grass seeds	2,060	±15
4	272.0	Unidentified plant material/Digesta	2,465	±15
5	298.0	Unidentified plant material/Digesta	2,715	±20
6	314.0	Legume pod	2,850	±20
7	321.0	Unidentified plant material/Digesta	3,540	±20
8	325.0	Grass stem and Grass seeds	3,005	±20
9	371.0	Unidentified plant material/Digesta	3,220	±20
10	381.0	Grass stem, Grass seed, and Cinquefoil seeds	3,680	±20
11	392.0	Unidentified plant material/Digesta	4,030	±20
12	396.0	Grass stem and Grass seed	4,175	±20
13	410.0	Spruce needle	4,500	±20
14	415.0	Unidentified plant material/Digesta	5,340	±20
15	422.0	Wildrye seed, Cinquefoil seed, and Digesta	4,825	±20
16	431.0	Grass seed, Digesta, and Insect chitin	5,220	±20
17	435.0	Grass stem and Bluegrass seeds	5,185	±20
18	443.0	Grass stem and Wildrye seeds	5,460	±20
19	451.0	Unidentified plant material/Digesta	5,980	±25
20	473.0	Grass stem	6,095	±25
21	487.0	Cinquefoil seeds	7,165	±30
22	512.5	Grass stem, Wildrye seed, and Digesta	8,085	±30
23	529.5	Grass stem, Grass seed, and Digesta	8,065	±30
24	537.5	Grass stem	8,045	±30
25	539.5	Grass stem	8,080	±30
26	542.5	Unidentified plant material/Digesta	8,255	±30
27	555.5	Grass seeds and Bluegrass seeds	8,725	±30
28	557.5	Pine needle	8,765	±35
29	560.5	Grass seeds	9,215	±35

Table 1. Depths, materials, and radiocarbon dates used to develop the ice core chronology.

Sample	Depth (cm)	Material Selected	Uncalibrated Radiocarbon Age	Radiocarbon Age Stddev
33	16	Pollen	700	±29
71	35	Pollen	1512	±28
109	54	Pollen	2377	±31
149	73	Pollen	2978	±27
185	92	Pollen	3731	±28
223	111	Pollen	5455	±33
261	130	Pollen	8218	±80
299	149	Pollen	9374	±75

Table 2. Depths, materials, and radiocarbon dates[28] used to develop the Island Lake chronology.

References

1. Kuper, R.; Kropelin, S., Climate-controlled Holocene occupation in the Sahara: Motor of Africa's evolution. *Science* **2006,** *313*, (5788), 803-807.
2. Buntgen, U.; Tegel, W.; Nicolussi, K.; McCormick, M.; Frank, D.; Trouet, V.; Kaplan, J. O.; Herzig, F.; Heussner, K. U.; Wanner, H.; Luterbacher, J.; Esper, J., 2500 Years of European Climate Variability and Human Susceptibility. *Science* **2011,** *331*, (6017), 578-582.
3. deMenocal, P. B., Cultural responses to climate change during the Late Holocene. *Science* **2001,** *292*, (5517), 667-673.
4. Anderson, L., Holocene record of precipitation seasonality from lake calcite delta O-18 in the central Rocky Mountains, United States. *Geology* **2011,** *39*, (3), 211-214.
5. Shuman, B., Recent Wyoming temperature trends, their drivers, and impacts in a 14,000-year context. *Climatic Change* **2012,** *112*, (2), 429-447.
6. Shuman, B. N.; Marsicek, J., The structure of Holocene climate change in mid-latitude North America. *Quaternary Sci. Rev.* **2016,** *141*, 38-51.
7. Pederson, G. T.; Gray, S. T.; Woodhouse, C. A.; Betancourt, J. L.; Fagre, D. B.; Littell, J. S.; Watson, E.; Luckman, B. H.; Graumlich, L. J., The Unusual Nature of Recent Snowpack Declines in the North American Cordillera. *Science* **2011,** *333*, (6040), 332-335.
8. Salzer, M. W.; Bunn, A. G.; Graham, N. E.; Hughes, M. K., Five millennia of paleotemperature from tree-rings in the Great Basin, USA. *Clim. Dynam.* **2014,** *42*, (5-6), 1517-1526.
9. Lundeen, Z.; Brunelle, A.; Burns, S. J.; Polyak, V.; Asmerom, Y., A speleothem record of Holocene paleoclimate from the northern Wasatch Mountains, southeast Idaho, USA. *Quatern. Int.* **2013,** *310*, 83-95.
10. Chellman, N.; McConnell, J. R.; Arienzo, M.; Pederson, G. T.; Aarons, S. M.; Csank, A., Reassessment of the Upper Fremont Glacier Ice-Core Chronologies by Synchronizing of Ice-Core-Water Isotopes to a Nearby Tree-Ring Chronology. *Environ. Sci. Tech.* **2017,** *51*, (8), 4230-4238.
11. Kelly, R. L.; Surovell, T. A.; Shuman, B. N.; Smith, G. M., A continuous climatic impact on Holocene human population in the Rocky Mountains. *P. Natl. Acad. Sci. USA* **2013,** *110*, (2), 443-447.
12. Lee, C. M.; Puseman, K., Ice patch hunting in the Greater Yellowstone Area, Rocky Mountains, USA: Wood shafts, chipped stone projectile points, and bighorn sheep (Ovis canadensis). *Am. Antiquity* **2017,** *82*, (2), 223-243.
13. Reckin, R. Ice Patch Archaeology in Global Perspective: Archaeological Discoveries from Alpine Ice Patches Worldwide and Their Relationship with Paleoclimates. *J. World Prehist.* **2013,** 26, 323-385.
14. Lee, C.M. "Continuing Archeological and Paleobiological Reconnaissance of Perennial Ice and Snow Patches" (US Forest Service ARPA Permit Report CFK317, 2018).
15. Lee, C.M. Global warming reveals wooden artefact frozen over 10,000 years ago in the Rocky Mountains. *Antiquity* **2010,** 325.

16. Kyne, J.; McConnell, J., The PrairieDog: A double-barrel coring drill for 'hand' augering. *Ann. Glaciol.* **2007,** *47*, 99-100.

17. Reimer, P. J. et al., IntCal13 and Marine13 radiocarbon age calibration curves 0-50,000 years cal BP. *Radiocarbon* **2013,** *55*, (4), 1869-1887.

18. Blaauw, M.; Christen, J. A., Flexible Paleoclimate Age-Depth Models Using an Autoregressive Gamma Process. *Bayesian Anal.* **2011,** *6*, (3), 457-474.

19. R Development Core Team, 2013. R: A language and environment for statistical computing. R Foundation for Statistical Computing, Vienna, Austria. ISBN 3-900051-07-0, URL http://www.r-project.org.

20. Naftz, D. L.; Susong, D. D.; Schuster, P. F.; Cecil, L. D.; Dettinger, M. D.; Michel, R. L.; Kendall, C., Ice core evidence of rapid air temperature increases since 1960 in alpine areas of the Wind River Range, Wyoming, United States. *J. Geophys. Res.-Atmos.* **2002,** *107*, (D13), 1-16.

21. Anderson, L.; Berkelhammer, M.; Mast, M. A., Isotopes in North American Rocky Mountain Snowpack 1993-2014. *Quaternary Sci. Rev.* **2016,** *131*, 262-273.

22. Meulendyk, T.; Moorman, B. J.; Andrews, T. D.; MacKay, G., Morphology and Development of Ice Patches in Northwest Territories, Canada. *Arctic* **2012,** *65*, 43-58.

23. Craig, H., Isotopic variations in meteoric waters. *Science* **1961,** *133*, 1702-1703.

24. Thompson, L. G.; Mosley-Thompson, E.; Davis, M. E.; Zagorodnov, V. S.; Howat, I. M.; Mikhatenko, V. N.; Lin, P. N., Annually Resolved Ice Core Records of Tropical Climate Variability over the Past similar to 1800 Years. *Science* **2013,** *340*, (6135), 945-950.

25. Fisher, D. A.; Koerner, R. M.; Paterson, W. S. B.; Dansgaard, W.; Gundestrup, N.; Reeh, N., Effect of wind scouring on climatic records from ice-core oxygen-isotope profiles. *Nature* **1983,** *301*, (5897), 205-209.

26. Welker, J. M., ENSO effects on delta O-18, delta H-2 and d-excess values in precipitation across the U.S. using a high-density, long-term network (USNIP). *Rapid Commun. Mass Sp.* **2012,** *26*, (17), 1893-1898.

27. Liu, Z. F.; Yoshimura, K.; Bowen, G. J.; Buenning, N. H.; Risi, C.; Welker, J. M.; Yuan, F. S., Paired oxygen isotope records reveal modern North American atmospheric dynamics during the Holocene. *Nat. Comm.* **2014,** *5*, 3701.

28. Brown, S., Multi-proxy Holocene fire history reconstruction in the Beartooth Mountains, Wyoming. M.S. Thesis, Indiana State University **2016.**

29. Marsicek, J.; Shuman, B. N.; Bartlein, P. J.; Shafer, S. L.; Brewer, S., Reconciling divergent trends and millennial variations in Holocene temperatures. *Nature* **2018,** *554*, (7690), 92-96.

30. Carter, V. A.; Shinker, J. J.; Preece, J., Drought and vegetation change in the central Rocky Mountains and western Great Plains: potential climatic mechanisms associated with megadrought conditions at 4200 cal yr BP. *Clim. Past* **2018,** *14*, (8), 1195-1212.

31. Menounos, B.; Osborn, G.; Clague, J. J.; Luckman, B. H., Latest Pleistocene and Holocene glacier fluctuations in western Canada. *Quaternary Sci. Rev.* **2009,** *28*, (21-22), 2049-2074.

32. Yuan, F. S.; Koran, M. R.; Valdez, A., Late Glacial and Holocene record of climatic change in the southern Rocky Mountains from sediments in San Luis Lake, Colorado, USA. *Palaeogeogr. Palaeocl.* **2013,** *392*, 146-160.

33. Kemp, D. B.; Eichenseer, K.; Kiessling, W., Maximum rates of climate change are systematically underestimated in the geological record. *Nat. Comm.* **2015,** *6*, 8890.

34. Zahid, H. J.; Robinson, E.; Kelly, R. L., Agriculture, population growth, and statistical analysis of the radiocarbon record. *P. Natl. Acad. Sci. USA* **2016,** *113*, (4), 931-935.

35. Peros, M. C.; Munoz, S. E.; Gajewski, K.; Viau, A. E., Prehistoric demography of North America inferred from radiocarbon data. *J. Archaeol. Sci.* **2010,** *37*, (3), 656-664.

36. Trouet, V.; Diaz, H. F.; Wahl, E. R.; Viau, A. E.; Graham, R.; Graham, N.; Cook, E. R., A 1500-year reconstruction of annual mean temperature for temperate North America on decadal-to-multidecadal time scales. *Environ. Res. Lett.* **2013,** *8*, (2), 024008.

Chapter 4

Assessment of black carbon deposition in two high-elevation Wyoming lakes

Nathan Chellman[1,2]*, Sabrina Brown[3], Alan Heyvaert[1], Jeffery Stone[4], Monica M. Arienzo[1], and Joseph R. McConnell[1]

[1]Division of Hydrologic Sciences, Desert Research Institute, Reno, Nevada
[2]Graduate Program of Hydrologic Sciences, University of Nevada, Reno, Nevada
[3]Earth and Atmospheric Sciences, University of Nebraska-Lincoln, Lincoln, Nebraska
[4]Indiana State University, Department of Earth and Environmental Systems, Terra Haute, Indiana

Abstract

Reconstructions of past wildfire activity using lake sediment cores, most traditionally through charcoal measurements, are crucial for understanding both the frequency and spatial variability of forest fire history. Sub-micron, refractory black carbon (rBC) is an alternative proxy to charcoal to develop fire histories in lakes sediments. rBC records from ice cores have been used extensively to understand hemispheric-scale past fire history and pollution, but few rBC records have been developed from lake sediment cores. Here, we apply a method for rBC quantification in lake sediments to two Wyoming lakes with contrasting catchments, Island Lake and North Lake. At Island Lake, which has a large, vegetated catchment, rBC concentration and flux parallel charcoal measurements, suggesting rBC in this lake setting is subject to similar depositional mechanisms as charcoal, and is therefore more representative of local burning. At North Lake, which has a comparatively smaller catchment devoid of vegetation, rBC flux parallels regional temperature and moisture, indicating rBC is more representative of regional biomass burning. rBC flux at Island Lake is ~5-fold higher than at North Lake, where rBC flux agrees well with measurements from a nearby ice core and modeling results. The differences in the magnitude of rBC flux and physical lake characteristics indicate that mobilization in the watershed via runoff and erosion resulting in secondary deposition of rBC may contribute to the Island Lake record, while North Lake likely is dominated by atmospheric deposition.

1. Introduction

Paleoclimate records from lake sediments are used to infer past environmental conditions, including temperature[1, 2] and hydrologic changes.[3-5] Lake sediment cores are also commonly used to reconstruct changes in past wildfire activity, most routinely based on measurements of macroscopic charcoal deposition in a lake.[6-10] Charcoal particles are emitted by incomplete combustion of biomass and are generally ~50 to 1000 μm in size. The larger macroscopic particles are thought to be more representative of local fire events, while smaller microscopic particles are more representative of watershed-scale or extra-local burning within tens of kilometers of the lake.[7, 11, 12]

Charcoal records from lakes at the landscape scale can be influenced by local dynamics such as ignition sources, local flora, and physical setting.[13] Therefore, charcoal records from a spatial array of lakes must be combined to develop burning records representative of a broader regional scale.[9, 10, 14] Additionally, charcoal records can be complicated by factors including secondary deposition resulting from runoff or sediment mixing, as well as a limited understanding of the interaction between fire type or intensity, charcoal formation, and aerial transport of charcoal particles.[10, 12, 15, 16]

Black carbon (BC) is an alternative proxy for reconstructing past fire history in lake sediments.[17-19] Like charcoal, BC is emitted from incomplete combustion, though BC particles can also be sourced from industrial emissions of fossil fuels in addition to natural biomass burning.[20, 21] Here, we use refractory BC (rBC) to refer to the most highly-condensed soot byproducts of combustion.[22, 23] The morphological characteristics and formation of rBC particles, which are highly-combusted elemental carbon, are fundamentally different than those for charcoal, which can be affected by varying degrees of charring and retain some of the original properties and chemistry of the initial biomass.[22] rBC particles typically have a diameter of less than one micron, orders of magnitude smaller in diameter than charcoal, and can be transported

long distances through the atmosphere. Therefore, rBC records from distal archives, such as ice cores, can represent regional burning from areas as far away as hundreds or thousands of kilometers.[21, 24-26]

rBC records from lakes are sparse, however, because of relatively intensive analytical techniques that can be hampered by uncertainties associated with measurement artefacts and interferences.[22, 27, 28] Furthermore, the depositional setting of a lake, including catchment or lake size, secondary deposition from runoff or erosion, and redeposition, can affect the records of fire history preserved in lake sediments.[10] Better understanding the deposition of pyrogenic carbon in sediments, including rBC and charcoal, is important not only for reconstructing past fire history, but also because pyrogenic carbon in sediments increasingly is recognized as a significant component of the global carbon cycle,[29, 30] with important implications for radiative forcing.[31, 32]

Here, we apply a recently developed, incandescence-based method for measuring rBC in lake sediments[17] to two lakes in Wyoming with the goal of developing local (within a few kilometers)-to-regional (within tens to hundreds of kilometers) burning records over past millennia. This method relies on an instrument used extensively for rBC quantification in the atmosphere, ice cores, and snow samples,[21, 24, 31, 33, 34] and recently has been adapted to lake sediment cores.[17, 35] As this study is an early implementation of this new method, this rBC method was evaluated through comparison to other burning proxies as well as to regional climate. At Island Lake, located on the Beartooth Plateau, rBC measurements were compared to co-registered charcoal data[36] to evaluate if the rBC record documented regional to local burning over the past 10,000 years. Lacking charcoal measurements in the same sediment core, rBC measurements in a core from North Lake in the Wind River Range were compared to rBC deposition measured in a nearby ice core[37] over recent centuries and to other lake sediment records of climate[1] over the past 2,000 years.

2. Methods

2.1 Study sites

rchived core NOR08-02[38, 39] from North Lake (Fig. 1; Table 1; 42.76 °N, 109.06 °W; 3085 masl), stored at the National Lacustrine Core Facility (LacCore), was subsampled at 1-cm resolution. This 88 cm percussion core was collected in 2008 CE and the depth-age scale was developed using eight radiocarbon dates and plutonium isotopes in the upper section.[39] Other measurements and interpretation, including a depth-age scale and geochemical, diatom, and isotope measurements, have been previously published in Brahney et al.[38, 39]

A 1.5 m core collected using a Griffith corer from Island Lake in 2013 CE[36] (Fig. 1; Table 1; 44.95 °N, 109.54 °W; 2904 masl) was subsampled at 0.5-cm resolution. A depth-age model (Fig. 3a) was developed in the R-package Bacon v2.2 from eight extracted pollen samples that were radiocarbon dated at the Accelerator Mass Spectrometry Lab (directAMS, Bothell WA) and calibrated using IntCal13,[40-42] in addition to lead-210 measurements in the upper 9 cm. Charcoal quantities for the Island Lake core were previously published in Brown.[36] For charcoal analysis, samples were bleached with 3% hydrogen peroxide, wet-sieved through 250, 125, and 63 μm mesh, and counted using a 20x Nikon stereomicroscope on a 1-cm grid.[36]

2.2 rBC measurements

Protocols for rBC analysis are detailed in Chellman et al.[17]. Sediment samples were dried and homogenized using a planetary ball mill. Homogenized sediment (~50 mg) was resuspended in ultrapure 18.2 MΩ water (~50 ml), sonicated for 15 mins, and placed on a shaker table for 16 hrs. Samples were subsequently sonicated for another 30 mins and allowed to settle for ~24 hrs to allow large sediment particles to settle before rBC analysis, assuming the smaller and less-dense rBC particles will preferentially remain in suspension. Samples were not chemically pretreated at any step of the preparation process. After settling, the samples were introduced into the analytical

system. Aqueous sample containing the resuspended sediment was passed through sequential 20 μm and 10 μm stainless steel filters and diluted with DI water in-line by a ratio of 11:1 and 14:1 for North Lake and Island Lake, respectively. The dilution was required to protect downstream instrumentation, including sensitive optics within the rBC instrument. The sample stream was introduced to an Apex-Q jet-type nebulizer to create a dry aerosol that was sent to a Single Particle Soot Photometer (SP2, Droplet Measurement Technologies) for rBC quantification.

The SP2 was calibrated in two steps. First, the SP2 was internally calibrated using a Differential Mobility Analyzer (DMA) and the rBC-like material Aquadag following manufacturer specifications. This internal calibration relates the instrument response to single-particle rBC masses from 0.01 to 60 fg. Second, an external calibration was performed daily to account for drift in nebulization efficiency and sample delivery using a suite of aqueous standards made from three rBC-like materials: Cabojet 200, Regal Black, and Aquadag. Quality control standards were run periodically during sample analysis. rBC concentrations were corrected for under-recovery, which was quantified by subjecting representative samples to repeated preparation cycles. The recovery of the first measurement of rBC was 49±12% (±1σ, n=3) and 58±6% (±1σ, n=3) for North Lake and Island Lake, respectively.

It is possible that a portion of the rBC signal was derived from fragmented macrocharcoal generated during sample homogenization. However, the SP2 is most sensitive to highly-condensed combustion byproducts.[43, 44] Furthermore, the rBC mass distribution of the samples is comparable to that of rBC distribution in snow[24, 45] and ice samples from the Upper Fremont Glacier (UFG), Wyoming (Fig. 2), suggesting that it is unlikely that fragmented charcoal, which would have to be reduced in size by at least ~2 orders of magnitude to be efficiently nebulized and detected by the SP2, is the primary driver of the rBC signal.

The SP2 color ratio, calculated as the log base 10 of the ratio of the broadband to narrowband peak heights, was used to evaluate potential interferences on the rBC measurement,

namely from iron oxides within the sediments. The SP2 is much less sensitive to iron oxides than rBC and detects a different color ratio for iron oxides than for rBC, allowing for quantification and correction of potential interferences.[17, 46] For any given sample, particles with color ratios outside of the optimum rBC range of -0.15 to 0.45 were discarded during post-processing.

The amount of the SP2 signal attributable to any interference within this color ratio range was determined by fitting two distributions to the total color ratio distribution – one representing the interference signal and one representing the rBC signal – then calculating the fraction of the rBC to interference signal based on the fitted distributions within the color ratio range.[17] This fraction was used to correct the final rBC concentration in post-processing. A Cauchy distribution was fit to the potential interference signal, and either a Cauchy or a normal distribution was fit to the rBC signal, with the final fit determined by which distribution had a lower root mean squared error (RMSE) to the observations. The color ratio indicated that rBC, on average, was responsible for 73±13% (±1σ, n=173) and 78±4% (±1σ, n=288) of the signal detected by the SP2 for North Lake and Island Lake, respectively (Fig. 2).

rBC concentrations (reported in ng rBC per mg sediment, or ng mg^{-1}) were converted to rBC depositional flux (reported in mg m^{-2} yr^{-1}) by multiplying the rBC concentration with the mass accumulation rate determined by density measurements and sediment accumulation rate from the depth-age scale.

2.3 Upper Fremont Glacier rBC flux

rBC flux was calculated for the UFG ice cores by multiplying rBC concentrations (Chellman et al. 2017) by the water equivalent accumulation rate at the site of 0.91 m yr^{-1} (ice accumulation of 1 m yr^{-1}) (Schuster et al. 2002), following the description for calculating mercury flux in the UFG ice cores in Chapter 2.

3. Results and discussion

3.1 Lake chronologies

The depth-age model for North Lake was previously published in Brahney et al.[39]. The record covers the time period from 1850 to -68 ybp with a maximum age uncertainty of ±97 years. The depth-age model for Island Lake[36] (Fig. 3a) indicates the record covers the time period from 10500 to -65 ybp with an average uncertainty of ±330 years.

3.2 Method reproducibility

Replicate measurements were used to evaluate variability in rBC measurements resulting from the sample preparation process (Figs. 3 and 4). For North Lake, the average relative percent difference (RPD; calculated as the absolute value of the difference between two measurements divided by their average) for replicate samples was 41±32% (±1σ, n=85). However, a number of replicate samples from North Lake had rBC concentrations below the detection limit of the prescribed dilutions. When excluding these samples by discounting samples from the lower first quartile of rBC data (concentrations less than 4.3 ng BC per mg sediment), the average RPD improved to 34±27% (±1σ, n=70). Similar reproducibility was observed for Island Lake, with an average RPD of 38±26% (±1σ, n=30). The source of variability between replicate measurements is uncertain. Overall rBC mass distributions for replicate samples were similar, suggesting that while the same rBC mass distributions are replicated by the sample preparation and analytical process, the overall concentration of resuspended rBC is more variable. This variability likely is linked to initial sediment homogenization but also could be influenced by subtle differences in the shaking and sonication steps of preparation (e.g. position of sample within sonic bath). We note that many samples from Island Lake contained rounded, coarse (up to 5 mm diameter) clastic grains that likely prevented complete homogenization of the sediment in the planetary ball mill. The good reproducibility of rBC mass distributions and stability of quality-control standard

measurements suggest instrument calibration or daily changes in filtration or nebulization efficiency were stable.

While the overall high RPD for replicate measurements indicated significant variability on a sample-by-sample basis, the overall trends observed between replicate sets of samples for both lakes were in good agreement (Figs. 3 and 4). Thus, though there was lower confidence in individual rBC spikes and high-frequency variability, the average rBC profile effectively captured low-frequency multi-decadal to centennial-scale trends.

3.3 Controls on rBC deposition at Island Lake

rBC concentration for Island Lake samples ranged from 20 to 500 ng mg^{-1}, corresponding to depositional fluxes of 5 to 80 mg m^{-2} yr^{-1} from 10,000 to ~250 years before present (ybp; defined here as years before 1950 CE) and of ~80-250 mg m^{-2} yr^{-1} from 250 ybp to modern (Fig. 3). rBC concentration compares well with charcoal counts from the same core, especially over the most recent 4,000 years (Fig. 5). From 10,000 to 7,000 ybp, rBC had several centennial-scale increases, while charcoal counts (both 150 μm and 60 μm particles) remained low. At 6,800 ybp, both rBC and charcoal increased for a millennium, before charcoal declined and remained low until 3,800 ybp. rBC also returned to overall lower baseline interrupted by multiple short-lived spikes. Starting at around 4,000 ybp, rBC concentration and charcoal counts, both 60 μm and 150 μm sizes, closely paralleled each other until present.

Changes in rBC depositional flux at Island Lake were largely driven by changes in mass accumulation rate, which varied significantly throughout the record and proportionally overwhelmed the observed temporal variability of rBC concentration. The mass accumulation rate was ~0.0175 g cm^{-2} yr^{-1} from 10,000 to 8,500 ybp and 0.007 to 0.009 g cm^{-2} yr^{-1} from 8,500 to 4,200 ybp before increasing to 0.021 to 0.032 g cm^{-2} yr^{-1} from 4,200 to 700 ybp. After 700 ybp, the accumulation rate briefly dropped to 0.013 g cm^{-2} yr^{-1} for a century before increasing over 10-

fold to 0.15 g cm^{-2} yr^{-1} since 100 ybp (Fig. 3). When calculating rBC flux, these rapid and large changes in accumulation were superimposed onto the rBC flux record. rBC flux largely was below 30 mg m^{-2} yr^{-1} from 10,000 to 4,000 ybp. From 4,000 to 1,000 ybp, coincident with increased sedimentation rates, rBC flux increased to between 20 to 80 mg m^{-2} yr^{-1}. Between 1,000 and 100 ybp, rBC flux decreased to 15-30 mg m^{-2} yr^{-1} before increasing ~10 fold to 120 to 160 mg m^{-2} yr^{-1} since 100 ybp.

Processes affecting rBC transport and deposition are poorly constrained in the context of lake sediment records. Upon initial emission from a fire, rBC primarily is injected into the atmosphere and subsequently transported via eolian processes. rBC can travel for hundreds or thousands of kilometers[48, 49] and has an atmospheric lifetime of 4 to 12 days.[50] In natural archives far removed from emissions sources and therefore where rBC deposition is dominated by long-range transport, such as polar or alpine ice cores, rBC records represent a regional-to-hemispheric scale signal of burning or pollution.[21, 25, 26, 34] However, at sites such as Island Lake, which are proximal to emissions sources and have large upstream catchments—which can contribute rBC via secondary deposition from runoff or erosion—the long-range, atmospheric rBC signal could be overwhelmed by local sources, such as fires within or adjacent to the lake's watershed. rBC is thought to be inert in soils with a half-life of 5-7 millennia,[20, 30] potentially longer in environments that enhance preservation. Thus, it is unlikely that rBC was degraded in the lake sediments presented in this study.

Three factors suggest that local emissions, including secondary deposition, control rBC deposition at Island Lake, as opposed to long-range transported emissions from distal emissions sources. First, the lake setting and geometry is prone to influence from local emissions. The lake is situated in a forested watershed and surrounded by a region with a known natural fire cycle.[51, 52] Thus, there are likely frequent rBC and charcoal inputs from wildfires within and immediately adjacent to the lake's watershed. Furthermore, the lake has a catchment area (19 km^2) to surface

area (0.6 km^2) ratio of 30 (Fig. 1; Table 1). The large catchment area relative to the size of the lake suggests that there could be significant secondary, terrestrial rBC contributions to the lake from runoff compared to the likely smaller contributions from direct atmospheric deposition. Furthermore, the large upstream drainage at Island Lake is complicated by a multitude of flow paths through numerous lakes (Fig. 1).

Second, the covariance of the rBC and charcoal data imply a similar emissions source and depositional mechanism for both of these fire proxies at Island Lake. Charcoal deposited in lake sediments is limited to fires within, at most, tens of kilometers of the lake itself[12, 16] and therefore is biased towards local burning. While charcoal fragments are initially dispersed and deposited through the atmosphere, secondary deposition from fluvial processes can contribute charcoal from local fires for a number of years post-fire until revegetation occurs.[7, 10, 12] These depositional processes likely can be extended to rBC deposition at Island Lake given its covariance with charcoal data.

Third, the magnitude of rBC flux at Island Lake since 150 ybp was between 120 and 160 mg m^{-2} yr^{-1}, over ten times higher than expected from direct atmospheric deposition inferred from model simulations[48] and observations from a glacial ice core from the Wind River Range, WY. Global model simulations, which do not have the resolution to capture small-scale local burning, predicted rBC atmospheric depositional fluxes of ~10 mg m^{-2} yr^{-1} since 150 ybp for this region,[48] and rBC flux at UFG, which has been shown to represent continental-scale rBC emissions, were between 2 and 10 mg m^{-2} yr^{-1} since 250 ybp . The overall higher flux at Island Lake suggests that atmospheric rBC deposition only accounted for part of the total rBC flux entering the lake and other mechanisms, such as fluvial transport, contributed a significant portion of rBC. Prior to 150 ybp, however, the observed fluxes at Island Lake (15 to 30 mg m^{-2} yr^{-1}) are in better agreement, but still higher by a factor of 2-15 of those from the model and UFG ice core.

3.4 Island Lake rBC links to regional climate

From the Early Holocene to 4,000 ybp, rBC and charcoal flux was low with little variability (Fig. 5). The increased rBC variability compared to the charcoal data during this time could represent contributions from extra-local or smaller fires that did not result in charcoal deposition. Despite overall warmer temperatures[1, 53] and frequent drought conditions[2, 3] during the Early- and Mid-Holocene compared to Late-Holocene conditions in Wyoming and nearby regions of the Rocky Mountains, there was little fire activity at Island Lake. The lack of fire activity may have resulted from a fuel-limited system or decreased secondary deposition resulting from less runoff, inferred from the low mass accumulation rates during this time.

rBC flux suggests there was a transition to a more active fire regime at Island Lake beginning at ~4,000 ybp (Fig. 5). This coincides with the establishment of a coupled tropical-North Pacific control on hydroclimate in western North America driven by patterns such as ENSO, inferred from an array of oxygen isotopic records from sediments and caves,[5] as well as continued Mid- and Late- Holocene cooling.[2, 53, 54] Increased sedimentation rate coincident with the higher rBC flux could also indicate enhanced fluvial contributions and therefore more secondary rBC deposition. The onset of increased rBC flux at Island Lake corresponded to a brief decrease in effective moisture after a preceding millennium of wetter conditions inferred from a lake sediment core from the Wind River Range, WY,[53, 55] however, a nearby lake on the Beartooth Plateau did not show a significant decrease in lake level at this time.[3]

Fire activity remained relatively high during the Late Holocene, inferred from both the rBC and charcoal flux records (Fig. 5). A possible mechanism for increased fire activity would be increased fuel growth associated with overall wetter conditions; a lake at Yellowstone National Park documented increased fuel biomass beginning at 4,500 ybp.[56] Island Lake documented peak Late-Holocene fire activity at 2,800 ybp, after which it declined to 2,000 ybp before subsequently increasing to a local maximum centered at 1,200 ybp, roughly coinciding with warmer

temperatures during the Medieval Warm Period.[13] The lowest rBC flux occurred from 500 to 200 ybp, coeval with the Little Ice Age. rBC flux rapidly increased by 8 to 10 fold at 150 ybp, largely driven by the rapid increase in sedimentation rate. The increased rBC flux at modern could be the result of increased secondary rBC deposition or industrial or recreational emissions from increased anthropogenic activity in the area.

3.5 North Lake rBC

At North Lake, located in the Wind River Range approximately 250 km to the south of Island Lake (Fig. 1), rBC fluxes ranged from 0 to 200 ng mg^{-1} over the past 2,000 years (Fig. 4). The mass accumulation rate ranged between 0.01 and 0.06 g cm^{-2} yr^{-1}, though for the most of the record it smoothly varied between 0.01 and 0.02 g cm^{-2} yr^{-1},[39] resulting in rBC fluxes ranging from 0 to 50 mg m^{-2} yr^{-1}. rBC flux had a short-lived spike at 1770 ybp, after which rBC concentrations were below detection limits from 1750 to 1350 ybp. Between 1350 and 750 ybp, BC flux gradually increased from 0 to 12 mg m^{-2} yr^{-1} before declining to 5 mg m^{-2} yr^{-1} from 750 to 30 ybp. Over the past 70 years, rBC increased rapidly to 50 mg m^{-2} yr^{-1} in -30 ybp before decreasing to present.

The magnitude of rBC flux before 0 ybp at North Lake —5 and 20 mg m^{-2} yr^{-1}—is in good agreement with rBC flux at the UFG, located 50 km to the north, where rBC flux varied between 1 and 10 mg m^{-2} yr^{-1} since 200 ybp (Fig. 6). It also agrees well with the modeled rBC flux for the region of ~10 mg m^{-2} yr^{-1} since 100 ybp [48]. This suggests that unlike Island Lake, where rBC fluxes that were significantly higher than at UFG or predicted by models were attributed to secondary deposition and local burning, rBC deposition at North Lake plausibly could be dominated by more regional-scale, direct atmospheric contributions. Though the lake catchment to surface area ratio of North Lake is higher (~59) than at Island Lake (~30) (Table 1), the catchment is largely bare rock devoid of vegetation, minimizing the amount of rBC that can

be eroded from soils or shed by burnt biomass. Furthermore, the catchment at North Lake of 1.7 km^2 is roughly a tenth of that for Island Lake, further reducing potential inputs from secondary deposition.

The extremely low rBC flux from 1750 to 1350 ybp, corresponding to core depths of 60 to 80 cm, could be attributed to numerous factors including: 1) a turbidity flow or mass movement that altered the depositional processes at these depths in the core, 2) rBC decomposition or degradation, 3) ineffective rBC mobilization from sediments during sample preparation, or 4) very low rBC deposition in sediments at North Lake for these 400 years. A turbidity flow is unlikely, as there are two radiocarbon dates within this depth range that fit well within the context of deeper and shallower dates.[39] Furthermore, there were no major changes in mass accumulation, sediment geochemistry, or diatom assemblages[39] at the lake or visually-detectable disturbances in the cores that would indicate a major shift in deposition. rBC decomposition also is an unlikely explanation, as rBC is thought to be relatively inert[20] and there was rBC both above and below this depth range. The low rBC concentrations do not appear to be related to the sample preparation process—homogenization times of up to 20 minutes did not increase rBC concentrations for these samples, and the standard preparation process yielded repeatable measurements for the rest of the core. Thus, the most likely explanation is that there was very low rBC deposition at North Lake during this period.

Few millennial-scale climate records from lake sediment cores or trees exist from the Wind River Range,[57] and to our knowledge, there are no charcoal reconstructions. The only existing rBC record in this region is from the UFG ice cores, ~50 km to the north of North Lake, which extends to 200 ybp. rBC at UFG parallels trends observed in Greenland, with significant increases associated with industrial pollution beginning in 100 ybp and peaking in ~40 ybp.[37] Though this period only corresponds to the upper 10 cm at North Lake, the ice core and lake-sediment trends generally agree until 0 ybp (Fig. 6). Both records have an rBC minimum around

150 ybp before increasing to a peak at ~50 ybp followed by a decline. However, while rBC at UFG declined to present, rBC at North Lake declined only until 0 ybp, after which rBC rapidly increased. This decoupling of the two signals could indicate a shift to a more dominant local rBC emissions source for North Lake, and the sharp rBC increase coincided with dramatic increases in dust deposition (Fig. 6) at North Lake attributed to industrial activity in the adjacent Green River Basin, namely oil and gas extraction.[39] This large increase in dust deposition, a salient feature at North Lake on the western side of the continental divide, was not evident at nearby Lonesome Lake[39] or at UFG,[58] both on the eastern side of the divide.

The rBC record at North Lake parallels regional temperature (mean temperature of the warmest month [MTWM]) and moisture reconstructions (Fig. 4) based on a network of lake sediment cores.[1] Low rBC flux until 1150 ybp corresponded with overall cooler and wetter conditions. rBC flux began to increase at North Lake as temperature increased between 1150 and 950 ybp, and subsequently increased further to a maximum at 550 ybp, coeval with a rapid moisture increase—inferred from increased lake levels—between 1150 and 750 ybp. Decreasing rBC flux from 550 to 50 ybp also paralleled decreasing temperatures into the Little Ice Age. This suggests that a combination of temperature and moisture controls wildfire in this region. North Lake rBC flux, excluding the pre-1750 ybp and post-0 ybp peaks is highly correlated with both the temperature ($r=0.66$, $p<0.01$) and moisture ($r=0.70$, $p<0.01$) reconstructions. The correlation to temperature improves to greater than $r=0.80$ when the temperature reconstruction is lagged by 180 to 300 years, while the correlation to moisture decreases. The increased correlation with a time shift suggests that climate influences natural burning in the region and` there are century-scale lags in the system related to climate change, successional processes, and burning.[13, 59]

Conclusion

The application of this recently-developed method to two Wyoming lakes shows that it can be used to develop rBC records of both regional and local fire, and emphasizes the importance of site selection for future applications. Because rBC is orders of magnitude smaller than charcoal and therefore can be transported long distances through the atmosphere, rBC measurements in lake sediments potentially can be used to reconstruct regional burning on a broader scale than macroscopic charcoal currently permits, as well as inform atmospheric rBC modeling efforts. The strong covariance of the rBC record from Island Lake with coregistered charcoal measurements and high rBC flux values, however, indicate that in larger catchments in close proximity to areas with frequent burning, local burning and secondary deposition likely overwhelm regional atmospheric inputs. While in settings similar to Island Lake, this method for measuring rBC may not prove advantageous over traditional charcoal measurements, rBC measurements from North Lake effectively captured the magnitude of atmospheric rBC flux and paralleled regional climate, suggesting that in lakes with a smaller, more barren catchments that limit local inputs and secondary deposition, rBC records can provide meaningful constraints on atmospheric deposition and regional burning.

Acknowledgements

We thank the Sulo and Aileen Maki Endowment at the Desert Research Institute for funding this research. We thank J. Davidson and N. Hayes for their assistance in the lab, and we also thank LacCore for storing and subsampling the North Lake core.

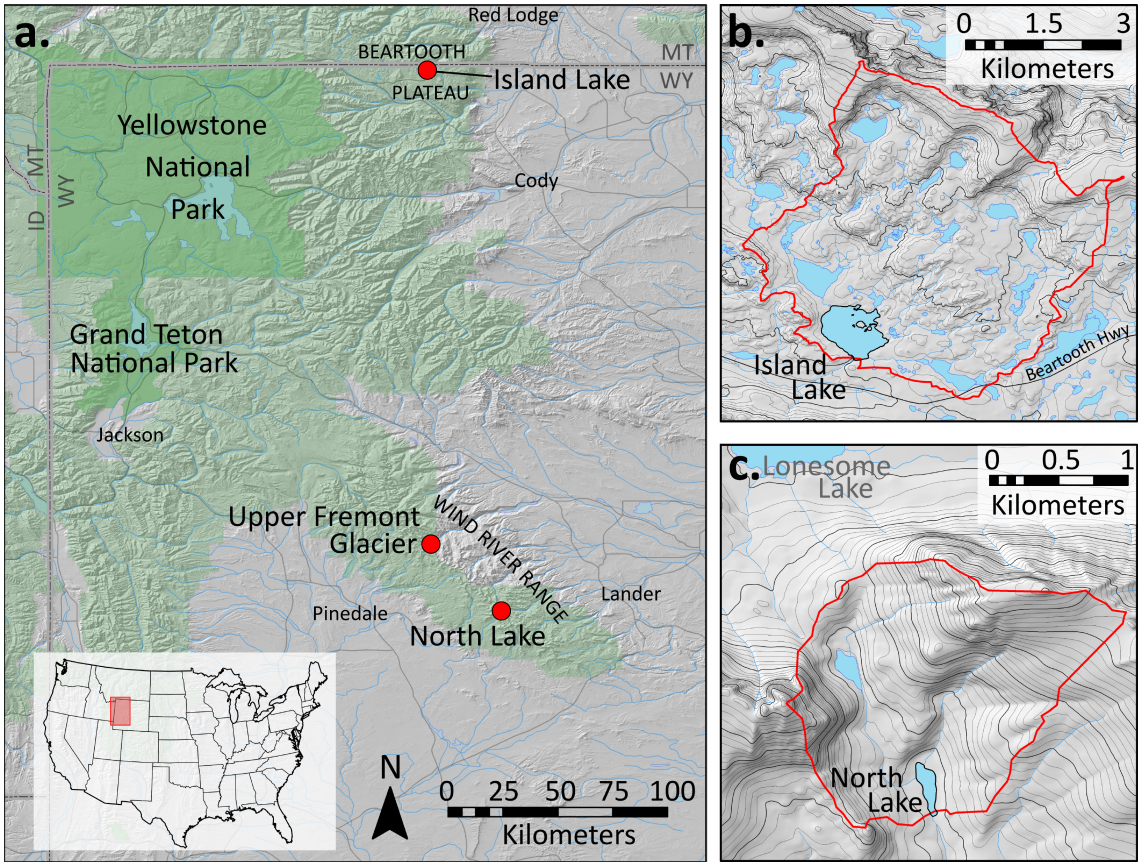

Figure 1.Map of study sites. (a) Locations of all study sites. (b) Detail of Island Lake. (c) Detail of North Lake. Island Lake and North Lake outlined in black. Red line delineates approximate catchment.

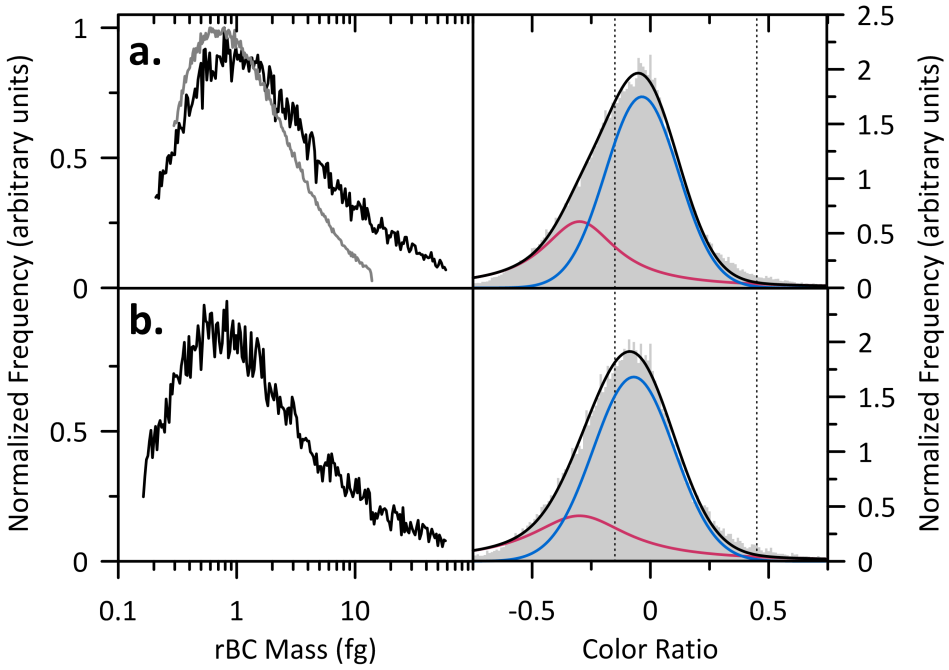

Figure 2. rBC color ratio and mass distributions. (a) rBC particle mass distributions (left) for North Lake (black) and Upper Fremont Glacier (gray) and corresponding color ratio for North Lake sample (right). (b) rBC particle mass distributions (left) for Island Lake and corresponding color ratio. All data from samples dated to ~200 ybp. For color ratios, black distribution represents fit to data (gray), calculated as the sum of two distributions fit to the rBC (blue) and interference (red) portions of the color ratio. Particles with color ratio less than -0.15 or greater than 0.45, indicated by dashed vertical lines, were excluding in post-processing.

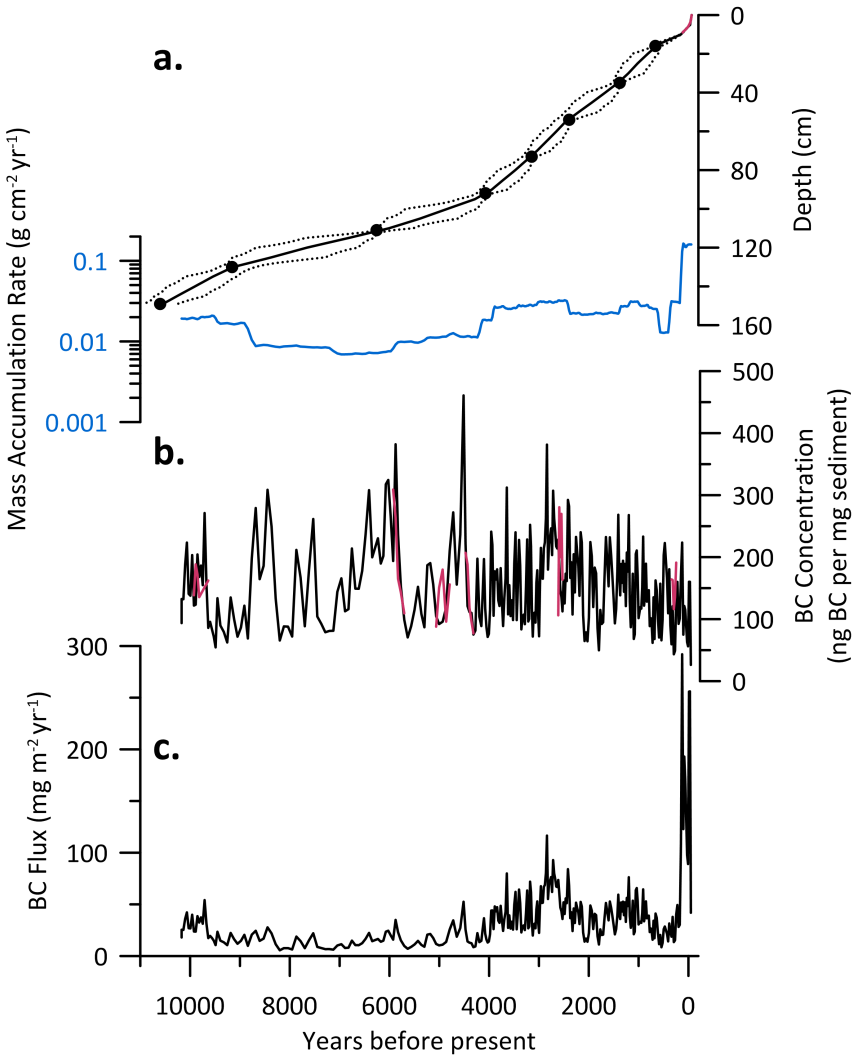

Figure 3. Island Lake results. (a) Island Lake depth-age scale (black, dotted lines indicate 98% confidence interval) with age control points (points for radiocarbon dates; red line in upper 10 cm for lead-210 dates) nd mass accumulation rate (blue). (b) rBC concentration. Red lines are replicate measurements. (c) Island Lake rBC flux.

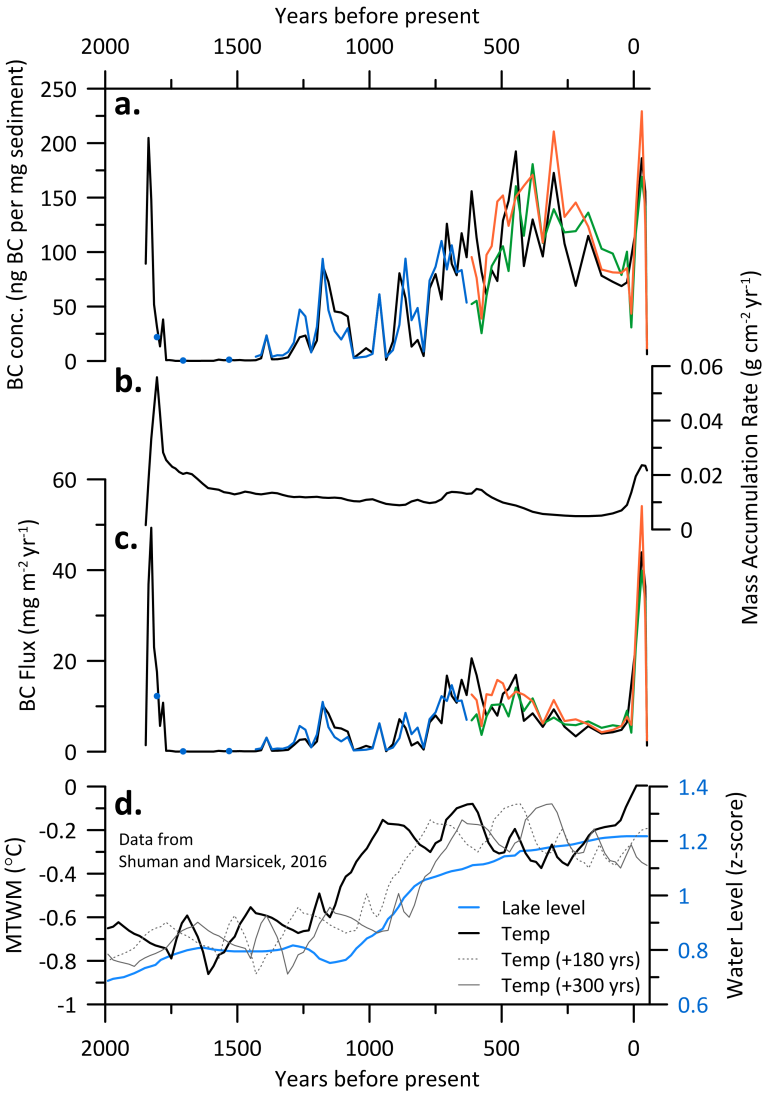

Figure 4. North Lake results. (a) North Lake rBC concentration (a), mass accumulation rate (b), and rBC flux (c). Each colored line in panels (a) and (c) represents a replicate set of measurements. (d) Regional reconstructions (Shuman and Marsicek 2016) of mean temperature of the warmest month (MTWM) and lake water levels, a proxy for moisture.

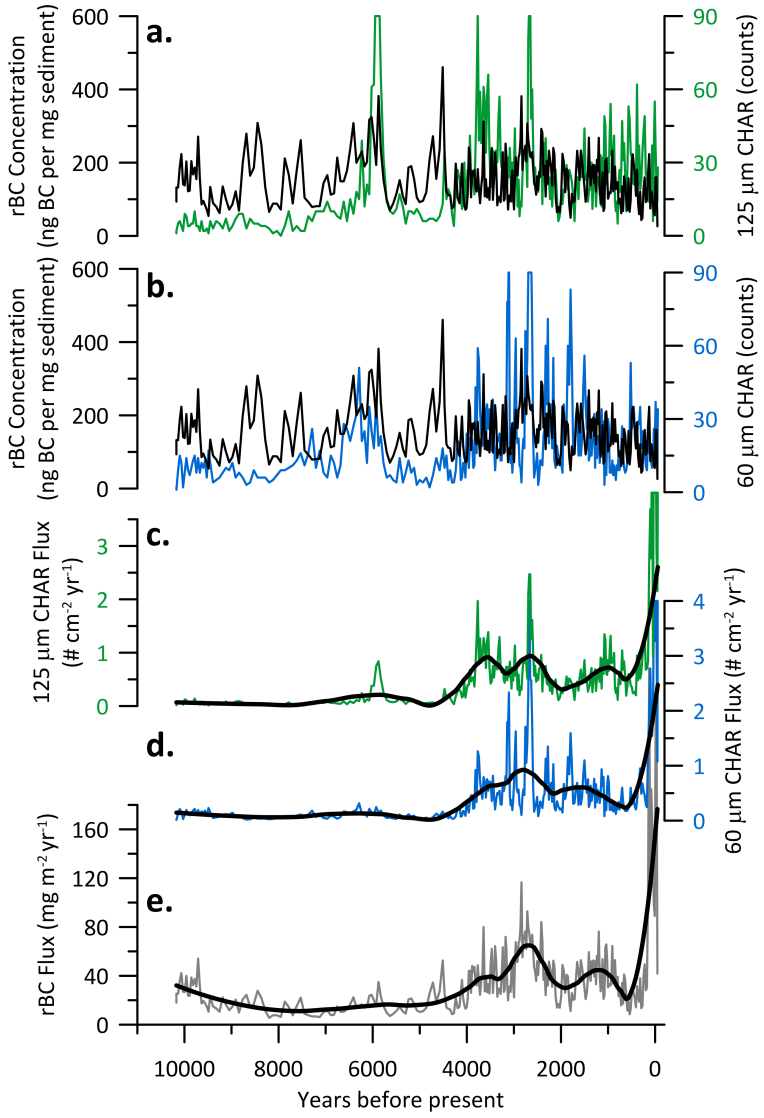

Figure 5. Comparison of Island Lake rBC and charcoal data (Brown 2016). rBC concentration compared to 125 µm (a) and 60 µm (b) CHAR counts. 125 µm (c) and 60 µm (d) CHAR flux (c) compared to rBC flux (e). Lowess filter was applied to flux data.

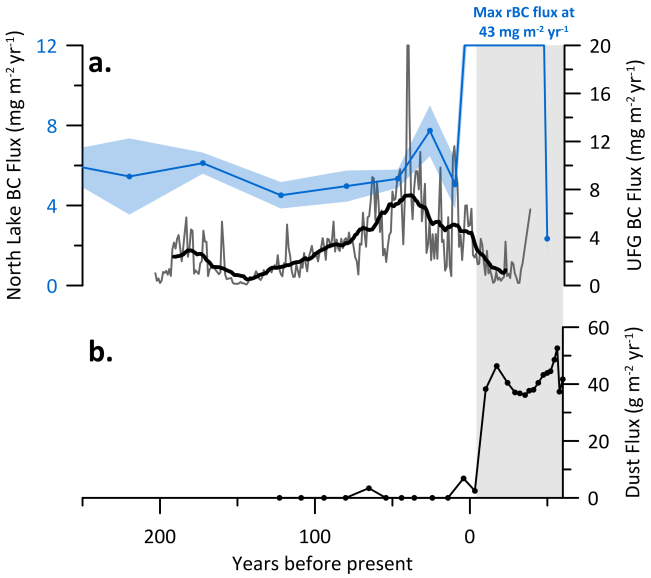

Figure 6. Comparison of North Lake and UFG data. (a) North Lake rBC flux (mean±1σ of replicate measurements) and UFG BC flux. (b) Dust flux from parallel core NOR09-02 (Brahney et al. 2015) that documents increased dust flux at -5 ybp attributed to gas and oil production in the nearby Green River Basin.

Lake	Latitude	Longitude	Elevation (masl)	Lake Area (km^2)	Lake Catchment (km^2)	Catchment Area: Lake Area
North Lake	42.76	-109.06	3085	0.03	1.7	59
Island Lake	44.95	-109.54	2904	0.6	19	32

Table 1. Lake location and physical characteristics. North Lake data from Brahney et al.[39]

References

1. Shuman, B. N.; Marsicek, J., The structure of Holocene climate change in mid-latitude North America. *Quaternary Sci. Rev.* **2016,** *141*, 38-51.
2. Mensing, S.; Korfmacher, J.; Minckley, T.; Musselman, R., A 15,000 year record of vegetation and climate change from a treeline lake in the Rocky Mountains, Wyoming, USA. *Holocene* **2012,** *22*, (7), 739-748.
3. Shuman, B. N.; Serravezza, M., Patterns of hydroclimatic change in the Rocky Mountains and surrounding regions since the last glacial maximum. *Quaternary Sci. Rev.* **2017,** *173*, 58-77.
4. Stone, J. R.; Saros, J. E.; Pederson, G. T., Coherent late-Holocene climate-driven shifts in the structure of three Rocky Mountain lakes. *Holocene* **2016,** *26*, (7), 1103-1111.
5. Anderson, L.; Berkelhammer, M.; Barron, J. A.; Steinman, B. A.; Finney, B. P.; Abbott, M. B., Lake oxygen isotopes as recorders of North American Rocky Mountain hydroclimate: Holocene patterns and variability at multi-decadal to millennial time scales. *Global Planet. Change* **2016,** *137*, 131-148.
6. Higuera, P. E.; Whitlock, C.; Gage, J. A., Linking tree-ring and sediment-charcoal records to reconstruct fire occurrence and area burned in subalpine forests of Yellowstone National Park, USA. *Holocene* **2011,** *21*, (2), 327-341.
7. Whitlock, C.; Millspaugh, S. H., Testing the assumptions of fire history studies: An examination of modern charcoal accumulation in Yellowstone National Park, USA. *Holocene* **1996,** *6*, (1), 7-15.
8. Marlon, J. R.; Bartlein, P. J.; Daniau, A.-L.; Harrison, S. P.; Maezumi, S. Y.; Power, M. J.; Tinner, W.; Vanniere, B., Global biomass burning: a synthesis and review of Holocene paleofire records and their controls. *Quaternary Sci. Rev.* **2013,** *65*, 5-25.
9. Vanniere, B.; Blarquez, O.; Rius, D.; Doyen, E.; Brucher, T.; Colombaroli, D.; Connor, S.; Feurdean, A.; Hickler, T.; Kaltenrieder, P.; Lemmen, C.; Leys, B.; Massa, C.; Olofsson, J., 7000-year human legacy of elevation-dependent European fire regimes. *Quaternary Sci. Rev.* **2016,** *132*, 206-212.
10. Whitlock, C.; Larsen, C. P. S., Charcoal as a fire proxy. In *Tracking environmental change using lake sediments*, Smol, J. P.; Birks, H. J. B.; Last, W. M., Eds. Kluwer Academic Publishers: Dordrecht, The Netherlands, 2002; Vol. Volume 3: Terrestrial, Algal, and siliceous Indicators, pp 1-23.
11. Marlon, J. R.; Bartlein, P. J.; Carcaillet, C.; Gavin, D. G.; Harrison, S. P.; Higuera, P. E.; Joos, F.; Power, M. J.; Prentice, I. C., Climate and human influences on global biomass burning over the past two millennia. *Nat. Geosci.* **2008,** *1*, (10), 697-702.
12. Higuera, P. E.; Peters, M. E.; Brubaker, L. B.; Gavin, D. G., Understanding the origin and analysis of sediment-charcoal records with a simulation model. *Quaternary Sci. Rev.* **2007,** *26*, (13-14), 1790-1809.
13. Calder, W. J.; Parker, D.; Stopka, C. J.; Jimenez-Moreno, G.; Shuman, B. N., Medieval warming initiated exceptionally large wildfire outbreaks in the Rocky Mountains. *P. Natl. Acad. Sci. USA* **2015,** *112*, (43), 13261-13266.

14. McWethy, D. B.; Whitlock, C.; Wilmshurst, J. M.; McGlone, M. S.; Fromont, M.; Li, X.; Dieffenbacher-Krall, A.; Hobbs, W. O.; Fritz, S. C.; Cook, E. R., Rapid landscape transformation in South Island, New Zealand, following initial Polynesian settlement. *P. Natl. Acad. Sci. USA* **2010,** *107*, (50), 21343-21348.

15. Duffin, K. I.; Gillson, L.; Willis, K. J., Testing the sensitivity of charcoal as an indicator of fire events in savanna environments: quantitative predictions of fire proximity, area and intensity. *Holocene* **2008,** *18*, (2), 279-291.

16. Vachula, R. S.; Richter, N., Informing sedimentary charcoal-based fire reconstructions with a kinematic transport model. *Holocene* **2018,** *28*, (1), 173-178.

17. Chellman, N. J.; McConnell, J. R.; Heyvaert, A.; Vanniere, B.; Arienzo, M. M.; Wennrich, V., Incandescence-based single-particle method for black carbon quantification in lake sediment cores. *Limnol. Oceanogr.-Meth.* **2018,** *16*, (11), 711-721.

18. Ruppel, M. M.; Gustafsson, O.; Rose, N. L.; Pesonen, A.; Yang, H.; Weckstrom, J.; Palonen, V.; Oinonen, M. J.; Korhola, A., Spatial and Temporal Patterns in Black Carbon Deposition to Dated Fennoscandian Arctic Lake Sediments from 1830 to 2010. *Environ. Sci. Tech.* **2015,** *49*, (24), 13954-13963.

19. Han, Y. M.; Cao, J. J.; Yan, B. Z.; Kenna, T. C.; Jin, Z. D.; Cheng, Y.; Chow, J. C.; An, Z. S., Comparison of Elemental Carbon in Lake Sediments Measured by Three Different Methods and 150-Year Pollution History in Eastern China. *Environ. Sci. Tech.* **2011,** *45*, (12), 5287-5293.

20. Forbes, M. S.; Raison, R. J.; Skjemstad, J. O., Formation, transformation and transport of black carbon (charcoal) in terrestrial and aquatic ecosystems. *Sci. Total Environ.* **2006,** *370*, (1), 190-206.

21. McConnell, J. R.; Edwards, R.; Kok, G. L.; Flanner, M. G.; Zender, C. S.; Saltzman, E. S.; Banta, J. R.; Pasteris, D. R.; Carter, M. M.; Kahl, J. D. W., 20th-century industrial black carbon emissions altered arctic climate forcing. *Science* **2007,** *317*, (5843), 1381-1384.

22. Hammes, K. et al., Comparison of quantification methods to measure fire-derived (black/elemental) carbon in soils and sediments using reference materials from soil, water, sediment and the atmosphere. *Global Biogeochemical Cycles* **2007,** *21*, (3), GB3016.

23. Petzold, A.; Ogren, J. A.; Fiebig, M.; Laj, P.; Li, S. M.; Baltensperger, U.; Holzer-Popp, T.; Kinne, S.; Pappalardo, G.; Sugimoto, N.; Wehrli, C.; Wiedensohler, A.; Zhang, X. Y., Recommendations for reporting "black carbon" measurements. *Atmos. Chem. Phys.* **2013,** *13*, (16), 8365-8379.

24. Schwarz, J. P.; Gao, R. S.; Perring, A. E.; Spackman, J. R.; Fahey, D. W., Black carbon aerosol size in snow. *Sci. Rep.-UK* **2013,** *3*, 1356.

25. Bisiaux, M. M.; Edwards, R.; McConnell, J. R.; Curran, M. A. J.; Van Ommen, T. D.; Smith, A. M.; Neumann, T. A.; Pasteris, D. R.; Penner, J. E.; Taylor, K., Changes in black carbon deposition to Antarctica from two high-resolution ice core records, 1850-2000 AD. *Atmos. Chem. Phys.* **2012,** *12*, (9), 4107-4115.

26. Zennaro, P.; Kehrwald, N.; McConnell, J. R.; Schuepbach, S.; Maselli, O. J.; Marlon, J.; Vallelonga, P.; Leuenberger, D.; Zangrando, R.; Spolaor, A.; Borrotti, M.; Barbaro, E.; Gambaro, A.; Barbante, C., Fire in ice: two millennia of boreal forest fire history from the Greenland NEEM ice core. *Clim. Past* **2014,** *10*, (5), 1905-1924.

27. Gustafsson, O.; Bucheli, T. D.; Kukulska, Z.; Andersson, M.; Largeau, C.; Rouzaud, J. N.; Reddy, C. M.; Eglinton, T. I., Evaluation of a protocol for the quantification of black carbon in sediments. *Global Biogeochem. Cy.* **2001,** *15*, (4), 881-890.

28. Han, Y. N.; Cao, J. J.; An, Z. S.; Chow, J. C.; Watson, J. G.; Jin, Z.; Fung, K.; Liu, S. X., Evaluation of the thermal/optical reflectance method for quantification of elemental carbon in sediments. *Chemosphere* **2007,** *69*, (4), 526-533.

29. Bird, M. I.; Wynn, J. G.; Saiz, G.; Wurster, C. M.; McBeath, A., The Pyrogenic Carbon Cycle. *Annu. Rev. Earth Pl. Sc., Vol 43* **2015,** *43*, 273-298.

30. Preston, C. M.; Schmidt, M. W. I., Black (pyrogenic) carbon: a synthesis of current knowledge and uncertainties with special consideration of boreal regions. *Biogeosciences* **2006,** *3*, (4), 397-420.

31. Gleason, K. E.; McConnell, J. R.; Arienzo, M. M.; Chellman, N.; Calvin, W. M., Four-fold increase in solar forcing on snow in western U.S. burned forests since 1999. *Nat. Comm.* **2019,** *10*, 2026.

32. Bond, T. C. et al., Bounding the role of black carbon in the climate system: A scientific assessment. *J. Geophys. Res.-Atmos.* **2013,** *118*, (11), 5380-5552.

33. Laborde, M.; Crippa, M.; Tritscher, T.; Juranyi, Z.; Decarlo, P. F.; Temime-Roussel, B.; Marchand, N.; Eckhardt, S.; Stohl, A.; Baltensperger, U.; Prevot, A. S. H.; Weingartner, E.; Gysel, M., Black carbon physical properties and mixing state in the European megacity Paris. *Atmos. Chem. Phys.* **2013,** *13*, (11), 5831-5856.

34. Arienzo, M. M.; McConnell, J. R.; Murphy, L. N.; Chellman, N.; Das, S.; Kipfstuhl, S.; Mulvaney, R., Holocene black carbon in Antarctica paralleled Southern Hemisphere climate. *J. Geophys. Res.-Atmos.* **2017,** *122*, (13), 6713-6728.

35. Arienzo, M. M.; Maezumi, S. Y.; Chellman, N. J.; Iriarte, J., Pre-Colombian fire management linked to refractory black carbon emissions in the Amazon. *Fire* **2019,** *2*, (2), 31.

36. Brown, S., Multi-proxy Holocene fire history reconstruction in the Beartooth Mountains, Wyoming. M.S. Thesis, Indiana State University **2016.**

37. Chellman, N.; McConnell, J. R.; Arienzo, M.; Pederson, G. T.; Aarons, S. M.; Csank, A., Reassessment of the Upper Fremont Glacier Ice-Core Chronologies by Synchronizing of Ice-Core-Water Isotopes to a Nearby Tree-Ring Chronology. *Environ. Sci. Tech.* **2017,** *51*, (8), 4230-4238.

38. Brahney, J.; Ballantyne, A. P.; Turner, B. L.; Spaulding, S. A.; Otu, M.; Neff, J. C., Separating the influences of diagenesis, productivity and anthropogenic nitrogen deposition on sedimentary delta N-15 variations. *Org. Geochem.* **2014,** *75*, 140-150.

39. Brahney, J.; Ballantyne, A. P.; Kociolek, P.; Leavitt, P. R.; Farmer, G. L.; Neff, J. C., Ecological changes in two contrasting lakes associated with human activity and dust transport in western Wyoming. *Limnol. Oceanogr.* **2015,** *60*, (2), 678-695.

40. Blaauw, M.; Christen, J. A., Flexible Paleoclimate Age-Depth Models Using an Autoregressive Gamma Process. *Bayesian Anal.* **2011,** *6*, (3), 457-474.

41. Reimer, P. J. et al., IntCal13 and Marine13 radiocarbon age calibration curves 0-50,000 years cal BP. *Radiocarbon* **2013,** *55*, (4), 1869-1887.

42. R Development Core Team, 2013. R: A language and environment for statistical computing. R Foundation for Statistical Computing, Vienna, Austria. ISBN 3-900051-07-0, URL http://www.r-project.org.

43. Laborde, M.; Mertes, P.; Zieger, P.; Dommen, J.; Baltensperger, U.; Gysel, M., Sensitivity of the Single Particle Soot Photometer to different black carbon types. *Atmos. Meas. Tech.* **2012,** *5*, (5), 1031-1043.

44. Kondo, Y.; Saho, L.; Moteki, N.; Khan, F.; Takegawa, N.; Liu, X.; Koike, M.; Miyakawa, T., Consistency and Traceability of Black Carbon Measurements Made by Laser-Induced Incandescence, Thermal-Optical Transmittance, and Filter-Based Photo-Absorption Techniques. *Aerosol Sci. Tech.* **2011,** *45*, (2), 295-312.

45. Wendl, I. A.; Menking, J. A.; Faerber, R.; Gysel, M.; Kaspari, S. D.; Laborde, M. J. G.; Schwikowski, M., Optimized method for black carbon analysis in ice and snow using the Single Particle Soot Photometer. *Atmos. Meas. Tech.* **2014,** *7*, (8), 2667-2681.

46. Yoshida, A.; Moteki, N.; Ohata, S.; Mori, T.; Tada, R.; Dagsson-Waldhauserova, P.; Kondo, Y., Detection of light-absorbing iron oxide particles using a modified single-particle soot photometer. *Aerosol Sci. Tech.* **2016,** *50*, (3), 1-4.

47. Schuster, P. F.; Krabbenhoft, D. P.; Naftz, D. L.; Cecil, L. D.; Olson, M. L.; Dewild, J. F.; Susong, D. D.; Green, J. R.; Abbott, M. L., Atmospheric mercury deposition during the last 270 years: A glacial ice core record of natural and anthropogenic sources. *Environ. Sci. Tech.* **2002,** *36*, (11), 2303-2310.

48. Lee, Y. H. et al., Evaluation of preindustrial to present-day black carbon and its albedo forcing from Atmospheric Chemistry and Climate Model Intercomparison Project (ACCMIP) (vol 13, pg 2607, 2013). *Atmos. Chem. Phys.* **2013,** *13*, (13), 6553-6554.

49. Ramanathan, V.; Carmichael, G., Global and regional climate changes due to black carbon. *Nat. Geosci.* **2008,** *1*, (4), 221-227.

50. Cape, J. N.; Coyle, M.; Dumitrean, P., The atmospheric lifetime of black carbon. *Atmos. Environ.* **2012,** *59*, 256-263.

51. Whitlock, C.; Dean, W.; Rosenbaum, J.; Stevens, L.; Fritz, S.; Bracht, B.; Power, M., A 2650-year-long record of environmental change from northern Yellowstone National Park based on a comparison of multiple proxy data. *Quatern. Int.* **2008,** *188*, 126-138.

52. Huerta, M. A.; Whitlock, C.; Yale, J., Holocene vegetation-fire-climate linkages in northern Yellowstone National Park, USA. *Palaeogeogr. Palaeocl.* **2009,** *271*, (1-2), 170-181.

53. Kelly, R. L.; Surovell, T. A.; Shuman, B. N.; Smith, G. M., A continuous climatic impact on Holocene human population in the Rocky Mountains. *P. Natl. Acad. Sci. USA* **2013,** *110*, (2), 443-447.

54. Shuman, B., Recent Wyoming temperature trends, their drivers, and impacts in a 14,000-year context. *Climatic Change* **2012,** *112*, (2), 429-447.

55. Shuman, B.; Pribyl, P.; Minckley, T. A.; Shinker, J. J., Rapid hydrologic shifts and prolonged droughts in Rocky Mountain headwaters during the Holocene. *Geophys. Res. Lett.* **2010,** *37*, L06701.

56. Whitlock, C.; Dean, W. E.; Fritz, S. C.; Stevens, L. R.; Stone, J. R.; Power, M. J.; Rosenbaum, J. R.; Pierce, K. L.; Bracht-Flyr, B. B., Holocene seasonal variability inferred

from multiple proxy records from Crevice Lake, Yellowstone National Park, USA. *Palaeogeogr. Palaeocl.* **2012,** *331*, 90-103.

57. Fall, P. L.; Davis, P. T.; Zielinski, G. A., Late Quaternary vegetation and climate of the Wind-River Range, Wyoming. *Quaternary Res.* **1995,** *43*, (3), 393-404.
58. Aarons, S. M.; Aciego, S. M.; Gabrielli, P.; Delmonte, B.; Koornneef, J. M.; Uglietti, C.; Wegner, A.; Blakowski, M. A.; Bouman, C., Ice core record of dust sources in the western United States over the last 300 years. *Chemical Geology* **2016,** *442*, 160-173.
59. Minckley, T. A.; Shriver, R. K.; Shuman, B., Resilience and regime change in a southern Rocky Mountain ecosystem during the past 17 000 years. *Ecol. Monogr.* **2012,** *82*, (1), 49-68.

Dissertation Conclusions

This dissertation contributes to a better understanding of northern Rocky Mountain Holocene climate and pollution, and introduces semi-permanent ice patches as a new climate archive. Since 1750 CE, the UFG ice cores documented pervasive, ubiquitous pollution from the Industrial Revolution, apparent in increased heavy metal and black carbon concentrations. Both the UFG ice cores and nearby tree rings, when adjusted for radial translocation of mercury, also documented 20th-century increases in atmospheric mercury deposition and concentration, suggesting that industrial-era fossil fuel burning was the main contributor to atmospheric mercury budgets over recent centuries with relatively minor contributions from Gold Rush-era mining.

From a climate perspective, the strong covariance of the tree ring-width chronology with the ice-core water isotopes demonstrate how these two natural archives documented a coherent climate signal over the past two and half centuries. The magnitude and trend of black carbon deposition at North Lake was similar to that at UFG, 50 km to the north, from 1750 to 1950 CE. Over the past 2,000 years, black carbon deposition at North Lake paralleled regional temperature and moisture, indicating a link between regional burning and climate. Over longer timescales, the Beartooth Plateau ice patch water isotope and ice accumulation records documented peak Holocene warmth in the region at 4,200 ybp, before a rapid transition to cooler and wetter conditions coincident with the Neoglaical period. The ice patch climate record also paralleled human activity in the nearby Bighorn Mountains, suggesting a link between climate and habitability of the region.

These studies are unified by a theme fundamental to interpreting paleoclimate records from any natural proxy: accurate dating. Developing robust, valid records of climate and pollution requires well-constrained chronologies to accurately attribute changes observed in chemical records within natural archives to a specific time in earth history.

The reassessment of the UFG ice cores emphasizes the importance of accurate dating and introduces a novel strategy to constrain the dating of alpine ice cores. The original, inaccurate depth-age scales of the ice cores led to misinterpretation of the mercury profile, suggesting significant pollution from 19th century mining. This conclusion was used to inform studies of mercury budgets[1, 2] and large-scale reconstructions of past anthropogenic mercury emissions that are still debated today[3, 4]. By revisiting the chronology with a new approach of synchronizing climate records from adjacent tree cores, which have very little dating uncertainty, to the ice-core water isotope records, it was possible to significantly improve and refine the dating of the UFG ice cores, leading to a more accurate understanding of mercury deposition over the past 250 years. This approach leveraged the strength of tree-ring chronologies to address a weakness in the difficult-to-date UFG ice cores.

Another important conclusion for the UFG ice cores is the control of glacier and basin geometry on the chronology of glacial ice cores. An ice flow model[5], driven only by the glacial surface topography, bedrock topography, ice accumulation rate, and an estimate of basal melt, was able to provide an excellent approximation of the general shape of the final UFG depth-age scale. If this modeling exercise was performed in early stages of glacial ice core studies, it would be an effective approach to guide initial dating, especially for cores where there are no clear annual cycles or where volcanic synchronization is inconclusive because of significant melt and high impurity loading.

The emphasis on ensuring valid temporal attribution of trends continued in the study of tree-ring mercury. While the dating of individual tree rings themselves had little uncertainty in this study, mercury may move radially between individual rings so that mercury concentrations measured within a tree-ring are not necessarily representative of the year that ring formed. Trees, as biological organisms, actively process nutrients and contaminants in their tissues, and such mobility across ring boundaries had been noted for mercury and other chemical species in trees[6-

[10]. The co-located mercury record from the UFG ice cores on the revised depth-age scale served as a benchmark for atmospheric mercury loadings against which these tree records could be evaluated to identify and quantify potential radial movement—without such a record, it would be difficult to assess potential radial movement, likely leading to misinterpretation of the tree-ring mercury profiles.

For the Beartooth ice patch, the robust chronology of 29 radiocarbon dates throughout the 6 meter- deep ice core was essential for interpretation. The unique depositional environment of the ice patch of extremely high surface melt with an average accumulation rate on the order of a few millimeters per year precludes dating by any traditional approaches. The spatial coherence of the organic layers between the three cores recovered from the ice patch, as well as the regular frequency of the layers that formed on average every few centuries, narrowly constrained the age of the clean ice units between such layers, allowing for meaningful temporal interpretation of the record.

The study of black carbon in Island Lake and North Lake emphasized how site characteristics govern whether lake sediment black carbon records are representative of a regional or local signal. Generally, lakes with a smaller catchment to surface area ratio are more likely to record atmospheric deposition because of proportionally smaller inputs from runoff. The lakes in this study, however, did not agree with this assumption—Island Lake and North Lake had catchment to surface area ratios of 59 and 30, respectively, but the black carbon records indicated that North Lake was more regionally-representative than Island Lake. This discrepancy likely results from other characteristics of the watersheds, namely the watershed for North Lake is much smaller and consists largely of exposed rock, minimizing black carbon inputs from soil erosion or burnt biomass, while the Island Lake watershed is comparatively large and vegetated and therefore more likely to contribute black carbon via secondary deposition.

Recommendations for future work

The results of this dissertation highlight a number of areas for future research. Chapter 2 points to the need for a better understanding of mercury uptake and preservation in trees. While the radial movement of atmospherically-derived chemical species across tree ring boundaries can be studied on shorter timescales in controlled lab experiments or by comparing to direct atmospheric measurements over recent decades, better evaluating potential post-depositional modification on century-scale timescales requires comparison to other proxy records. Future work developing higher resolution records of mercury in tree rings, ideally at annual resolution, that are paired with other co-located or nearby mercury records from more well-established proxies (e.g., ice cores, lake sediment cores, or direct atmospheric measurements) would be valuable for better evaluating potential radial movement. Higher-resolution measurements would allow for detection of sharp changes in mercury concentrations, which is limited in current studies by smoothing inherent to sampling at five- or ten-year resolution. Furthermore, more laboratory or process-level studies evaluating pathways of mercury uptake and mobility in trees of different ages and different species are necessary to understand the significant inter- and intra-tree variability of mercury concentrations.

The development of a climate record from a semi-permanent ice patch based on water isotopes and ice accumulation rates that compares well to other proxies, as demonstrated in Chapter 3, indicates the potential to develop ice-based paleoclimate records from similar ice patches in other mountainous regions. Developing a better understanding of how these ice patches persist on the landscape by long-term instrumental monitoring would be valuable for better constraining interpretations of ice-patch chemical records. Such monitoring, however, will be challenging because of the large variability in seasonal conditions. While the surface of the Beartooth Plateau ice patch was exposed in 2016 CE, there were over 8 meters of seasonal snow

covering the ice patch on attempted coring attempts at the same time of year in 2018 CE following two winters of above-average precipitation.

Under a warming climate, there is urgency for reconnaissance and sampling of ice patches in the Rockies and other mountain ranges before they melt and disappear from the landscape. An 8-meter-long ice core recovered from an ice patch in the Sierra Nevada mountains near Sonora Pass, California showed significant isotopic variability. Attempts to date the core, however, using radiocarbon dating of a small piece of organic matter, were unsuccessful. Future work studying this ice patch in more depth, with alternative dating approaches such as heavy metal synchronization or by identifying plutonium fallout from nuclear weapons testing, as well as sampling of other eastern Sierra ice patches, is the focus of a recently-submitted proposal to the Sulo and Aileen Maki Endowment at the Desert Research Institute.

Finally, Chapter 4 demonstrated that a new method for black carbon measurements can be successfully implemented to develop records of fire history. The implications of each black carbon record, however, depend on the lake's physical characteristics. Future work includes developing black carbon records from lakes dominated by atmospheric deposition, with a small, non-vegetated catchment and small catchment-to-surface-area ratio, as well as refining the rBC method to improve measurement reproducibility. Further comparison of black carbon and charcoal measurements from lakes with these characteristics will test the hypothesis that black carbon records represent regional burning. Also, evaluation of black carbon depositional processes in lakes would help with interpreting records developed with this new method. Potential work includes quantifying secondary deposition by measuring black carbon influx via tributaries and evaluating black carbon cycling and deposition within the lake.

References

1. Streets, D. G.; Devane, M. K.; Lu, Z. F.; Bond, T. C.; Sunderland, E. M.; Jacob, D. J., All-Time Releases of Mercury to the Atmosphere from Human Activities. *Environ. Sci. Technol.* **2011,** *45*, (24), 10485-10491.
2. Horowitz, H. M.; Jacob, D. J.; Amos, H. M.; Streets, D. G.; Sunderland, E. M., Historical Mercury Releases from Commercial Products: Global Environmental Implications. *Environ. Sci. Technol.* **2014,** *48*, (17), 10242-10250.
3. Outridge, P. M.; Mason, R. P.; Wang, F.; Guerrero, S.; Heimburger-Boavida, L. E., Updated Global and Oceanic Mercury Budgets for the United Nations Global Mercury Assessment 2018. *Environ. Sci. Technol.* **2018,** *52*, (20), 11466-11477.
4. Streets, D. G.; Horowitz, H. M.; Jacob, D.; Lu, Z. F.; Levin, L.; ter Schure, A. F. H.; Sunderland, E. M., Total Mercury Released to the Environment by Human Activities. *Environ. Sci. Technol.* **2017,** *51*, (11), 5969-5977.
5. Pattyn, F., Antarctic subglacial conditions inferred from a hybrid ice sheet/ice stream model. *Earth Planet. Sc. Lett.* **2010,** *295*, (3-4), 451-461.
6. Arnold, J.; Gustin, M. S.; Weisberg, P. J., Evidence for Nonstomatal Uptake of Hg by Aspen and Translocation of Hg from Foliage to Tree Rings in Austrian Pine. *Environ. Sci. Technol.* **2018,** *52*, (3), 1174-1182.
7. Navratíl, T.; Šimeček, M.; Shanley, J. B.; Rohovec, J.; Hojdová, M.; Houška, J., The history of mercury pollution near the Spolana chlor-alkali plant (Neratovice, Czech Republic) as recorded by Scots pine tree rings and other bioindicators. *Sci. Total Environ.* **2017,** *586*, 1182-1192.
8. Watmough, S. A.; Hutchinson, T. C., Historical changes in lead concentrations in tree-rings of sycamore, oak and Scots pine in north-west England. *Sci. Total Environ.* **2002,** *293*, (1-3), 85-96.
9. Edmands, J. D.; Brabander, D. J.; Coleman, D. S., Uptake and mobility of uranium in black oaks: implications for biomonitoring depleted uranium-contaminated groundwater. *Chemosphere* **2001,** *44*, (4), 789-795.
10. Bunn, A. G.; Helfield, J. M.; Gerdts, J. R.; Gleaves, D. A.; Drake, D. C.; Sheppard, P. R., A solvent-based extraction fails to remove mobile nitrogen from western redcedar (Thuja plicata). *Dendrochronologia* **2017,** *44*, 19-21.